
Towards graph neural networks for provably solving convex optimization problems

Chendi Qian¹ Christopher Morris¹

Abstract

Recently, message-passing graph neural networks (MPNNs) have shown potential for solving combinatorial and continuous optimization problems due to their ability to capture variable-constraint interactions. While existing approaches leverage MPNNs to approximate solutions or warm-start traditional solvers, they often lack guarantees for feasibility, particularly in convex optimization settings. Here, we propose an iterative MPNN framework to solve convex optimization problems with provable feasibility guarantees. First, we demonstrate that MPNNs can provably simulate standard interior-point methods for solving quadratic problems with linear constraints, covering relevant problems such as SVMs. Secondly, to ensure feasibility, we introduce a variant that starts from a feasible point and iteratively restricts the search within the feasible region. Experimental results show that our approach outperforms existing neural baselines in solution quality and feasibility, generalizes well to unseen problem sizes, and, in some cases, achieves faster solution times than state-of-the-art solvers such as Gurobi.

1. Introduction

Message-passing graph neural networks (MPNNs) have recently been widely applied to optimization problems, including continuous and combinatorial domains (Bengio et al., 2021; Cappart et al., 2023; Scavuzzo et al., 2024). Due to their inherent ability to capture structured data, MPNNs are well-suited as proxies for representing and solving such problems, e.g., in satisfiability problems, literals and clauses can be modeled as different node types within a bipartite graph (Selsam et al., 2018). At the same time, in *linear programming* (LP), the variable-constraint interaction naturally forms a bipartite graph structure (Gasse et al., 2019).

¹Department of Computer Science, RWTH Aachen University, Aachen, Germany. Correspondence to: Chendi Qian <chendi.qian@log.rwth-aachen.de>.

Under review.

Consequently, MPNNs are used as a lightweight proxy to solve such optimization problems in a data-driven fashion.

Most *combinatorial optimization* (CO) problems are NP-hard (Ausiello et al., 1999), making exact solutions computationally intractable for larger instances. To address this, it is often more practical to relax the integrality constraints and solve the corresponding continuous optimization problems instead. This approach involves formulating a *continuous relaxation* as a proxy for the original problem. After solving the relaxed problem, the resulting continuous solutions guide the search in the discrete solution space (Schrijver, 1986). For example, solving the underlying *linear programming relaxation* in *mixed-integer linear programming* (MILP) is a crucial step for scoring candidates in strong branching (Achterberg et al., 2005), also using MPNNs (Gasse et al., 2019; Qian et al., 2024). Recent studies have extended MPNN-based modeling to other continuous optimization problems, especially *quadratic programming* (QP) (Li et al., 2024a; Gao et al., 2024; Xiong et al., 2024). Some existing methods integrate neural networks with traditional solvers (Fan et al., 2023; Jung et al., 2022; Li et al., 2022b; 2024a; Liu et al., 2024). These approaches either replace components of the solver with neural networks or use neural networks to warm-start the solver. In the former case, the methods remain limited by the solver’s framework. In contrast, in the latter, the solver is still required to solve a related problem to produce feasible and optimal solutions.

However, the above works mainly aim to predict a near-optimal solution without ensuring the feasibility of such a solution. For example, Fioretto et al. (2020); Qian et al. (2024) propose penalizing constraint violations by adding an extra loss term during training without offering strict feasibility guarantees. Existing strategies typically fall into two categories: relying on solvers to produce feasible solutions or projecting neural network outputs into the feasible region. The first approach, where the neural network serves primarily as a warm-start for the solver, still relies on the solver for final solutions. The second approach, which involves projecting outputs into the feasible region, often requires solving an additional optimization problem and can be efficient only for specific cases. Moreover, this projection

may degrade solution quality (Li et al., 2024b). More recently, approaches leveraging Lagrangian duality theory have emerged, aiming to design neural networks capable of producing dual-feasible solutions (Fioretto et al., 2021; Klamkin et al., 2024; Park & Van Hentenryck, 2023). While promising, these methods often require many iterations and still lack guarantees for strict feasibility.

Present work We propose an MPNN architecture that directly outputs high-quality, feasible solutions to convex optimization problems, closely approximating the optimal ones. Building on Qian et al. (2024), which pioneered using MPNNs for simulating polynomial-time *interior-point methods* (IPM) for LPs, we extend this approach to *linearly constrained quadratic programming* (LCQP), covering relevant problems such as SVMs. Unlike Qian et al. (2024), where each MPNN layer corresponds to an IPM iteration, our fixed-layer MPNN predicts the next interior point from the current one, decoupling the number of MPNN layers from IPM iterations. We further prove that such MPNNs can simulate IPMs for solving LCQPs. In addition, we incorporate a computationally lightweight projection step that restricts the search direction to the feasible region to ensure feasibility, leveraging the constraints’ linear algebraic structure. Experiments show our method outperforms neural network baselines, generalizes well to larger, unseen problem instances, and, in some cases, achieves faster solution times than state-of-the-art exact solvers such as Gurobi (Gurobi Optimization, LLC, 2024).

In summary, our contributions are as follows.

1. We propose an MPNN-based approach for predicting solutions of LCQP instances.
2. We theoretically show that an MPNN with $\mathcal{O}(1)$ distinct layers, where each layer has unique weights, and $\mathcal{O}(m+n)$ total message-passing steps and each step executes a layer that may be reused across steps, can simulate an IPM for LCQP.
3. We introduce an efficient and feasibility-guaranteed variant that incorporates a projection step to ensure the predicted solutions strictly satisfy the constraints of the LCQP.
4. Empirically, we show that both methods achieve high-quality predictions and outperform traditional QP solvers in solving time for certain problems. Furthermore, our approach can generalize to larger, unseen problem instances in specific cases.

1.1. Related work

Here, we discuss relevant related work.

MPNNs MPNNs (Gilmer et al., 2017; Scarselli et al., 2008) have been extensively studied in recent years. Notable architectures can be categorized into spatial models (Duvenaud et al., 2015; Hamilton et al., 2017; Bresson & Laurent, 2017; Veličković et al., 2018; Xu et al., 2019) and spectral MPNNs (Bruna et al., 2014; Defferrard et al., 2016; Kipf & Welling, 2017; Levie et al., 2019; Monti et al., 2018; Geisler et al., 2024). The former conforms to the message-passing framework of Gilmer et al. (2017), while the latter leverage the spectral property of the graph.

Machine learning for convex optimization In this work, we focus on convex optimization and direct readers interested in combinatorial optimization problems to the surveys Bengio et al. (2021); Cappart et al. (2023); Peng et al. (2021); see a more detailed discussion on related work in Appendix A.2.

A few attempts have been made to apply machine learning to LPs. Li et al. (2022b) learned to reformulate LP instances, and Fan et al. (2023) learned the initial basis for the simplex method, both aimed at accelerating the solver. Liu et al. (2024) imitated simplex pivoting, and Qian et al. (2024) proposed using MPNNs to simulate IPMs for LPs (Nocedal & Wright, 2006). Li et al. (2024a) introduced PDHG-Net to approximate and warm-start the *primal-dual hybrid gradient algorithm* (PDHG) (Applegate et al., 2021; Lu, 2024). Li et al. (2024b) bounded the depth and width of MPNNs while simulating a specific LP algorithm. Quadratic programming (QP) has seen limited standalone exploration. Notable works include Bonami et al. (2018), who analyzed solver behavior to classify linearization needs, and Getzleman & Balaprakash (2021), who used reinforcement learning for solver selection. Others accelerated solvers by learning step sizes (Ichnowski et al., 2021; Jung et al., 2022) or warm-started them via end-to-end learning (Sambharya et al., 2023). Graph-based representations have been applied to quadratically constrained quadratic programming (QCQP) (Wu et al., 2024; Xiong et al., 2024), while Gao et al. (2024) extended Qian et al. (2024) to general nonlinear programs. On the theoretical side, Chen et al. (2022; 2024); Wu et al. (2024) examined the expressivity of MPNNs in approximating LP and QP solutions, offering insights into their capabilities and limitations.

See Appendix A.2 for a discussion on machine learning for constrained optimization.

1.2. Background

Here, we introduce notation, MPNNs, and convex optimization problems.

Notation Let $\mathbb{N} := \{0, 1, 2, \dots\}$. For $n \geq 1$, let $[n] := \{1, \dots, n\} \subset \mathbb{N}$. We use $\{\!\{ \dots \}\!\}$ to denote multisets, i.e.,

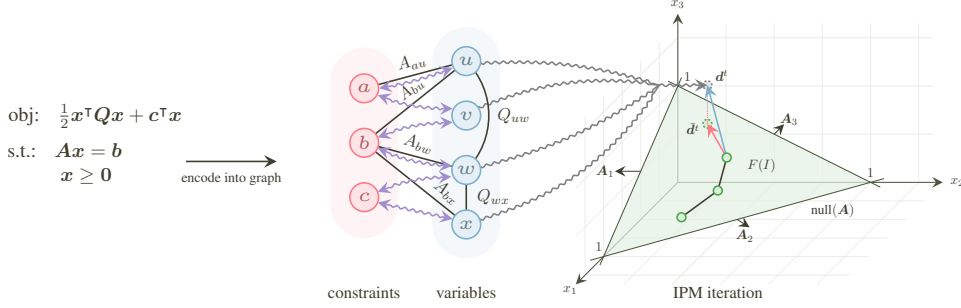


Figure 1. Overview of our MPNN architectures for solving LCQPs.

the generalization of sets allowing for multiple instances for each of its elements. A graph G is a pair $(V(G), E(G))$ with finite sets of vertices or nodes $V(G)$ and edges $E(G) \subseteq \{\{u, v\} \subseteq V(G) \mid u \neq v\}$. For ease of notation, we denote the edge $\{u, v\}$ in $E(G)$ by (u, v) or (v, u) . Throughout the paper, we use standard notation, e.g., we denote the neighborhood of a node v by $N(v)$; see Appendix A.1 for details. By default, a vector $x \in \mathbb{R}^d$ is a column vector.

MPNNs Intuitively, MPNNs learn a vectorial representation, i.e., a d -dimensional real-valued vector, representing each vertex in a graph by aggregating information from neighboring vertices. Let G be an n -order attributed graph with node feature matrix $\mathbf{X} \in \mathbb{R}^{n \times d}$, for $d > 0$, following, Gilmer et al. (2017) and Scarselli et al. (2008), in each layer, $t > 0$, for vertex $v \in V(G)$, we compute a vertex feature $h_v^{(t)} :=$

$$\text{UPD}^{(t)}\left(h_v^{(t-1)}, \text{AGG}^{(t)}(\{h_u^{(t-1)} \mid u \in N(v)\})\right) \in \mathbb{R}^d,$$

where $\text{UPD}^{(t)}$ and $\text{AGG}^{(t)}$ may be parameterized functions, e.g., neural networks, and $h_v^{(0)} := \mathbf{X}_v$.

Convex optimization problems In this work, we focus on convex optimization problems, namely LCQPs, of the following form,

$$\min_{x \in \mathbb{Q}_{\geq 0}^n} \frac{1}{2} x^\top Q x + c^\top x \text{ such that } Ax = b, x \geq \mathbf{o}. \quad (1)$$

Here, an LCQP instance I is a tuple (Q, A, b, c) , where $Q \in \mathbb{Q}^{n \times n}$ and $c \in \mathbb{Q}^n$ are the quadratic and linear coefficients of the objective, $A \in \mathbb{Q}^{m \times n}$ and $b \in \mathbb{Q}^m$ form the constraints. We assume that the quadratic matrix Q is positive semi-definite (PSD), i.e., $v^\top Q v \geq 0$, for all $v \in \mathbb{R}^n$; otherwise, the problem is non-convex. We assume $m \leq n$ and that A has full rank m ; otherwise, either the problem is infeasible, or some linear constraints can be eliminated using resolving techniques (Andersen & Andersen, 1995). Furthermore, if constraints are inequalities, we can always transform them into equalities by adding slack variables (Boyd & Vandenberghe,

2004). We denote the feasible region of the instance I as $F(I) := \{x \in \mathbb{Q}^n \mid A_j x = b_j \text{ for } j \in [m] \text{ and } x_i \geq 0 \text{ for } i \in [n]\}$. The optimal solution $x^* \in F(I)$ is defined such as $\frac{1}{2} x^\top Q x + c^\top x \geq \frac{1}{2} x^{*\top} Q x^* + c^\top x^*$, for $x \in F(I)$, which we assume to be unique.

2. Towards MPNNs for solving convex optimization problems

Here, we provide a detailed overview of our MPNN architectures. We first describe how to represent an LCQP instance as a graph. Next, we present an MPNN architecture that provably simulates IPMs for solving LCQPs. Finally, we introduce a null space projection method to ensure feasibility throughout the search.

Encoding LCQP instances as graphs Previous works have demonstrated that LP instances can be effectively encoded as a bipartite or tripartite graph (Gasse et al., 2019; Khalil et al., 2022; Qian et al., 2024). In the case of LCQPs, following Chen et al. (2024), we encode a given LCQP instance I into a graph $G(I)$ with constraint node set $C(I)$ and variable node set $V(I)$. We define the constraint-variable node connections via the non-zero entries of the A matrix and define the edge features via $e_{cv} := A_{cv}$, for $v \in V(I), c \in C(I)$. In addition, the constraint vector b acts as features for the constraint nodes, i.e., we design the constraint node feature matrix as $C := \text{reshape}(b) \in \mathbb{Q}^{m \times 1}$. The feature matrix for the variable nodes is set to the objective vector $V := \text{reshape}(c) \in \mathbb{Q}^{n \times 1}$. To encode the Q matrix, we follow Chen et al. (2024) and encode the non-zero entries Q_{vu} as edges between variable nodes v, u , and use the value Q_{vu} as the edge attribute, $e_{vu} := Q_{vu}, v, u \in V(I)$. Moreover, we add a global node $\{g(I)\}$ to $G(I)$, similar to Qian et al. (2024) for LPs, and connect it to all the variable and constraint nodes with uniform edge features $e_{cg} := 1, c \in C(I)$, and $e_{vg} := 1, v \in V(I)$.

MPNNs for simulating IPMs Here, we derive an MPNN architecture to provably simulate IPMs for solving LCQPs. For more details on IPM for LCQP, we refer to Ap-

Algorithm 1 Training phase of our MPNN architecture simulating IPM steps.

Require: An LCQP instance $I = (\mathbf{Q}, \mathbf{A}, \mathbf{b}, \mathbf{c})$, an arbitrary initial solution $\mathbf{x}^{(0)}$, an L -layer MPNN architecture following Equations (2) to (6), number of iterations T , the ground-truth interior points $\{\mathbf{x}^{*(t)} \mid t \in [T]\}$.

Ensure: Supervised loss \mathcal{L} .

- 1: **for** $t \in [T]$ **do**
- 2: $\mathbf{x}^{(t)} \leftarrow \text{MPNN}(I, \mathbf{x}^{(t-1)})$
- 3: Calculate $\mathcal{L}^{(t)}(\mathbf{x}^{*(t)}, \mathbf{x}^{(t)})$ as in Equation (7)
- 4: **end for**
- 5: **return** The loss $\mathcal{L} \leftarrow \frac{1}{T} \sum_{t=1}^T \mathcal{L}^{(t)}(\mathbf{x}^{*(t)}, \mathbf{x}^{(t)})$

pendix A.6. Similar to Gao et al. (2024), we decouple the number of layers L of the MPNN and the number of iterations T . Additionally, the learnable parameters of the L -layer MPNN are shared across the iterations. At each iteration $t \in [T]$, the L -layer MPNN takes the graph $G(I)$ together with the current solution $\mathbf{x}^{(t-1)}$ as input. The MPNN outputs a scalar per variable node as the prediction for the next interior point $\mathbf{x}^{(t)}$, with an arbitrary initial solution $\mathbf{x}^{(0)} \geq \mathbf{0}$. We denote the node embedding at layer $l \in [L]$ and iteration $t \in [T]$ as $\mathbf{h}_\circ^{(l,t)}$, $\circ \in V(I) \cup C(I) \cup \{g(I)\}$. At the beginning of each iteration, we initialize the node embeddings as

$$\begin{aligned} \mathbf{h}_c^{(0,t)} &:= \mathbf{C}_c \in \mathbb{Q}, c \in C(I), \\ \mathbf{h}_v^{(0,t)} &:= \text{CONCAT}(\mathbf{V}_v, \mathbf{x}_v^{(t-1)}) \in \mathbb{Q}^2, v \in V(I), \\ \mathbf{h}_g^{(0,t)} &:= \mathbf{0}. \end{aligned} \quad (2)$$

Each message passing layer consists of three sequential steps, similar to Qian et al. (2024). First, the embeddings of the constraint nodes are updated, using the embeddings of the variable nodes and the global node $\mathbf{h}_c^{(l,t)} :=$

$$\begin{aligned} &\text{UPD}_c^{(l)} \left[\mathbf{h}_c^{(l-1,t)}, \right. \\ &\text{MSG}_{v \rightarrow c}^{(l)} \left(\left\{ \left\{ \mathbf{h}_v^{(l-1,t)}, \mathbf{e}_{cv} \mid v \in N(c) \cap V(I) \right\} \right\} \right), \\ &\left. \text{MSG}_{g \rightarrow c}^{(l)} \left(\mathbf{h}_g^{(l-1,t)}, \mathbf{e}_{cg} \right) \right] \in \mathbb{Q}^d. \end{aligned} \quad (3)$$

Next, the global node embeddings are updated based on the embeddings of the variable nodes and the most recently updated constraint node embeddings $\mathbf{h}_g^{(l,t)} :=$

$$\begin{aligned} &\text{UPD}_g^{(l)} \left[\mathbf{h}_g^{(l-1,t)}, \right. \\ &\text{MSG}_{v \rightarrow g}^{(l)} \left(\left\{ \left\{ \mathbf{h}_v^{(l-1,t)}, \mathbf{e}_{vg} \mid v \in V(I) \right\} \right\} \right), \\ &\left. \text{MSG}_{c \rightarrow g}^{(l)} \left(\left\{ \left\{ \mathbf{h}_c^{(l,t)}, \mathbf{e}_{cg} \mid c \in C(I) \right\} \right\} \right) \right] \in \mathbb{Q}^d. \end{aligned} \quad (4)$$

Algorithm 2 Inference phase of our MPNN architecture simulating IPM steps.

Require: An LCQP instance $I = (\mathbf{Q}, \mathbf{A}, \mathbf{b}, \mathbf{c})$, an arbitrary initial solution $\mathbf{x}^{(0)}$, an L -layer MPNN architecture following Equations (2) to (6), number of iterations T , threshold δ for solution selection.

Ensure: Best found solution \mathbf{x} .

- 1: Define $\text{obj}(\mathbf{x}) := \frac{1}{2} \mathbf{x}^\top \mathbf{Q} \mathbf{x} + \mathbf{c}^\top \mathbf{x}$
- 2: Define $\text{cons}(\mathbf{x}) := \max\{|\mathbf{A}_i \mathbf{x} - \mathbf{b}_i| \mid i \in [m]\}$
- 3: **if** $\text{cons}(\mathbf{x}^{(0)}) < \delta$ **then**
- 4: $\mathbf{x} \leftarrow \mathbf{x}^{(0)}$
- 5: **end if**
- 6: **for** $t \in [T]$ **do**
- 7: $\mathbf{x}^{(t)} \leftarrow \text{MPNN}(I, \mathbf{x}^{(t-1)})$
- 8: **if** $\text{cons}(\mathbf{x}^{(t)}) < \delta$ and $\text{obj}(\mathbf{x}^{(t)}) < \text{obj}(\mathbf{x})$ **then**
- 9: $\mathbf{x} \leftarrow \mathbf{x}^{(t)}$
- 10: **end if**
- 11: **end for**
- 12: **return** \mathbf{x} .

Finally, the embeddings of the variable nodes are updated by aggregating information from their neighboring variable nodes and the updated constraint node and global node embeddings $\mathbf{h}_v^{(l,t)} :=$

$$\begin{aligned} &\text{UPD}_v^{(l)} \left[\mathbf{h}_v^{(l-1,t)}, \right. \\ &\text{MSG}_{v \rightarrow v}^{(l)} \left(\left\{ \left\{ \mathbf{h}_u^{(l-1,t)}, \mathbf{e}_{uv} \mid u \in N(v) \cap V(I) \right\} \right\} \right), \\ &\text{MSG}_{c \rightarrow v}^{(l)} \left(\left\{ \left\{ \mathbf{h}_c^{(l,t)}, \mathbf{e}_{cv} \mid c \in N(v) \cap C(I) \right\} \right\} \right), \\ &\left. \text{MSG}_{g \rightarrow v}^{(l)} \left(\mathbf{h}_g^{(l,t)}, \mathbf{e}_{vg} \right) \right] \in \mathbb{Q}^d. \end{aligned} \quad (5)$$

Finally, we use a multi-layer perceptron for predicting the current variable assignments,

$$\mathbf{x}_v^{(t)} := \text{MLP}(\mathbf{h}_v^{(L,t)}) \in \mathbb{Q}, \quad (6)$$

whose output vector $\mathbf{x}^{(t)} \in \mathbb{Q}^n$ serves as the prediction of the next interior point.

For training, we use the mean-squared error between our intermediate predictions $\mathbf{x}^{(t)}$, $t \in [T]$, and the ground truth interior point given by the IPM $\mathbf{x}^{*(t)}$, $t \in [T]$,

$$\mathcal{L}^{(t)}(\mathbf{x}^{*(t)}, \mathbf{x}^{(t)}) := \|\mathbf{x}^{*(t)} - \mathbf{x}^{(t)}\|_2^2. \quad (7)$$

During training, we pre-set the iterations and supervise all predicted interior points. During inference, however, our framework allows for an arbitrary number of iterations and picks the best solution simultaneously. The training and inference processes are summarized in Algorithm 1 and Algorithm 2.

Now, the following result shows that there exists an MPNN architecture, $f_{\text{MPNN,IPM}}$, of $\mathcal{O}(1)$ layers and $\mathcal{O}(m)$ message passing steps in the form of Equations (2) to (5), that is capable of simulating the IPM algorithm for LCQPs. For the detailed proof, please see Appendix A.7.

Theorem 1. *There exists an MPNN $f_{\text{MPNN,IPM}}$ composed of $\mathcal{O}(1)$ layers and $\mathcal{O}(m+n)$ successive message-passing steps that reproduces each iteration of the IPM algorithm for LCQPs, in the sense that for any LCQP instance $I = (\mathbf{Q}, \mathbf{A}, \mathbf{b}, \mathbf{c})$ and any primal-dual point $(\mathbf{x}^{(t)}, \boldsymbol{\lambda}^{(t)}, \mathbf{s}^{(t)})$ with $t > 0$, $f_{\text{MPNN,IPM}}$ maps the graph $G(I)$ carrying $[\mathbf{x}^{(t-1)}, \mathbf{s}^{(t-1)}]$ on the variable nodes, $[\boldsymbol{\lambda}^{(t-1)}]$ on the constraint nodes, and $[\mu, \sigma]$ on the global node to the same graph $G(I)$ carrying the output $[\mathbf{x}^{(t)}, \mathbf{s}^{(t)}]$ and $[\boldsymbol{\lambda}^{(t)}]$ of Algorithm 7 on the variable and constraint nodes, respectively.*

Ensuring feasible solutions In supervised learning, ensuring feasibility is challenging due to training and validation errors in Algorithm 1 and Algorithm 2. Correcting infeasible solutions typically involves additional optimization, which adds computational overhead and may degrade solution quality. To address this, we propose an iterative method that maintains strict feasibility throughout optimization. Starting from a feasible point $\mathbf{x}^{(0)}$, the search is constrained to the feasible region $\mathbf{x}^{(t)} \in F(I)$, for all $t \in [T]$. We also discard intermediate steps from the expert solver, focusing only on the optimal solution to enhance flexibility. This section details our approach, answering two key questions: (1) How is an initial feasible solution constructed? (2) How can feasibility be preserved during updates? We also describe MPNN modifications and the search algorithm.

We can obtain a feasible initial solution by solving a trivial LP with the given constraints and a simple objective, such as $\mathbf{c} = \mathbf{0}$. This incurs moderate overhead, as solving an LP is computationally cheaper than a quadratic problem. Existing methods, like the big-M and two-phase simplex methods (Bertsimas & Tsitsiklis, 1998), efficiently compute feasible basic solutions, while MOSEK’s IPM Andersen & Andersen (2000) achieves feasibility within a few updates.

We follow the generic framework of iterative optimization methods (Nocedal & Wright, 2006), where, at each iteration, a search direction $\mathbf{d}^{(t)} \in \mathbb{Q}^n$ is determined and corresponding step length $\alpha^{(t)} > 0$ is computed. However, our approach differs in that we train an MPNN in a supervised way to predict the displacement $\mathbf{d}^{*(t)} := \mathbf{x}^* - \mathbf{x}^{(t-1)}$ from the current solution $\mathbf{x}^{(t-1)}$ to the optimal solution \mathbf{x}^* .¹

To correct the predicted displacement $\mathbf{d}^{(t)}$, we com-

¹We distinguish the terms *direction* and *displacement*; the former focuses on the orientation only, with normalized magnitude by default, while the latter emphasizes both the magnitude and direction of the movement from one point to another.

pute a feasibility-preserving displacement $\tilde{\mathbf{d}}^{(t)}$ such that $\mathbf{A}(\mathbf{x}^{(t-1)} + \tilde{\mathbf{d}}^{(t)}) = \mathbf{b}$. If $\mathbf{A}\mathbf{x}^{(t-1)} = \mathbf{b}$, this reduces to $\mathbf{A}\tilde{\mathbf{d}}^{(t)} = \mathbf{0}$, meaning $\tilde{\mathbf{d}}^{(t)}$ lies in the null space $\{\mathbf{v} \in \mathbb{Q}^n \mid \mathbf{A}\mathbf{v} = \mathbf{0}\}$. For full-rank $\mathbf{A} \in \mathbb{Q}^{m \times n}$, the null space has dimension $n - m$, represented by $\{\mathbf{v}_1, \dots, \mathbf{v}_{n-m}\}$. We project $\mathbf{d}^{(t)}$ onto this space as $\tilde{\mathbf{d}}^{(t)} = \sum_{i=1}^{n-m} a_i \mathbf{v}_i$ where $a_i := \frac{\mathbf{v}_i^\top \mathbf{d}^{(t)}}{\mathbf{v}_i^\top \mathbf{v}_i}$. Thus, $\tilde{\mathbf{d}}^{(t)} := \sum_{i=1}^{n-m} \frac{\mathbf{v}_i^\top \mathbf{d}^{(t)}}{\mathbf{v}_i^\top \mathbf{v}_i} \mathbf{v}_i$, ensuring $\mathbf{A}\tilde{\mathbf{d}}^{(t)} = \mathbf{0}$. Updating $\mathbf{x}^{(t)} = \mathbf{x}^{(t-1)} + \tilde{\mathbf{d}}^{(t)}$ preserves feasibility, assuming $\mathbf{x}^{(0)}$ is feasible. In practice, *singular value decomposition* (SVD) (Strang, 2000) provides the orthonormal null space of \mathbf{A} . The projection operator is expressed as $\Pi_{\mathbf{A}} = \sum_{i=1}^{n-m} \frac{\mathbf{v}_i \mathbf{v}_i^\top}{\mathbf{v}_i^\top \mathbf{v}_i}$, satisfying $\Pi_{\mathbf{A}}^2 = \Pi_{\mathbf{A}}$ and has no effect on vectors already in the null space.

If the prediction of the MPNN is exact, i.e., $\tilde{\mathbf{d}}^{(t)} = \mathbf{d}^{(t)}$, and we take a step along $\tilde{\mathbf{d}}^{(t)}$ with step length $\alpha^{(t)} = 1$ and we end up with the optimal solution. Therefore, by default, we set the step length $\alpha^{(t)} = 1$. However, if a full step using $\alpha^{(t)} = 1$ leads to the violation of the positivity constraint, we take a maximal possible $\alpha^{(t)} < 1$ so that all variables would still lie in the positive orthant, specifically

$$\alpha^{(t)} := \min \left\{ 1, \sup \left\{ \alpha \mid \mathbf{x}_i^{(t)} + \alpha \tilde{\mathbf{d}}_i^{(t)} \geq 0, i \in [n] \right\} \right\}. \quad (8)$$

Formally, the update step is

$$\mathbf{x}^{(t)} := \mathbf{x}^{(t-1)} + \alpha^{(t)} \Pi_{\mathbf{A}} \mathbf{d}^{(t)}. \quad (9)$$

The MPNN architecture is similar to the IPM-guided approach introduced above. We drop the global node to enhance computational efficiency and align with the theorem outlined below. At each iteration $t \in [T]$, the L -layer MPNN takes the graph together with the current solution $\mathbf{x}^{(t-1)}$ as input but, unlike above, predicts the displacement $\mathbf{d}^{(t)}$ instead of subsequent point. In each iteration, we initialize the node embeddings as

$$\begin{aligned} \mathbf{h}_c^{(0,t)} &:= \mathbf{C}_c \in \mathbb{Q}, \\ \mathbf{h}_v^{(0,t)} &:= \text{CONCAT}(\mathbf{V}_v, \mathbf{x}^{(t-1)}) \in \mathbb{Q}^2. \end{aligned} \quad (10)$$

The message passing on the heterogeneous graph is defined as

$$\begin{aligned} \mathbf{h}_c^{(l,t)} &:= \text{UPD}_c^{(l)} \left[\mathbf{h}_c^{(l-1,t)}, \right. \\ &\quad \left. \text{MSG}_{v \rightarrow c}^{(l)} \left(\left\{ \left(\mathbf{h}_v^{(l-1,t)}, \mathbf{e}_{cv} \mid v \in N(c) \cap V(I) \right\} \right) \right) \right], \\ \mathbf{h}_v^{(l,t)} &:= \text{UPD}_v^{(l)} \left[\mathbf{h}_v^{(l-1,t)}, \right. \\ &\quad \left. \text{MSG}_{v \rightarrow v}^{(l)} \left(\left\{ \left(\mathbf{h}_u^{(l-1,t)}, \mathbf{e}_{uv} \mid u \in N(v) \cap V(I) \right\} \right) \right), \right. \\ &\quad \left. \text{MSG}_{c \rightarrow v}^{(l)} \left(\left\{ \left(\mathbf{h}_c^{(l,t)}, \mathbf{e}_{cv} \mid u \in N(v) \cap C(I) \right\} \right) \right) \right], \end{aligned} \quad (11)$$

where we first update the constraint node embeddings and then the variable ones. In addition, we use a multi-layer

perceptron to predict the displacement from the current solution $\mathbf{x}^{(t-1)}$ to the optimal solution \mathbf{x}^* ,

$$\mathbf{d}_v^{(t)} := \text{MLP}\left(\mathbf{h}_v^{(L,t)}\right) \in \mathbb{Q}. \quad (12)$$

We denote the exact displacement pointing from the current solution at iteration t to the optimal solution as the oracle displacement, $\mathbf{d}^{*(t)} = \mathbf{x}^* - \mathbf{x}^{(t-1)}$, and define the supervised loss

$$\mathcal{L}^{(t)}\left(\mathbf{d}^{*(t)}, \mathbf{d}^{(t)}\right) := \|\mathbf{d}^{*(t)} - \mathbf{d}^{(t)}\|_2^2. \quad (13)$$

In practice, when the current solution $\mathbf{x}^{(t)}$ approaches the boundary of the positive orthant $\mathbb{Q}_{\geq 0}^n$ and the prediction $\mathbf{d}^{(t)}$ is inaccurate, the step length $\alpha^{(t)}$ can be too small to ensure the non-negativity constraints. Due to the continuous nature of neural networks, the prediction $\mathbf{d}^{(t+1)}$ will hardly change since $\mathbf{x}^{(t+1)} \approx \mathbf{x}^{(t)}$ and a small $\alpha^{(t+1)}$ will be picked. This makes the search process stagnant. To address this vanishing step length issue, we introduce a correction term $\frac{\tau}{\alpha^{(t)} + \epsilon}$, where the bias ϵ ensures numerical stability and τ adjusts the correction's magnitude, encouraging the solution $\mathbf{x}^{(t)}$ to move away from the orthant boundary. Details of this design are provided in Appendix A.5. Algorithms 3 and 4 show the training and inference using the MPNNs.

Now, the following result shows that our proposed MPNN architecture is expressive enough to predict the displacement arbitrarily close.

Theorem 2. *Given a LCQP instance I , assume I is feasible with solution \mathbf{x}^* , $\mathbf{x}^{(0)} \geq \mathbf{0}$ is an initial feasible point, for any $\epsilon, \delta > 0$, there exists an MPNN architecture $f_{\text{MPNN},2}$ such that*

$$P\left[\|f_{\text{MPNN},2}(I, \mathbf{x}^{(0)}) - (\mathbf{x}^* - \mathbf{x}^{(0)})\|_2 > \delta\right] < \epsilon.$$

2.1. Complexity analysis

It is straightforward to show that our IPM-guided approach lies within the framework of MPNN. Thus, the runtime is linear to the number of nodes and edges, i.e., $\mathcal{O}(n + m + |E(G)|)$, where m, n are the numbers of constraints and variables. In the worst case, where the \mathbf{A} and \mathbf{Q} matrices are dense, the complexity amounts to $\mathcal{O}(mn + n^2)$. However, we need further investigation for the feasibility approach. The two-phase method, for the feasible initial solution, requires solving an extra LP and finding the initial feasible point, which is in $\mathcal{O}(nm)$ (Bertsimas & Tsitsiklis, 1998). The null space calculation is based on SVD or QR decomposition and is of complexity $\mathcal{O}(nm^2)$ (Strang, 2000). Fortunately, finding a feasible solution and calculating the null space and corresponding projection matrix only need to be done once in the pre-processing phase. The projection of the predicted direction on the null space of \mathbf{A}

is $\mathcal{O}(n(n - m))$. The message passing scheme between the two node types has the same complexity $\mathcal{O}(|E(G)|)$, which depends on the number of edges, i.e., the nonzero entries of the \mathbf{A} and \mathbf{Q} matrices, also $\mathcal{O}(mn + n^2)$ in the worst case. The remaining part of the algorithm, such as the line search and variable update, is in $\mathcal{O}(n)$.

Algorithm 3 Training phase of our MPNN architecture ensuring feasibility.

Require: An LCQP instance $I = (\mathbf{Q}, \mathbf{A}, \mathbf{b}, \mathbf{c})$, a feasible initial solution $\mathbf{x}^{(0)}$, projection matrix of \mathbf{A} as $\mathbf{\Pi}_A$, an L -layer MPNN initialized as Equations (10) to (12), number of iterations T , scaling factor τ , small bias ϵ .

Ensure: Supervised loss \mathcal{L} .

- 1: **for** $t \in [T]$ **do**
 - 2: $\mathbf{d}^{(t)} \leftarrow \text{MPNN}(I, \mathbf{x}^{(t-1)}) + \frac{\tau}{\alpha^{(t-1)} + \epsilon}$
 - 3: $\tau \leftarrow \tau/2$
 - 4: Calculate loss $\mathcal{L}^{(t)}(\mathbf{d}^{*(t)}, \mathbf{d}^{(t)})$ given by Equation (13)
 - 5: $\tilde{\mathbf{d}}^{(t)} \leftarrow \mathbf{\Pi}_A \mathbf{d}^{(t)}$
 - 6: Get step length $\alpha^{(t)}$ as given by Equation (8)
 - 7: Update $\mathbf{x}^{(t)}$ with Equation (9)
 - 8: **end for**
 - 9: **return** The loss $\mathcal{L} \leftarrow \frac{1}{T} \sum_{t=1}^T \mathcal{L}^{(t)}(\mathbf{d}^{*(t)}, \mathbf{d}^{(t)})$.
-

Algorithm 4 Inference phase of our MPNN architecture ensuring feasibility.

Require: An LCQP instance $I = (\mathbf{A}, \mathbf{b}, \mathbf{c})$ or QP instance $I = (\mathbf{Q}, \mathbf{A}, \mathbf{b}, \mathbf{c})$, a feasible initial solution $\mathbf{x}^{(0)}$, projection matrix of \mathbf{A} as $\mathbf{\Pi}_A$, an L -layer MPNN initialized as Equations (10) to (12), number of iterations T , scaling factor τ , small bias ϵ .

Ensure: Best found solution \mathbf{x} .

- 1: $\mathbf{x} \leftarrow \mathbf{x}^{(0)}$
 - 2: Define $\text{obj}(\mathbf{x}) := \frac{1}{2} \mathbf{x}^\top \mathbf{Q} \mathbf{x} + \mathbf{c}^\top \mathbf{x}$
 - 3: **for** $t \in [T]$ **do**
 - 4: $\mathbf{d}^{(t)} \leftarrow \text{MPNN}(I, \mathbf{x}^{(t-1)}) + \frac{\tau}{\alpha^{(t-1)} + \epsilon}$
 - 5: $\tau \leftarrow \tau/2$
 - 6: $\tilde{\mathbf{d}}^{(t)} \leftarrow \mathbf{\Pi}_A \mathbf{d}^{(t)}$
 - 7: Compute step length $\alpha^{(t)}$ as given by Equation (8)
 - 8: Update $\mathbf{x}^{(t)}$ with Equation (9)
 - 9: **if** $\text{obj}(\mathbf{x}^{(t)}) < \text{obj}(\mathbf{x})$ **then**
 - 10: $\mathbf{x} \leftarrow \mathbf{x}^{(t)}$
 - 11: **end if**
 - 12: **end for**
 - 13: **return** Best found solution \mathbf{x} .
-

3. Experimental study

In the following, we investigate to what extent our theoretical results translate into practice. The implementation is open source at <https://github.com/chendiqian/FeasMPNN>.

- Q1** How good is the solution quality of our MPNN architectures regarding objective value and constraint violation?
- Q2** How well can our (pre-)trained MPNN architectures generalize to larger unseen instances?
- Q3** How fast are our MPNN architectures compared with baselines and traditional solvers?

We evaluate three types of synthetic LCQP problems: generic, soft-margin support vector machine (SVM), and Markowitz portfolio optimization problems, following Jung et al. (2022). Details of dataset generation are provided in Appendix A.4. For each problem type, we generate 1000 instances, split into training, validation, and test sets with an 8:1:1 ratio. Hyperparameters for all neural networks are tuned on our feasibility variant and shared across baselines. Specifically, we train an MPNN of 8 layers with hidden dimension 128 using the Adam optimizer (Kingma & Ba, 2015) for up to 1000 epochs with early stopping after 300 epochs. During training, our IPM- and feasibility-based architectures use 8 iterations, which are increased to 32 during inference. For our feasibility approach, the instances are preprocessed using SciPy (Virtanen et al., 2020) for null space computation and an IPM solver (Frenk et al., 2013) to obtain feasible initial solutions from the linear constraints. Training is conducted on four Nvidia L40s GPUs. Timing evaluations for neural network methods in Table 17 are performed on a single Nvidia L40s. In contrast, solver and preprocessing evaluations are carried out on a MacBook Air with an Apple M2 chip.²

Solution quality (Q1) We benchmark all approaches regarding the relative objective gap and constraint violation metrics. Given the ground truth optimal solution \mathbf{x}^* , MPNN-predicted solution \mathbf{x} of an LCQP instance, and the objective function $\text{obj}(\mathbf{x}) := \frac{1}{2}\mathbf{x}^\top \mathbf{Q}\mathbf{x} + \mathbf{c}^\top \mathbf{x}$ the relative objective gap is calculated as

$$\left| \frac{\text{obj}(\mathbf{x}) - \text{obj}(\mathbf{x}^*)}{\text{obj}(\mathbf{x}^*)} \right| \times 100\%,$$

and the constraint violation metric is computed as

$$\frac{1}{m} \sum_{i=1}^m \frac{|\mathbf{A}_i \mathbf{x} - \mathbf{b}_i|}{\max\{|\mathbf{b}_i|, \max_j |\mathbf{A}_{ij}|\}},$$

²We found that conducting the CPU-based experiments on the M2 chip was faster than executing them on our compute server.

Table 1. Comparisons of our IPM- and feasibility-oriented approaches with the MPNN-based prediction from Chen et al. (2024) and Qian et al. (2024), all **with the global node**. The table reports the relative objective gap (in percentage) and constraint violation (in normalized absolute value). Training was repeated three times with different random seeds, and we report the mean and standard deviation across runs. For our feasibility method, the standard deviation of constraint violation is omitted as it is not meaningful.

	Method	MPNN	Generic	SVM	Portfolio	
Obj. gap [%]	Naive 2024	GCN	2.281±0.150	0.352±0.032	2.446±0.756	
		GIN	2.782±0.056	0.148±0.086	0.295±0.024	
	IPM 2024	GCN	1.829±0.079	0.162±0.009	0.717±0.353	
		GIN	1.581±0.044	0.141±0.034	0.416±0.052	
	IPM(ours)	GCN	1.661±0.199	0.485±0.176	1.838±0.720	
		GIN	2.746±0.152	0.109±0.017	0.486±0.041	
	Feas.(ours)	GCN	0.070±0.004	0.190±0.008	1.005±0.159	
		GIN	0.084±0.005	0.192±0.017	1.078±0.121	
	Cons. vio.	Naive 2024	GCN	0.018±0.001	0.007±0.001	0.017±0.006
			GIN	0.019±0.001	0.002±0.001	0.002±0.001
		IPM 2024	GCN	0.016±0.0003	0.003±0.0001	0.006±0.003
			GIN	0.011±0.001	0.002±0.001	0.003±0.001
IPM(ours)		GCN	0.029±0.009	0.012±0.005	0.015±0.005	
		GIN	0.029±0.003	0.003±0.001	0.004±0.001	
Feas.(ours)		GCN	1.142 × 10 ⁻⁷	3.489 × 10 ⁻⁷	3.427 × 10 ⁻⁷	
		GIN	1.167 × 10 ⁻⁷	3.418 × 10 ⁻⁷	3.427 × 10 ⁻⁷	

i.e., for each constraint i , we calculate the absolute violation number $|\mathbf{A}_i \mathbf{x} - \mathbf{b}_i|$, normalized by the scale of \mathbf{A}_i , \mathbf{b}_i , and we calculate the mean value across all the constraints. To show the model-agnostic property of our approaches, we use the GIN (Xu et al., 2019) and GCN (Kipf & Welling, 2017) as our MPNN layers. The selected baselines are: (1) a naive MPNN approach that directly predicts the LCQP solution, following Chen et al. (2024), and (2) a variant of IPM-MPNN for LCQPs (Qian et al., 2024), where the output of each layer represents an intermediate step of the search process.

Our IPM-guided search theoretically requires a global node in the graph, but our feasibility method does not. To ensure fairness, we conduct experiments with and without the global node; see Table 1 and Table 2. Our feasibility method generally achieves lower relative objective gaps, indicating better approximations of optimal solutions, particularly for generic LCQP and portfolio problems. However, the advantage is less pronounced on SVM tasks, where the quadratic matrix has a diagonal structure. While both IPM approaches exhibit constraint violations, similar to naive MPNN predictions, our feasibility method ensures strict feasibility up to numerical precision (10⁻⁷). Differences between global-node and non-global-node settings are typically minor, except for the Chen et al. (2024) approach on portfolio optimization, where problem-specific factors may account for an order-of-magnitude difference.

Furthermore, to compare against feasibility-related work, we generate another synthetic dataset of 1000 LCQP instances with 200 variables, 50 equality constraints, and 200

Table 2. Comparisons of our IPM- and feasibility-oriented approaches with the MPNN-based prediction from Chen et al. (2024) and Qian et al. (2024), all **without the global node**. The table reports the relative objective gap (in percentage) and constraint violation (in normalized absolute value). Training was repeated three times with different random seeds, and we report the mean and standard deviation across runs. For our feasibility method, the standard deviation of constraint violation is omitted as it is not meaningful.

	Method	MPNN	Generic	SVM	Portfolio	
Obj. gap [%]	Naive 2024	GCN	2.547±0.126	0.446±0.102	11.075±0.363	
		GIN	2.330±0.151	0.191±0.094	10.801±0.184	
	IPM 2024	GCN	1.894±0.166	0.175±0.022	1.497±0.686	
		GIN	1.298±0.148	0.098±0.006	0.438±0.080	
	IPM(ours)	GCN	2.236±0.249	0.696±0.236	1.168±0.048	
		GIN	2.746±0.152	0.478±0.244	0.657±0.121	
	Feas.(ours)	GCN	0.049±0.015	0.126±0.034	0.935±0.062	
		GIN	0.142±0.034	0.091±0.016	1.105±0.094	
	Cons. vio.	Naive 2024	GCN	0.012±0.004	0.013±0.009	0.083±0.001
			GIN	0.010±0.001	0.004±0.001	0.146±0.018
		IPM 2024	GCN	0.013±0.001	0.004±0.001	0.011±0.005
			GIN	0.009±0.002	0.002±0.001	0.003±0.001
IPM(ours)		GCN	0.031±0.008	0.020±0.010	0.008±0.001	
		GIN	0.029±0.003	0.011±0.003	0.005±0.001	
Feas.(ours)		GCN	1.216 × 10 ⁻⁷	3.433 × 10 ⁻⁷	2.179 × 10 ⁻⁷	
		GIN	1.221 × 10 ⁻⁷	3.470 × 10 ⁻⁷	2.135 × 10 ⁻⁷	

trivial inequality constraints ($x_i \geq 0$). The dataset is split into training, validation, and test sets with the ratio 8:1:1. The constraint matrix A , quadratic matrix Q , and objective vector c are shared across all instances. In contrast, only the right-hand side (RHS) b is randomized, following the setup described in DC3 (Donti et al., 2021) and IPM-LSTM (Gao et al., 2024). Using their default hyperparameters, we evaluate DC3, IPM-LSTM, and our GCN-based feasibility method (without a global node, 32 inference steps). As shown in Table 3, our method achieves the lowest objective gap and ensures strong feasibility. DC3 suffers from worse objective gaps due to post-processing and significant inequality violations, while IPM-LSTM exhibits higher equality constraint violations. DC3 is the fastest due to its simple architecture, followed by our method, with IPM-LSTM being the slowest owing to the computational expense of its LSTM-based architecture. For inference time, we benchmark these methods alongside three traditional solvers: OSQP (Stellato et al., 2020), CVXOPT (Andersen et al., 2013), and Gurobi (Gurobi Optimization, LLC, 2024). While DC3 achieves solver-comparable performance, our method shows no advantage on these small, dense problems. These baselines have inflexible architectures, therefore restricted to fixed problem sizes, and cannot handle sparsity in large problems. In contrast, our MPNN-based approach is trainable on varying-sized datasets, captures problem sparsity, and performs efficiently on larger problem instances.

Size generalization (Q2) In response to Q2, we pre-train GCN-based architecture and evaluate them on larger prob-

Table 3. Experiments on fixed-size instances. We compare our feasibility approach with DC3 (Donti et al., 2021) and IPM-LSTM (Gao et al., 2024). We train each neural network once and report the mean and deviation on the test set. The table shows the relative objective gap, the equality and inequality constraint violations, and the inference time. The inference time of our approach includes the preprocessing time.

Method	Rel. obj. (%)	Eq. cons. vio.	Ineq. cons. vio.	Time (sec)
CVXOPT	–	–	–	0.009±0.003
OSQP	–	–	–	0.003±0.0003
Gurobi	–	–	–	0.006±0.0003
DC3	63.714±34.837	7.534 × 10 ⁻¹⁴	0.372±0.069	0.005±0.002
IPM-LSTM	0.762±0.028	2.272 × 10 ⁻⁴	4.721 × 10 ⁻⁶	1.435±0.232
Feas. (ours)	0.578±0.032	5.377 × 10 ⁻⁷	0	0.281±0.031

lem instances, exploring two scaling approaches: (1) increasing size parameters while keeping the density constant and (2) increasing size parameters while maintaining a constant average node degree. We test with 16 and 32 iterations for both approaches to assess the impact of iteration count. As shown in Table 16, objective gaps increase for all methods on larger instances, but our approach consistently outperforms the baselines. Violation values also rise for methods lacking feasibility guarantees. Maintaining a constant node degree yields better generalization than fixing density across all candidates. For additional results on SVM and portfolio problems, see Appendix A.3.

We evaluate on real-world QPLIB instances (Furini et al., 2019), where conventional train-validation splits are impractical due to limited, diverse-sized data. To address this, we pre-train a GCN model on 1000 large, sparse generic LCQP problems and test it on selected QPLIB instances with linear constraints, positive definite objectives, and memory manageable sizes (integer variables relaxed to continuous). As shown in Table 4, our feasibility approach generalizes well to real-world problems, e.g., it obtains a relative objective error of 0.597% on QPLIB_3547. While errors are larger for some instances, e.g., QPLIB_3547, absolute solution values remain satisfactory as the optimal value is near zero. Our method also generalizes to out-of-distribution unconstrained QPs (e.g., QPLIB_8790 to QPLIB_8991) with a relative error around 25%.

Efficiency (Q3) To investigate computational efficiency, we evaluate the runtime performance on three QP problems in Table 17 and visualize the results on generic QPs in Figure 2. We use the original test set for this evaluation and generate larger instances than those used in training. We compare our methods with the neural network baselines Chen et al. (2024); Qian et al. (2024) and solvers OSQP, CVXOPT, and Gurobi. We evaluate the neural network-based approaches with pre-trained GCN-based architecture. Both our approaches are evaluated with 16 and 32 iterations, and the impact of the global node on runtime is assessed. We

Table 4. The generalization performance on selected QPLIB instances. We show the details of problem size and density, the optimal objective value, and absolute value and relative error of our prediction.

QP ID	A dens.	Q dens.	#cons.	#vars.	Sol.	Pred.	Rel. error (%)
3547	0.001	0.167	3137	1998	2.125×10^4	2.138×10^4	0.597
3694	0.001	0.0003	3280	3240	0.794	1.359	71.255
3698	0.001	0.0003	3100	3030	1.116	1.688	51.318
3792	0.001	0.0003	3150	3020	1.903	2.571	35.069
3861	0.0008	0.0002	4650	4530	1.329	1.939	45.972
3871	0.004	0.001	1040	1025	0.735	1.276	73.493
4270	0.002	0.251	1603	1600	0.183	0.593	224.023
8790	–	0.0001	0	39204	-3.920×10^4	-2.940×10^4	25.000
8792	–	0.0003	0	15129	-1.513×10^4	-1.134×10^4	25.000
8991	–	0.0003	0	14400	-1.430×10^4	-1.077×10^4	24.690

also report data preparation time, including the null space calculation and finding the feasible solution. As shown in Table 17, Chen et al. (2024) and Qian et al. (2024) achieve the fastest runtime due to their simple MPNN architectures and their iteration-free behavior. Despite the same architecture, the runtime of our methods is higher, as it depends on the number of iterations. Notably, runtime differences between our two approaches are minimal, as line search and null-space projection are computationally inexpensive compared to message passing. On generic problems, all the neural network approaches are significantly faster than the traditional QP solvers, even accounting for data preparation time. This gap widens with increasing problem size, showcasing the scalability of neural solvers. Traditional solvers like OSQP and Gurobi excel on SVM problems as they are specifically tailored for sparse problems. As expected, runtime increases slightly when using a global node due to additional convolutions.

4. Conclusion

We demonstrated that MPNNs can effectively solve convex LCQPs, significantly extending their known capabilities. Thereto, first, we established that MPNNs can theoretically simulate standard interior-point methods for solving LCQPs. Next, we proposed an enhanced MPNN architecture that ensures the feasibility of the predicted solutions through a novel projection approach. Empirically, our architecture outperformed existing neural approaches regarding solution quality and feasibility in an extensive empirical evaluation. Furthermore, our approaches generalized well to larger problem instances beyond the training set and, in some cases, achieved faster solution times than state-of-the-art solvers such as Gurobi.

Acknowledgements

Christopher Morris and Chendi Qian are partially funded by a DFG Emmy Noether grant (468502433) and RWTH Junior Principal Investigator Fellowship under Germany’s Excellence Strategy. We thank Erik Müller for crafting the

figures.

Impact statement

This paper presents work that aims to advance the field of machine learning. Our work has many potential societal consequences, none of which must be specifically highlighted here.

References

- Achterberg, T., Koch, T., and Martin, A. Branching rules revisited. *Operations Research Letters*, 33(1):42–54, 2005. 1
- Alvarez, A. M., Louveaux, Q., and Wehenkel, L. A machine learning-based approximation of strong branching. *INFORMS Journal on Computing*, 29(1):185–195, 2017. 14
- Andersen, E. D. and Andersen, K. D. Presolving in linear programming. *Mathematical Programming*, 71:221–245, 1995. 3
- Andersen, E. D. and Andersen, K. D. *The Mosek Interior Point Optimizer for Linear Programming: An Implementation of the Homogeneous Algorithm*, pp. 197–232. Springer, 2000. 5
- Andersen, M. S., Dahl, J., Vandenberghe, L., et al. CVX-OPT: A python package for convex optimization. *Available at cvxopt.org*, 54, 2013. 8
- Applegate, D., Díaz, M., Hinder, O., Lu, H., Lubin, M., O’Donoghue, B., and Schudy, W. Practical large-scale linear programming using primal-dual hybrid gradient. *Advances in Neural Information Processing Systems*, 2021. 2
- Ausiello, G., Marchetti-Spaccamela, A., Crescenzi, P., Gambosi, G., Protasi, M., and Kann, V. *Complexity and Approximation: combinatorial optimization problems and their approximability properties*. Springer, 1999. 1
- Bengio, Y., Lodi, A., and Prouvost, A. Machine learning for combinatorial optimization: a methodological tour d’horizon. *European Journal of Operational Research*, 290(2):405–421, 2021. 1, 2, 14
- Bertsimas, D. and Tsitsiklis, J. *Introduction to Linear Optimization*. Athena Scientific, 1998. 5, 6
- Bishop, C. M. and Nasrabadi, N. M. *Pattern recognition and machine learning*, volume 4. Springer, 2006. 17
- Bonami, P., Lodi, A., and Zarpellon, G. Learning a classification of mixed-integer quadratic programming problems. In *International Conference on the Integration*

- of *Constraint Programming, Artificial Intelligence, and Operations Research*, 2018. 2
- Boyd, S. and Vandenberghe, L. *Convex optimization*. Cambridge University Press, 2004. 3
- Bresson, X. and Laurent, T. Residual gated graph convnets. *ArXiv preprint*, 2017. 2
- Bruna, J., Zaremba, W., Szlam, A., and LeCun, Y. Spectral networks and deep locally connected networks on graphs. In *International Conference on Learning Representation*, 2014. 2
- Cappart, Q., Chételat, D., Khalil, E. B., Lodi, A., Morris, C., and Veličković, P. Combinatorial optimization and reasoning with graph neural networks. *Journal of Machine Learning Research*, 24(130):1–61, 2023. 1, 2, 14
- Chatzos, M., Fioretto, F., Mak, T. W., and Van Hentenryck, P. High-fidelity machine learning approximations of large-scale optimal power flow. *ArXiv preprint*, 2020. 14
- Chen, W., Tanneau, M., and Van Hentenryck, P. End-to-end feasible optimization proxies for large-scale economic dispatch. *IEEE Transactions on Power Systems*, 2023. 14
- Chen, Z., Liu, J., Wang, X., Lu, J., and Yin, W. On representing linear programs by graph neural networks. *ArXiv preprint*, 2022. 2, 16, 18
- Chen, Z., Chen, X., Liu, J., Wang, X., and Yin, W. Expressive power of graph neural networks for (mixed-integer) quadratic programs. *ArXiv preprint*, 2024. 2, 3, 7, 8, 9, 15, 16, 17, 22, 23, 39, 40
- Chételat, D. and Lodi, A. Continuous cutting plane algorithms in integer programming. *Operations Research Letters*, 51(4):439–445, 2023. 14
- Defferrard, M., Bresson, X., and Vandergheynst, P. Convolutional neural networks on graphs with fast localized spectral filtering. *Advances in Neural Information Processing Systems*, 29, 2016. 2
- Ding, J.-Y., Zhang, C., Shen, L., Li, S., Wang, B., Xu, Y., and Song, L. Accelerating primal solution findings for mixed integer programs based on solution prediction. In *AAAI Conference on Artificial Intelligence*, 2020. 14, 16
- Donti, P. L., Rolnick, D., and Kolter, J. Z. DC3: A learning method for optimization with hard constraints. *ArXiv preprint*, 2021. 8, 14
- Duvenaud, D., Maclaurin, D., Aguilera-Iparraguirre, J., Gómez-Bombarelli, R., Hirzel, T., Aspuru-Guzik, A., and Adams, R. P. Convolutional networks on graphs for learning molecular fingerprints. In *Advances in Neural Information Processing Systems*, 2015. 2
- Fan, Z., Wang, X., Yakovenko, O., Sivas, A. A., Ren, O., Zhang, Y., and Zhou, Z. Smart initial basis selection for linear programs. In *International Conference on Machine Learning*, 2023. 1, 2
- Fey, M., Lenssen, J. E., Morris, C., Masci, J., and Kriege, N. M. Deep graph matching consensus. In *International Conference on Learning Representations*, 2020. 14
- Fioretto, F., Mak, T. W., and Van Hentenryck, P. Predicting ac optimal power flows: Combining deep learning and lagrangian dual methods. In *AAAI Conference on Artificial Intelligence*, 2020. 1, 14
- Fioretto, F., Van Hentenryck, P., Mak, T. W., Tran, C., Baldo, F., and Lombardi, M. Lagrangian duality for constrained deep learning. In *European Conference on Machine Learning and Knowledge Discovery in Databases*, 2021. 2, 14
- Frenk, H., Roos, K., Terlaky, T., and Zhang, S. *High performance optimization*, volume 33. Springer Science & Business Media, 2013. 7
- Frerix, T., Nießner, M., and Cremers, D. Homogeneous linear inequality constraints for neural network activations. In *IEEE/CVF Conference on Computer Vision and Pattern Recognition Workshops*, 2020. 14
- Furini, F., Traversi, E., Belotti, P., Frangioni, A., Gleixner, A., Gould, N., Liberti, L., Lodi, A., Misener, R., Mittelmann, H., et al. Qplib: a library of quadratic programming instances. *Mathematical Programming Computation*, 11:237–265, 2019. 8
- Gallier, J. et al. The Schur complement and symmetric positive semidefinite (and definite) matrices. *Penn Engineering*, pp. 1–12, 2010. 21
- Gao, X., Xiong, J., Wang, A., Duan, Q., Xue, J., and Shi, Q. IPM-LSTM: A learning-based interior point method for solving nonlinear programs. *ArXiv preprint*, 2024. 1, 2, 4, 8
- Gasse, M., Chételat, D., Ferroni, N., Charlin, L., and Lodi, A. Exact combinatorial optimization with graph convolutional neural networks. In *Advances in Neural Information Processing Systems*, 2019. 1, 3, 14
- Geisler, S., Kosmala, A., Herbst, D., and Günnemann, S. Spatio-spectral graph neural networks. *ArXiv preprint*, 2024. 2
- Getzelman, G. and Balaprakash, P. Learning to switch optimizers for quadratic programming. In *Asian Conference on Machine Learning*, 2021. 2

- Gilmer, J., Schoenholz, S. S., Riley, P. F., Vinyals, O., and Dahl, G. E. Neural message passing for quantum chemistry. In *International Conference on Machine Learning*, 2017. 2, 3
- Gros, S., Zanon, M., and Bemporad, A. Safe reinforcement learning via projection on a safe set: How to achieve optimality? *IFAC-PapersOnLine*, 53(2):8076–8081, 2020. 14
- Gurobi Optimization, LLC. Gurobi Optimizer Reference Manual, 2024. URL <https://www.gurobi.com>. 2, 8
- Hamilton, W. L., Ying, Z., and Leskovec, J. Inductive representation learning on large graphs. In *Advances in Neural Information Processing Systems*, 2017. 2
- Han, Q., Yang, L., Chen, Q., Zhou, X., Zhang, D., Wang, A., Sun, R., and Luo, X. A GNN-guided predict-and-search framework for mixed-integer linear programming. *ArXiv preprint*, 2023. 14
- He, H., Daumé, H., and Eisner, J. Learning to search in branch and bound algorithms. In *Neural Information Processing Systems*, 2014. 14
- Ichnowski, J., Jain, P., Stellato, B., Banjac, G., Luo, M., Borrelli, F., Gonzalez, J. E., Stoica, I., and Goldberg, K. Accelerating quadratic optimization with reinforcement learning. *Advances in Neural Information Processing Systems*, 2021. 2
- Jin, Y., Yan, X., Liu, S., and Wang, X. A unified framework for combinatorial optimization based on graph neural networks. *ArXiv preprint*, 2024. 14
- Joshi, C. K., Laurent, T., and Bresson, X. An efficient graph convolutional network technique for the travelling salesman problem. *ArXiv preprint*, 2019. 14
- Jung, H., Park, J., and Park, J. Learning context-aware adaptive solvers to accelerate quadratic programming. *ArXiv preprint*, 2022. 1, 2, 7
- Khalil, E., Le Bodic, P., Song, L., Nemhauser, G., and Dilkina, B. Learning to branch in mixed integer programming. In *AAAI Conference on Artificial Intelligence*, 2016. 14
- Khalil, E. B., Morris, C., and Lodi, A. MIP-GNN: A data-driven framework for guiding combinatorial solvers. In *AAAI Conference on Artificial Intelligence*, 2022. 3, 14
- Kingma, D. P. and Ba, J. Adam: A method for stochastic optimization. In *International Conference on Learning Representations*, 2015. 7
- Kipf, T. N. and Welling, M. Semi-supervised classification with graph convolutional networks. In *International Conference on Learning Representations*, 2017. 2, 7
- Klamkin, M., Tanneau, M., and Van Hentenryck, P. Dual interior-point optimization learning. *ArXiv preprint*, 2024. 2, 14
- Kotary, J. and Fioretto, F. Learning constrained optimization with deep augmented lagrangian methods. *ArXiv preprint*, 2024. 14
- Labassi, A. G., Chételat, D., and Lodi, A. Learning to compare nodes in branch and bound with graph neural networks. *Advances in Neural Information Processing Systems*, 2022. 14
- Lemos, H., Prates, M., Avelar, P., and Lamb, L. Graph colouring meets deep learning: Effective graph neural network models for combinatorial problems. In *IEEE International Conference on Tools with Artificial Intelligence*, 2019. 14
- Levie, R., Monti, F., Bresson, X., and Bronstein, M. M. Cayleynets: Graph convolutional neural networks with complex rational spectral filters. *IEEE Transactions on Signal Processing*, 67(1):97–109, 2019. 2
- Li, B., Yang, L., Chen, Y., Wang, S., Chen, Q., Mao, H., Ma, Y., Wang, A., Ding, T., Tang, J., et al. PDHG-unrolled learning-to-optimize method for large-scale linear programming. *ArXiv preprint*, 2024a. 1, 2
- Li, M., Kolouri, S., and Mohammadi, J. Learning to solve optimization problems with hard linear constraints. *IEEE Access*, 11:59995–60004, 2023. 14
- Li, Q., Ding, T., Yang, L., Ouyang, M., Shi, Q., and Sun, R. On the power of small-size graph neural networks for linear programming. In *Advances in Neural Information Processing Systems*, 2024b. 2, 14
- Li, W., Li, R., Ma, Y., Chan, S. O., Pan, D., and Yu, B. Rethinking graph neural networks for the graph coloring problem. *ArXiv preprint*, 2022a. 14
- Li, X., Qu, Q., Zhu, F., Zeng, J., Yuan, M., Mao, K., and Wang, J. Learning to reformulate for linear programming. *ArXiv preprint*, 2022b. 1, 2
- Liu, T., Pu, S., Ge, D., and Ye, Y. Learning to pivot as a smart expert. In *AAAI Conference on Artificial Intelligence*, 2024. 1, 2
- Lu, H. First-order methods for linear programming. *ArXiv preprint*, 2024. 2

- Min, Y., Bai, Y., and Gomes, C. P. Unsupervised learning for solving the travelling salesman problem. *Advances in Neural Information Processing Systems*, 2024. 14
- Monti, F., Otness, K., and Bronstein, M. M. Motifnet: a motif-based graph convolutional network for directed graphs. In *IEEE Data Science Workshop*, 2018. 2
- Nair, V., Bartunov, S., Gimeno, F., Von Glehn, I., Lichocki, P., Lobov, I., O’Donoghue, B., Sonnerat, N., Tjandraatmadja, C., Wang, P., et al. Solving mixed integer programs using neural networks. *ArXiv preprint*, 2020. 14
- Nelikkath, R. and Chatzivasileiadis, S. Physics-informed neural networks for ac optimal power flow. *Electric Power Systems Research*, 212:108412, 2022. 14
- Nocedal, J. and Wright, S. J. *Numerical optimization*. Springer, 2 edition, 2006. 2, 5, 19, 20, 21
- Pan, X., Zhao, T., Chen, M., and Zhang, S. Deepopf: A deep neural network approach for security-constrained dc optimal power flow. *IEEE Transactions on Power Systems*, 36(3):1725–1735, 2020. 14
- Park, S. and Van Hentenryck, P. Self-supervised primal-dual learning for constrained optimization. In *AAAI Conference on Artificial Intelligence*, 2023. 2, 14
- Paulus, M. B., Zarpellon, G., Krause, A., Charlin, L., and Maddison, C. Learning to cut by looking ahead: Cutting plane selection via imitation learning. In *International Conference on Machine Learning*, 2022. 14
- Peng, Y., Choi, B., and Xu, J. Graph learning for combinatorial optimization: a survey of state-of-the-art. *Data Science and Engineering*, 6(2):119–141, 2021. 2, 14
- Qian, C., Chételat, D., and Morris, C. Exploring the power of graph neural networks in solving linear optimization problems. In *International Conference on Artificial Intelligence and Statistics*, 2024. 1, 2, 3, 4, 7, 8, 9, 14, 15, 16, 17, 22, 23
- Sambharya, R., Hall, G., Amos, B., and Stellato, B. End-to-end learning to warm-start for real-time quadratic optimization. In *Learning for Dynamics and Control Conference*, 2023. 2
- Scarselli, F., Gori, M., Tsoi, A. C., Hagenbuchner, M., and Monfardini, G. The graph neural network model. *IEEE Transactions on Neural Networks*, 20(1):61–80, 2008. 2, 3
- Scavuzzo, L., Chen, F., Chételat, D., Gasse, M., Lodi, A., Yorke-Smith, N., and Aardal, K. Learning to branch with tree mdps. *Advances in Neural Information Processing Systems*, 2022. 14
- Scavuzzo, L., Aardal, K., Lodi, A., and Yorke-Smith, N. Machine learning augmented branch and bound for mixed integer linear programming. *ArXiv preprint*, 2024. 1, 14
- Schrijver, A. *Theory of Linear and Integer programming*. Wiley, 1986. 1
- Selsam, D. and Bjørner, N. Guiding high-performance SAT solvers with unsat-core predictions. In *Theory and Applications of Satisfiability Testing*, 2019. 14
- Selsam, D., Lamm, M., Bünz, B., Liang, P., de Moura, L., and Dill, D. L. Learning a SAT solver from single-bit supervision. *ArXiv preprint*, 2018. 1, 14
- Shi, Z., Li, M., Khan, S., Zhen, H.-L., Yuan, M., and Xu, Q. Satformer: Transformers for SAT solving. *ArXiv preprint*, 2022. 14
- Stellato, B., Banjac, G., Goulart, P., Bemporad, A., and Boyd, S. Osqp: An operator splitting solver for quadratic programs. *Mathematical Programming Computation*, 12(4):637–672, 2020. 8
- Strang, G. *Linear algebra and its applications*, 2000. 5, 6
- Tang, Y., Agrawal, S., and Faenza, Y. Reinforcement learning for integer programming: Learning to cut. In *International Conference on Machine Learning*, 2020. 14
- Toenshoff, J., Ritzert, M., Wolf, H., and Grohe, M. Graph neural networks for maximum constraint satisfaction. *Frontiers in Artificial Intelligence*, 3:580607, 2021. 14
- Turner, M., Koch, T., Serrano, F., and Winkler, M. Adaptive cut selection in mixed-integer linear programming. *ArXiv preprint*, 2022. 14
- Veličković, P., Cucurull, G., Casanova, A., Romero, A., Liò, P., and Bengio, Y. Graph attention networks. In *International Conference on Learning Representations*, 2018. 2
- Vinyals, O., Fortunato, M., and Jaitly, N. Pointer networks. *Advances in Neural Information Processing Systems*, 28, 2015. 14
- Virtanen, P., Gommers, R., Oliphant, T. E., Haberland, M., Reddy, T., Cournapeau, D., Burovski, E., Peterson, P., Weckesser, W., Bright, J., van der Walt, S. J., Brett, M., Wilson, J., Millman, K. J., Mayorov, N., Nelson, A. R. J., Jones, E., Kern, R., Larson, E., Carey, C. J., Polat, İ., Feng, Y., Moore, E. W., VanderPlas, J., Laxalde, D., Perktold, J., Cimrman, R., Henriksen, I., Quintero, E. A., Harris, C. R., Archibald, A. M., Ribeiro, A. H., Pedregosa, F., van Mulbregt, P., and SciPy 1.0 Contributors. SciPy 1.0: Fundamental Algorithms for Scientific Computing in Python. *Nature Methods*, 17:261–272, 2020. 7

- Wang, R., Yan, J., and Yang, X. Learning combinatorial embedding networks for deep graph matching. In *IEEE/CVF International Conference on Computer Vision*, 2019. 14
- Wang, R., Yan, J., and Yang, X. Combinatorial learning of robust deep graph matching: an embedding based approach. *IEEE Transactions on Pattern Analysis and Machine Intelligence*, 45(6):6984–7000, 2020. 14
- Wu, C., Chen, Q., Wang, A., Ding, T., Sun, R., Yang, W., and Shi, Q. On representing convex quadratically constrained quadratic programs via graph neural networks. *ArXiv preprint*, 2024. 2
- Xiong, Z., Zong, F., Ye, H., and Xu, H. Neuralqp: A general hypergraph-based optimization framework for large-scale qcqps. *ArXiv preprint*, 2024. 1, 2
- Xu, K., Hu, W., Leskovec, J., and Jegelka, S. How powerful are graph neural networks? In *International Conference on Learning Representations*, 2019. 2, 7
- Zarpellon, G., Jo, J., Lodi, A., and Bengio, Y. Parameterizing branch-and-bound search trees to learn branching policies. In *AAAI Conference on Artificial Intelligence*, 2021. 14

A. Appendix

A.1. Extended notation

A graph G is a pair $(V(G), E(G))$ with finite sets of vertices or nodes $V(G)$ and edges $E(G) \subseteq \{\{u, v\} \subseteq V(G) \mid u \neq v\}$. An attributed graph G is a triple $(V(G), E(G), a)$ with a graph $(V(G), E(G))$ and (vertex-)attribute function $a: V(G) \rightarrow \mathbb{R}^{1 \times d}$, for some $d > 0$. Then $a(v)$ are an (node) attributes or features of v , for v in $V(G)$. Equivalently, we define an n -vertex attributed graph $G := (V(G), E(G), a)$ as a pair $\mathbf{G} = (G, \mathbf{L})$, where $G = (V(G), E(G))$ and \mathbf{L} in $\mathbb{R}^{n \times d}$ is a node attribute matrix. Here, we identify $V(G)$ with $[n]$. For a matrix \mathbf{L} in $\mathbb{R}^{n \times d}$ and v in $[n]$, we denote by \mathbf{L}_v in $\mathbb{R}^{1 \times d}$ the v th row of \mathbf{L} such that $\mathbf{L}_v := a(v)$. The neighborhood of v in $V(G)$ is denoted by $N(v) := \{u \in V(G) \mid (v, u) \in E(G)\}$.

A.2. Additional related work

Here, we discuss additional related work.

Machine learning for constrained optimization Training a neural network as a computationally efficient proxy but with constraints is also a widely studied topic, especially in real-world problems such as optimal power flow (Chatzos et al., 2020; Fioretto et al., 2020; Nellikkath & Chatzivasileiadis, 2022). A naive approach would be adding a penalty of constraint violation term to the loss function (Chatzos et al., 2020; Fioretto et al., 2020; Nellikkath & Chatzivasileiadis, 2022; Qian et al., 2024). Recent methods fall into three categories: leveraging Lagrangian duality, designing specialized neural architectures, and post-processing outputs to enforce feasibility. The first category applies Lagrangian duality to reformulate problems and solve primal-dual objectives (Fioretto et al., 2021; Park & Van Hentenryck, 2023; Kotary & Fioretto, 2024; Klamkin et al., 2024). While these approaches guarantee feasibility under ideal conditions, minor constraint violations can persist. The second category focuses on architectural innovations. Frerix et al. (2020) embed homogeneous inequality constraints into activation functions. DC3 (Donti et al., 2021) partially satisfies constraints using gradient descent but struggles to generalize to unseen data. LOOP-LC (Li et al., 2023) projects problems into L_∞ spaces, which can be challenging to apply. The final category adjusts neural outputs to satisfy constraints. Chen et al. (2023) develop problem-specific algorithms, while others (Pan et al., 2020; Gros et al., 2020) use optimization to project results onto feasible regions. However, these methods are often computationally intensive, problem-specific, or limited in scope (Li et al., 2024b).

Machine learning for combinatorial optimization Machine learning has been applied widely to combinatorial problems (Bengio et al., 2021; Cappart et al., 2023; Peng et al., 2021). For example, in the field of mixed integer linear programming (MILP), machine learning methods are explored to predict an initial solution and guide the search (Ding et al., 2020; Khalil et al., 2022; Han et al., 2023; Nair et al., 2020). There are also extensive works for variable selection in branch and bound (Alvarez et al., 2017; Khalil et al., 2016; Gasse et al., 2019; Nair et al., 2020; Zarpellon et al., 2021; Scavuzzo et al., 2022), node selection (He et al., 2014; Labassi et al., 2022), and cutting-plane method (Paulus et al., 2022; Tang et al., 2020; Turner et al., 2022; Chételat & Lodi, 2023). Moreover, there are plenty works on other combinatorial problems, e.g., satisfiability (SAT) problem (Selsam et al., 2018; Selsam & Bjørner, 2019; Toenshoff et al., 2021; Shi et al., 2022), traveling salesman problem (TSP) (Joshi et al., 2019; Vinyals et al., 2015; Min et al., 2024), graph coloring (Lemos et al., 2019; Li et al., 2022a), graph matching (Wang et al., 2019; Fey et al., 2020; Wang et al., 2020), among many others. As noted by Jin et al. (2024), CO problems that are naturally designed on graphs—such as TSP and graph coloring—can be seamlessly encoded into graph structures. CO problems without an inherent graph structure, like SAT problems and mixed-integer linear programming, can also be represented as graphs. For more detailed and exhaustive reviews on MPNN for MILP and other combinatorial optimization problems, we refer to Scavuzzo et al. (2024); Jin et al. (2024).

A.3. Additional experiments

Here, we report on additional experiments.

A.3.1. SYNCHRONIZED MESSAGE PASSING

We study the update sequence of message passing. We denote the message passing in Equations (3) to (5) and Equation (11) as asynchronous, as the node embeddings of some node types are updated first, while some others are updated with the latest updated node embeddings. We design the ablation of synchronous message passing of the form as follows, for tripartite

Table 5. Ablation experiments of async-/synchronized message passing. We experiment on the generic dataset and GCN model. The table reports the relative objective gap (in percentage) and constraint violation (in normalized absolute value). The training was repeated three times with different random seeds, and we report the mean and standard deviation across runs. For our feasibility method, the standard deviation of constraint violation is omitted as it is not meaningful.

	Method	Global node	Async.	Sync.
Obj. gap [%]	Naive 2024	✗	2.547±0.126	2.447±0.091
		✓	2.281±0.150	2.400±0.143
	IPM 2024	✗	1.894±0.166	2.146±0.461
		✓	1.829±0.079	2.199±0.515
	IPM(ours)	✗	2.236±0.249	2.175±0.195
		✓	1.661±0.199	2.398±0.409
Feas.(ours)	✗	0.049±0.015	0.141±0.012	
	✓	0.070±0.004	0.207±0.047	
Cons. vio.	Naive 2024	✗	0.012±0.004	0.031±0.004
		✓	0.018±0.001	0.029±0.003
	IPM 2024	✗	0.013±0.001	0.020±0.002
		✓	0.016±0.0003	0.015±0.003
	IPM(ours)	✗	0.031±0.008	0.032±0.001
		✓	0.029±0.009	0.046±0.007
	Feas.(ours)	✗	1.216×10^{-7}	1.441×10^{-7}
		✓	1.142×10^{-7}	1.567×10^{-7}

Equation (14) and bipartite Equation (15), respectively.

$$\begin{aligned}
 \mathbf{h}_c^{(l,t)} &:= \text{UPD}_c^{(l)} \left[\mathbf{h}_c^{(l-1,t)}, \right. \\
 &\quad \text{MSG}_{v \rightarrow c}^{(l)} \left(\left\{ \left(\mathbf{h}_v^{(l-1,t)}, \mathbf{e}_{cv} \right) \mid v \in N(c) \cap V(I) \right\} \right), \\
 &\quad \left. \text{MSG}_{g \rightarrow c}^{(l)} \left(\mathbf{h}_g^{(l-1,t)}, \mathbf{e}_{cg} \right) \right] \in \mathbb{Q}^d, \\
 \mathbf{h}_g^{(l,t)} &:= \text{UPD}_g^{(l)} \left[\mathbf{h}_g^{(l-1,t)}, \right. \\
 &\quad \text{MSG}_{v \rightarrow g}^{(l)} \left(\left\{ \left(\mathbf{h}_v^{(l-1,t)}, \mathbf{e}_{vg} \right) \mid v \in V(I) \right\} \right), \\
 &\quad \left. \text{MSG}_{c \rightarrow g}^{(l)} \left(\left\{ \left(\mathbf{h}_c^{(l-1,t)}, \mathbf{e}_{cg} \right) \mid c \in C(I) \right\} \right) \right] \in \mathbb{Q}^d, \\
 \mathbf{h}_v^{(l,t)} &:= \text{UPD}_v^{(l)} \left[\mathbf{h}_v^{(l-1,t)}, \right. \\
 &\quad \text{MSG}_{v \rightarrow v}^{(l)} \left(\left\{ \left(\mathbf{h}_u^{(l-1,t)}, \mathbf{e}_{uv} \right) \mid u \in N(v) \cap V(I) \right\} \right), \\
 &\quad \text{MSG}_{c \rightarrow v}^{(l)} \left(\left\{ \left(\mathbf{h}_c^{(l-1,t)}, \mathbf{e}_{cv} \right) \mid c \in N(v) \cap C(I) \right\} \right), \\
 &\quad \left. \text{MSG}_{g \rightarrow v}^{(l)} \left(\mathbf{h}_g^{(l-1,t)}, \mathbf{e}_{vg} \right) \right] \in \mathbb{Q}^d.
 \end{aligned} \tag{14}$$

$$\begin{aligned}
 \mathbf{h}_c^{(l,t)} &:= \text{UPD}_c^{(l)} \left[\mathbf{h}_c^{(l-1,t)}, \text{MSG}_{v \rightarrow c}^{(l)} \left(\left\{ \left(\mathbf{h}_v^{(l-1,t)}, \mathbf{e}_{cv} \right) \mid v \in N(c) \cap V(I) \right\} \right) \right] \in \mathbb{Q}^d, \\
 \mathbf{h}_v^{(l,t)} &:= \text{UPD}_v^{(l)} \left[\mathbf{h}_v^{(l-1,t)}, \text{MSG}_{v \rightarrow v}^{(l)} \left(\left\{ \left(\mathbf{h}_u^{(l-1,t)}, \mathbf{e}_{uv} \right) \mid u \in N(v) \cap V(I) \right\} \right), \right. \\
 &\quad \left. \text{MSG}_{c \rightarrow v}^{(l)} \left(\left\{ \left(\mathbf{h}_c^{(l-1,t)}, \mathbf{e}_{cv} \right) \mid c \in N(v) \cap C(I) \right\} \right) \right] \in \mathbb{Q}^d.
 \end{aligned} \tag{15}$$

We select the GCN architecture and the generic QP dataset as representative; see Table 5 for results. Our feasibility-guaranteeing MPNNs get better results with asynchronous message passing, but there are no consistent and significant differences for other methods.

Table 6. Soft-margin SVM problem, size generalization. We fix the density hyperparameters or the average degree of nodes compared to the training set. The star symbol * indicates training sizes. The methods with postfix -G us the global node.

	Fix Size	Density			Degree		
		400*	600	800	600	800	
Obj. gap [%]	Naive 2024	0.446±0.102	5.416±1.242	15.913±2.946	1.066±0.295	1.003±0.285	
	Naive-G 2024	0.352±0.032	7.920±2.435	19.733±5.212	2.046±0.649	1.895±0.708	
	IPM 2024	0.175±0.022	5.775±1.171	16.257±4.036	0.946±0.153	0.890±0.183	
	IPM-G 2024	0.162±0.009	3.660±0.766	9.564±1.391	0.784±0.265	0.722±0.255	
	IPM ₁₆ (Ours)	2.352±0.525	5.601±1.383	9.342±1.674	4.965±1.597	5.051±1.616	
	IPM ₃₂ (Ours)	0.696±0.236	2.509±1.238	4.965±2.160	4.855±1.614	4.918±1.697	
	IPM-G ₁₆ (Ours)	1.744±0.108	2.238±0.893	3.705±1.874	2.367±0.841	2.340±0.937	
	IPM-G ₃₂ (Ours)	0.485±0.176	2.163±1.573	3.964±2.062	2.436±0.883	2.388±0.935	
	Feas. ₁₆ (Ours)	0.222±0.049	0.536±0.022	1.841±0.236	0.511±0.176	0.584±0.231	
	Feas. ₃₂ (Ours)	0.126±0.034	0.404±0.053	1.519±0.100	0.387±0.147	0.421±0.174	
	Feas.-G ₁₆ (Ours)	0.254±0.007	0.503±0.053	1.430±0.212	0.282±0.031	0.297±0.024	
	Feas.-G ₃₂ (Ours)	0.190±0.008	0.364±0.027	1.160±0.123	0.185±0.012	0.171±0.014	
	Cons. vio.	Naive 2024	0.013±0.009	0.051±0.011	0.133±0.025	0.017±0.002	0.016±0.002
		Naive-G 2024	0.007±0.001	0.066±0.021	0.179±0.047	0.019±0.003	0.018±0.003
IPM 2024		0.004±0.001	0.051±0.010	0.155±0.031	0.011±0.003	0.011±0.003	
IPM-G 2024		0.003±0.0001	0.035±0.006	0.107±0.018	0.007±0.001	0.007±0.001	
IPM ₁₆ (Ours)		0.015±0.007	0.074±0.025	0.136±0.027	0.079±0.008	0.080±0.008	
IPM ₃₂ (Ours)		0.020±0.010	0.082±0.026	0.145±0.024	0.074±0.012	0.075±0.012	
IPM-G ₁₆ (Ours)		0.010±0.005	0.047±0.011	0.106±0.023	0.055±0.011	0.055±0.012	
IPM-G ₃₂ (Ours)		0.012±0.005	0.051±0.012	0.111±0.023	0.054±0.012	0.053±0.013	
Feas. ₁₆ (Ours)		3.433 × 10 ⁻⁷	3.148 × 10 ⁻⁷	3.357 × 10 ⁻⁷	2.553 × 10 ⁻⁷	2.782 × 10 ⁻⁷	
Feas. ₃₂ (Ours)		3.486 × 10 ⁻⁷	3.204 × 10 ⁻⁷	3.412 × 10 ⁻⁷	2.627 × 10 ⁻⁷	2.859 × 10 ⁻⁷	
Feas.-G ₁₆ (Ours)		3.376 × 10 ⁻⁷	3.054 × 10 ⁻⁷	3.328 × 10 ⁻⁷	2.485 × 10 ⁻⁷	2.750 × 10 ⁻⁷	
Feas.-G ₃₂ (Ours)		3.489 × 10 ⁻⁷	3.127 × 10 ⁻⁷	3.369 × 10 ⁻⁷	2.489 × 10 ⁻⁷	2.962 × 10 ⁻⁷	

A.3.2. MORE EXPERIMENTS ON GENERALIZATION PERFORMANCE

We report size generalization experiments on SVM and portfolio problems in Tables 6 and 7.

A.3.3. LP AS SPECIAL QP

We observe that LPs are special cases of QPs. If we remove quadratic term in the objective of Equation (1), we arrive at a standard LP form

$$\begin{aligned} \min_{\mathbf{x} \in \mathbb{Q}_{\geq 0}^n} \quad & \mathbf{c}^\top \mathbf{x} \\ \text{s.t.} \quad & \mathbf{A}\mathbf{x} = \mathbf{b}. \end{aligned}$$

Since there is no quadratic matrix, no edges between variable nodes exist. The graph representation is similar to Chen et al. (2022) for bipartite graphs and Qian et al. (2024); Ding et al. (2020) for tripartite graphs. We generate LP instances by relaxing well-known mixed-integer linear programming problems, similar to Qian et al. (2024); see Table 8 for results.

A.4. Datasets

Here, we give details on dataset generation.

Generic QP For generic QP problems, we consider the standard form of QP but with inequalities,

$$\begin{aligned} \min_{\mathbf{x} \in \mathbb{R}_{\geq 0}^n} \quad & \frac{1}{2} \mathbf{x}^\top \mathbf{Q}\mathbf{x} + \mathbf{c}^\top \mathbf{x} \\ \text{s.t.} \quad & \mathbf{A}\mathbf{x} \leq \mathbf{b}. \end{aligned} \tag{16}$$

We generate the matrix \mathbf{A} and vectors \mathbf{c}, \mathbf{b} with entries drawn i.i.d. from the standard normal distribution $\mathcal{N}(0, 1)$. To maintain sparsity, we independently drop out each entry of \mathbf{A} with probability τ using a Bernoulli distribution $\mathcal{B}(\tau)$, setting the dropped entries to zero. We generate the quadratic matrix \mathbf{Q} simply with the `make_sparse_spd_matrix` function from SciPy given the desired density. Finally, we add slack variables to the constraints to make them into equalities.

Table 7. Markowitz portfolio problem, size generalization. We fix the density hyperparameters or the average degree of nodes as compared to the training set. The size with the star symbol * is where we train the models. The methods with postfix -G are with the global node.

	Fix Size	–	Density		Degree		
		800*	1000	1200	1000	1200	
Obj. gap [%]	Naive 2024	11.075±0.363	39.487±1.472	89.422±8.968	37.366±0.202	80.900±1.199	
	Naive-G 2024	2.446±0.756	50.303±2.226	114.081±2.407	43.062±3.737	103.827±4.694	
	IPM 2024	11.075±0.363	59.571±3.657	123.412±16.006	53.575±5.673	122.935±17.091	
	IPM-G 2024	0.717±0.353	60.532±2.009	123.601±6.519	53.641±3.141	127.39±10.328	
	IPM ₁₆ (Ours)	1.241±0.123	59.885±1.284	134.475±4.046	48.010±1.222	107.825±3.340	
	IPM ₃₂ (Ours)	1.168±0.048	58.791±0.902	133.522±3.104	46.299±0.963	104.649±3.020	
	IPM-G ₁₆ (Ours)	1.672±0.302	50.184±2.841	120.491±3.303	41.294±3.882	97.128±10.011	
	IPM-G ₃₂ (Ours)	1.838±0.720	48.149±3.959	116.984±3.736	39.947±4.891	95.537±10.651	
	Feas. ₁₆ (Ours)	1.069±0.135	30.945±7.768	69.905±19.248	24.286±7.778	44.202±12.299	
	Feas. ₃₂ (Ours)	0.935±0.062	18.755±0.100	43.238±13.631	13.420±4.255	25.170±6.707	
	Feas.-G ₁₆ (Ours)	1.076±0.161	8.211±2.691	22.804±7.514	5.348±1.463	10.702±3.327	
	Feas.-G ₃₂ (Ours)	1.005±0.159	5.303±1.279	14.530±4.671	3.412±0.835	6.389±1.285	
	Cons. vio.	Naive 2024	0.083±0.001	0.266±0.011	0.397±0.015	0.271±0.008	0.382±0.009
		Naive-G 2024	0.017±0.006	0.184±0.012	0.330±0.017	0.176±0.012	0.331±0.017
IPM 2024		0.011±0.005	0.237±0.027	0.435±0.039	0.235±0.034	0.440±0.048	
IPM-G 2024		0.006±0.003	0.239±0.004	0.409±0.011	0.231±0.002	0.422±0.013	
IPM ₁₆ (Ours)		0.007±0.001	0.192±0.010	0.352±0.015	0.175±0.007	0.331±0.008	
IPM ₃₂ (Ours)		0.008±0.000	0.187±0.012	0.347±0.016	0.169±0.008	0.319±0.009	
IPM-G ₁₆ (Ours)		0.011±0.003	0.156±0.019	0.288±0.040	0.153±0.015	0.288±0.039	
IPM-G ₃₂ (Ours)		0.015±0.005	0.162±0.015	0.297±0.038	0.160±0.011	0.293±0.037	
Feas. ₁₆ (Ours)		2.228 × 10 ⁻⁸	3.054 × 10 ⁻⁸	3.377 × 10 ⁻⁸	2.779 × 10 ⁻⁸	3.249 × 10 ⁻⁸	
Feas. ₃₂ (Ours)		2.179 × 10 ⁻⁸	2.873 × 10 ⁻⁸	3.491 × 10 ⁻⁸	2.693 × 10 ⁻⁸	3.386 × 10 ⁻⁸	
Feas.-G ₁₆ (Ours)		2.086 × 10 ⁻⁸	2.570 × 10 ⁻⁸	2.980 × 10 ⁻⁸	2.384 × 10 ⁻⁸	3.203 × 10 ⁻⁸	
Feas.-G ₃₂ (Ours)		3.427 × 10 ⁻⁸	8.568 × 10 ⁻⁸	2.235 × 10 ⁻⁸	2.692 × 10 ⁻⁸	2.160 × 10 ⁻⁸	

Soft margin SVM For the QP problems generated from SVMs (Bishop & Nasrabadi, 2006), we follow the form,

$$\begin{aligned}
 \min_{\mathbf{w}} \quad & \mathbf{w}^\top \mathbf{w} + \lambda \mathbf{1}^\top \boldsymbol{\xi} \\
 \text{s.t.} \quad & \mathbf{y} \odot \mathbf{X} \mathbf{w} \geq \mathbf{1} - \boldsymbol{\xi} \\
 & \boldsymbol{\xi} \in \mathbb{R}_{\geq 0}^n.
 \end{aligned}$$

The $\mathbf{w} \in \mathbb{R}^n$ above denotes the vector of learnable parameters in the SVM we try to optimize, and $(\mathbf{X} \mathbf{y} \in \mathbb{R}^m)$ are the data points. Note that we have no constraints on m, n , and \mathbf{X} must not be full rank. Here, $\boldsymbol{\xi} \in \mathbb{R}^m$ is the margin parameters we try to minimize, and \odot is element-wise multiplication. Given density hyperparameter $\tau \in (0, 1)$, we generate two sub-matrices $\mathbf{X}_1, \mathbf{X}_2 \in \mathbb{R}^{\frac{m}{2} \times n}$, with the entries drawn i.i.d. from the normal distributions $\mathcal{N}(-\frac{1}{n\tau}, \frac{1}{n\tau})$ and $\mathcal{N}(\frac{1}{n\tau}, \frac{1}{n\tau})$, respectively, and apply random drop for sparsity. The labels are $\{1, -1\}$ for the data points in the two sub-matrices. Finally, we also add slack variables to turn the inequalities into equalities.

Markowitz portfolio optimization There are various formulations of the Markowitz portfolio optimization problem. We consider the following form,

$$\begin{aligned}
 \min_{\mathbf{x} \in \mathbb{R}_{\geq 0}^n} \quad & \mathbf{x}^\top \boldsymbol{\Sigma} \mathbf{x} \\
 \text{s.t.} \quad & \boldsymbol{\mu}^\top \mathbf{x} = r \\
 & \mathbf{1}^\top \mathbf{x} = 1.
 \end{aligned}$$

We generate the symmetric, PSD matrix $\boldsymbol{\Sigma}$ again with the `make_sparse_spd_matrix` function from SciPy, and we sample the entries of $\boldsymbol{\mu}$ i.i.d. from the normal distribution $\mathcal{N}(0, 1)$. Here, r is sampled from the uniform distribution $\mathcal{U}(0, 1)$.

LP instances For the LP instances in Appendix A.3.3, we follow the setting of Qian et al. (2024).

Dataset hyperparameters Here, we list the hyperparameters of our dataset generation. For generic QP problems, we generate QPs of the form Equation (16) and use equality for the constraints. Table 9 lists the configurations for training and size generalization experiments and the hyperparameters with which we generate a dataset to train a GCN for QPLIB experiments.

Table 8. Experiment results on LP instances. The methods with postfix -G is with the global node. We do not show the violation of the feasibility method as it is not informative.

	Method	MPNN	Setcover	Indset	Cauc	Fac
Obj. gap [%]	Naive 2022	GCN	0.743±0.013	0.380±0.035	0.630±0.074	0.389±0.037
		GIN	0.681±0.017	0.408±0.019	0.465±0.008	0.329±0.003
	Naive-G 2022	GCN	0.706±0.036	0.357±0.021	0.557±0.092	0.336±0.028
		GIN	0.641±0.024	0.401±0.036	0.460±0.026	0.620±0.089
	Feas.	GCN	0.101±0.012	0.065±0.005	0.425±0.041	0.072±0.016
		GIN	0.123±0.026	0.088±0.014	0.529±0.007	0.063±0.034
	Feas.-G	GCN	0.120±0.026	0.089±0.030	0.338±0.034	0.069±0.007
		GIN	0.151±0.038	0.080±0.008	0.333±0.010	0.033±0.009
Cons. vio.	Naive 2022	GCN	0.024±0.003	0.023±0.003	0.028±0.002	0.012±0.001
		GIN	0.026±0.003	0.025±0.002	0.025±0.002	0.009±0.002
	Naive-G 2022	GCN	0.027±0.003	0.024±0.003	0.028±0.001	0.017±0.005
		GIN	0.033±0.007	0.025±0.001	0.025±0.001	0.014±0.003

Table 9. Hyperparameters for generating generic QP instances. The comments in the bracket indicate whether we fix the density or average node degree compared with the training data.

Dataset	#cons.	#vars.	A dens.	Q dens.	nums.
Training	400	400	0.01	0.01	1000
Larger (dens.)	600	600	0.01	0.01	100
Largest (dens.)	800	800	0.01	0.01	100
Larger (deg.)	600	600	0.005	0.007	100
Largest (deg.)	800	800	0.004	0.005	100
QPLIB	[2000, 3000]	[2000, 3000]	[1 × 10 ⁻⁴ , 1 × 10 ⁻³]	[1 × 10 ⁻⁵ , 1 × 10 ⁻³]	1000

We generate instances for SVM problems with the hyperparameters in Table 10. There is no hyperparameter for the density of the quadratic matrix, as it is always diagonal.

The hyperparameters of portfolio problems are shown in Table 11. There is no hyperparameter for the number of constraints, as it is a constant. However, we have control over the density of the quadratic matrix. Finally, the hyperparameters for the LP instances in Table 8 are shown in Tables 12 to 15.

A.5. Log-barrier function in search

In practical implementations, there are situations where the current solution $x^{(t)}$ is near the boundary of the positive orthant $Q_{\geq 0}^n$ and the prediction of displacement is inaccurate. In such cases, the step length would be small to not violate the

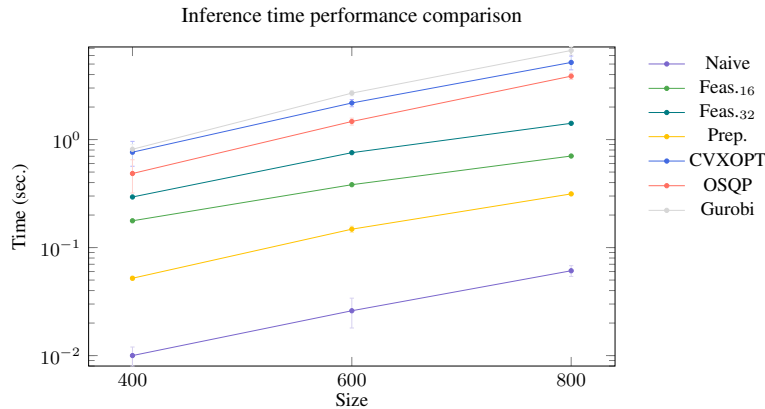


Figure 2. Comparison of inference runtimes on generic problem datasets, featuring GCN without the global node and three alternative solvers.

Table 10. Hyperparameters for generating SVM instances. The comments in the bracket indicate whether we fix the density or average node degree compared with the training data.

Dataset	#cons.	#vars.	\mathcal{A} dens.	nums.
Training	400	400	0.01	1000
Larger (dens.)	600	600	0.01	100
Largest (dens.)	800	800	0.01	100
Larger (deg.)	600	600	0.008	100
Largest (deg.)	800	800	0.006	100

Table 11. Hyperparameters for generating portfolio instances. The comments in the bracket indicate whether we fix the density or average node degree compared with the training data.

Dataset	#vars.	\mathcal{Q} dens.	nums.
Training	800	0.01	1000
Larger (dens.)	1000	0.01	100
Largest (dens.)	1200	0.01	100
Larger (deg.)	1000	0.008	100
Largest (deg.)	1200	0.006	100

non-negative constraint. At the next iteration, due to the continuous nature of neural networks, the prediction will again be inaccurate since the current solution hardly moved, and a small step size will be picked. Therefore, the current solution will likely be stuck at some suboptimal point. Recall the log barrier function in IPM (Nocedal & Wright, 2006), the function

$$f: \mathbb{Q}^n \rightarrow \mathbb{Q}, f(\mathbf{x}^{(t)}) := -\mathbf{1}^\top \log(\mathbf{x}^{(t)}), \quad (17)$$

where \log is an element-wise operation, is added in the objective function to prevent Newton’s step from being too aggressive and violating the non-negative constraint. Here, we incorporate the same function to encourage the current solution to move away from the orthant boundary. Calculating the gradient of this log barrier function w.r.t. $\mathbf{x}^{(t)}$, we have the direction vector $\nabla_{\mathbf{x}^{(t)}} f := -1/\mathbf{x}^{(t)}$. We directly subtract this vector from the predicted displacement vector $\mathbf{d}^{(t)}$ before applying null-space projection to them. Intuitively, this pushes the entries of the current solution that are very close to zero to larger positive numbers. To minimize the negative effect of the log barrier function on the convergence, we introduce a discount coefficient τ that scales itself down at each iteration. When $\tau \rightarrow 0$, the algorithm can still converge. However, the log barrier function still has a limitation. That is, it is not guaranteed that the entries in $1/\mathbf{x}^{(t)}$ after the projection $\Pi_A \frac{1}{\mathbf{x}^{(t)}}$ are still positive, which may drive some entries of $\mathbf{x}^{(t)}$ even closer to 0. In response to this challenge, we show that this log barrier force after the null space projection still effectively pushes the current solution away from the positive orthant boundary. Formally, based on the Equation (17), we want to show that

$$f\left(\mathbf{x} + \alpha \Pi_A \frac{1}{\mathbf{x}}\right) \leq f(\mathbf{x}), \quad (18)$$

for sufficiently small step length α . Since α is a small number, we treat the term $\alpha \Pi_A \frac{1}{\mathbf{x}}$ as a small perturbation and perform a Taylor expansion,

$$\begin{aligned} f\left(\mathbf{x} + \alpha \Pi_A \frac{1}{\mathbf{x}}\right) &\approx f(\mathbf{x}) + \nabla f(\mathbf{x})^\top \alpha \Pi_A \frac{1}{\mathbf{x}} \\ &= f(\mathbf{x}) - \alpha \frac{1}{\mathbf{x}}^\top \Pi_A \frac{1}{\mathbf{x}}. \end{aligned}$$

We notice the second term is an inner product, hence non-negative. So for sufficiently small α Equation (18) holds. Now, we would like to find an upper bound for α . We perform the second order Taylor expansion,

$$\begin{aligned} f\left(\mathbf{x} + \alpha \Pi_A \frac{1}{\mathbf{x}}\right) &\approx f(\mathbf{x}) + \nabla f(\mathbf{x})^\top \alpha \Pi_A \frac{1}{\mathbf{x}} + \left(\alpha \Pi_A \frac{1}{\mathbf{x}}\right)^\top \nabla^2 f(\mathbf{x}) \left(\alpha \Pi_A \frac{1}{\mathbf{x}}\right) \\ &= f(\mathbf{x}) - \alpha \frac{1}{\mathbf{x}}^\top \Pi_A \frac{1}{\mathbf{x}} + \left(\alpha \Pi_A \frac{1}{\mathbf{x}}\right)^\top \text{diag}\left(\frac{1}{\mathbf{x}^2}\right) \left(\alpha \Pi_A \frac{1}{\mathbf{x}}\right) \\ &< f(\mathbf{x}). \end{aligned}$$

Table 12. Hyperparameters for generating set cover problem instances.

Dataset	#cons.	#vars.	A dens.	nums.
Set cover	[200,300]	[300,400]	0.008	1000

Table 13. Hyperparameters for generating maximum independent set problem instances.

Dataset	#nodes	$p(u, v), u, v \in E(G)$	nums.
Max ind. set	[250,300]	0.01	1000

We want to ensure that

$$\alpha \frac{1}{x}^\top \Pi_A \frac{1}{x} - \left(\alpha \Pi_A \frac{1}{x} \right)^\top \text{diag} \left(\frac{1}{x^2} \right) \left(\alpha \Pi_A \frac{1}{x} \right) > 0.$$

We obtain the upper bound

$$\alpha < \frac{\frac{1}{x}^\top \Pi_A \frac{1}{x}}{\left(\Pi_A \frac{1}{x} \right)^\top \text{diag} \left(\frac{1}{x^2} \right) \left(\Pi_A \frac{1}{x} \right)}.$$

A.6. Derivation of the IPM

In this section, we only consider QPs as LPs are special cases of QPs where Q is set to an all-zero matrix. Let us first recap the standard form of QPs with linear equality constraints,

$$\begin{aligned} \min_{x \in \mathbb{R}_{\geq 0}^n} \quad & \frac{1}{2} x^\top Q x + c^\top x \\ \text{s.t.} \quad & A x = b. \end{aligned}$$

By adding Lagrangian multipliers, we obtain the Lagrangian,

$$\mathcal{L}(x, \lambda, s) := \frac{1}{2} x^\top Q x + c^\top x - \lambda^\top (A x - b) - s^\top x,$$

with $x, s \in \mathbb{R}_{\geq 0}^n, \lambda \in \mathbb{R}^m$. We can derive the *Karush–Kuhn–Tucker* (KKT) conditions for the Lagrangian,

$$\begin{aligned} A x &= b \\ Q x + c - A^\top \lambda - s &= 0 \\ x &\geq 0 \\ s &\geq 0 \\ x_i s_i &= 0. \end{aligned} \tag{19}$$

According to Lagrangian duality theory (Nocedal & Wright, 2006), the KKT condition is the necessary condition for optimality, and it is also a sufficient condition in our case of QPs. Thus, our goal is to find the solution (x, λ, s) that satisfies the KKT condition above. Let us consider the function

$$F(x, \lambda, s) := \begin{bmatrix} A x - b \\ Q x + c - A^\top \lambda - s \\ X S \mathbf{1} \end{bmatrix},$$

where X and S are diagonal matrices of the vectors x and s , respectively. The solution to the KKT condition is equivalent to the solution of $F(x, \lambda, s) = 0$, with $x, s \geq 0$. We search the zero point of the function F iteratively with Newton's method. That is, given current point of (x, λ, s) , we aim to find the search direction $(\Delta x, \Delta \lambda, \Delta s)$ by solving

$$J(F)(\Delta x, \Delta \lambda, \Delta s) = -F(x, \lambda, s),$$

where $J(\cdot)$ denotes the Jacobian of a function. The matrix form is

$$\begin{bmatrix} A & 0 & 0 \\ Q & -A^\top & -I \\ S & 0 & X \end{bmatrix} \begin{bmatrix} \Delta x \\ \Delta \lambda \\ \Delta s \end{bmatrix} = \begin{bmatrix} -A x + b \\ -Q x - c + A^\top \lambda + s \\ -X S \mathbf{1} \end{bmatrix}.$$

Table 14. Hyperparameters for generating combinatorial auction problem instances.

Dataset	#items.	#bids	nums.
Comb. auc.	[300,400]	[300,400]	1000

Table 15. Hyperparameters for generating capacitated facility location problem instances.

Dataset	#custom	#fac.	ratio	nums.
Cap. fac. loc.	[60,70]	5	0.5	1000

Ideally, by solving this equation, we can obtain the search direction. By doing a line search along the direction, the positivity constraints can be satisfied, and we can eventually converge to the optimal solution. However, the direction from Newton’s method might not ensure the positivity constraints, and the corresponding search step size might be too small. Thus similar to the IPM for LPs (Nocedal & Wright, 2006), we utilize the log barrier function and add the term $-\mu \log(\mathbf{x})^\top \mathbf{1}$ with $\mu \geq 0$ to the objective to replace the positivity constraints $\mathbf{x} \geq \mathbf{0}$. To be specific, the original QP problem becomes

$$\begin{aligned} \min_{\mathbf{x}} \quad & \frac{1}{2} \mathbf{x}^\top \mathbf{Q} \mathbf{x} + \mathbf{c}^\top \mathbf{x} - \mu \log(\mathbf{x})^\top \mathbf{1} \\ \text{s.t.} \quad & \mathbf{A} \mathbf{x} = \mathbf{b}. \end{aligned}$$

Correspondingly, we have a new Lagrangian

$$\mathcal{L}(\mathbf{x}, \boldsymbol{\lambda}, \mathbf{s}) := \frac{1}{2} \mathbf{x}^\top \mathbf{Q} \mathbf{x} + \mathbf{c}^\top \mathbf{x} - \boldsymbol{\lambda}^\top (\mathbf{A} \mathbf{x} - \mathbf{b}) - \mu \log(\mathbf{x})^\top \mathbf{1}.$$

The second equation in Equation (19) becomes $\mathbf{Q} \mathbf{x} + \mathbf{c} - \mathbf{A}^\top \boldsymbol{\lambda} - \frac{\mu}{\mathbf{x}} = \mathbf{0}$, which is nonlinear, making optimization via Newton’s method hard. Hence, we introduce the term $\mathbf{s} := \frac{\mu}{\mathbf{x}}$, and the new equation coincides with the second equation in Equation (19). However, the last equation in Equation (19) becomes $x_i s_i = \mu$. According to the path following definition (Nocedal & Wright, 2006), when $\mu \rightarrow 0$, the QP with log barrier function recovers the original problem. In practice, μ is defined as the dot product of the current solution $\mathbf{x}^\top \mathbf{s} / n$, multiplied with a scaling factor σ . The corresponding Newton equation is

$$\begin{bmatrix} \mathbf{A} & \mathbf{0} & \mathbf{0} \\ \mathbf{Q} & -\mathbf{A}^\top & -\mathbf{I} \\ \mathbf{S} & \mathbf{0} & \mathbf{X} \end{bmatrix} \begin{bmatrix} \Delta \mathbf{x} \\ \Delta \boldsymbol{\lambda} \\ \Delta \mathbf{s} \end{bmatrix} = \begin{bmatrix} -\mathbf{A} \mathbf{x} + \mathbf{b} \\ -\mathbf{Q} \mathbf{x} - \mathbf{c} + \mathbf{A}^\top \boldsymbol{\lambda} + \mathbf{s} \\ -\mathbf{X} \mathbf{S} \mathbf{1} + \sigma \mu \mathbf{1} \end{bmatrix}.$$

Now, let us take a closer look at the Newton equations. The last row gives us

$$\Delta \mathbf{s} := -\mathbf{X}^{-1} \mathbf{S} \Delta \mathbf{x} - \mathbf{s} + \mathbf{X}^{-1} \sigma \mu \mathbf{1},$$

applying this to the second row

$$\mathbf{Q} \Delta \mathbf{x} - \mathbf{A}^\top \Delta \boldsymbol{\lambda} - \Delta \mathbf{s} = -\mathbf{Q} \mathbf{x} - \mathbf{c} + \mathbf{A}^\top \boldsymbol{\lambda} + \mathbf{s},$$

we have

$$(\mathbf{Q} + \mathbf{X}^{-1} \mathbf{S}) \Delta \mathbf{x} - \mathbf{A}^\top \Delta \boldsymbol{\lambda} = \mathbf{X}^{-1} \sigma \mu \mathbf{1} - \mathbf{Q} \mathbf{x} - \mathbf{c} + \mathbf{A}^\top \boldsymbol{\lambda}.$$

Combining with the first row, we can see that we have reached an “atomic” linear system,

$$\begin{bmatrix} \mathbf{Q} + \mathbf{X}^{-1} \mathbf{S} & -\mathbf{A}^\top \\ -\mathbf{A} & \mathbf{0} \end{bmatrix} \begin{bmatrix} \Delta \mathbf{x} \\ \Delta \boldsymbol{\lambda} \end{bmatrix} = \begin{bmatrix} \mathbf{X}^{-1} \sigma \mu \mathbf{1} - \mathbf{Q} \mathbf{x} - \mathbf{c} + \mathbf{A}^\top \boldsymbol{\lambda} \\ \mathbf{A} \mathbf{x} - \mathbf{b} \end{bmatrix}, \quad (20)$$

where it is hard to perform Gaussian elimination due to the nontrivial computation of $(\mathbf{Q} + \mathbf{X}^{-1} \mathbf{S})^{-1}$. In contrast, in LPs, the \mathbf{Q} term in the matrix $\begin{bmatrix} \mathbf{Q} + \mathbf{X}^{-1} \mathbf{S} & -\mathbf{A}^\top \\ -\mathbf{A} & \mathbf{0} \end{bmatrix}$ vanishes, and we can further eliminate variable $\Delta \mathbf{x}$. However, the matrix $\begin{bmatrix} \mathbf{Q} + \mathbf{X}^{-1} \mathbf{S} & -\mathbf{A}^\top \\ -\mathbf{A} & \mathbf{0} \end{bmatrix}$ has full rank by definition. If we initialize the vectors \mathbf{x} , \mathbf{s} with positive values, we know the matrix is positive definite from Schur complement theory (Gallier et al., 2010). Hence, we use the conjugate gradient (CG) method (Nocedal & Wright, 2006) for the joint solution of $(\Delta \mathbf{x}, \Delta \boldsymbol{\lambda})$ by solving Equation (20). For the standard CG algorithm, see Algorithm 5. For a parametrized CG algorithm specific to our problem Equation (20), see Algorithm 6.

Table 16. Generic QP problem, size generalization. We fix the density hyperparameters or the average degree of nodes as compared to the training set. The size with the star symbol * is where we train the models on. The methods with postfix -G are with the global node.

	Fix Size	Density			Degree	
		400*	600	800	600	800
Obj. gap [%]	Naive 2024	2.547±0.126	11.480±0.297	20.663±0.813	1.787±0.196	1.402±0.127
	Naive-G 2024	2.281±0.150	8.461±1.078	15.443±1.500	1.744±0.134	1.302±0.091
	IPM 2024	1.894±0.166	10.521±1.057	20.936±1.106	1.510±0.126	1.153±0.063
	IPM-G 2024	1.829±0.079	10.987±1.132	20.129±1.782	1.541±0.021	1.062±0.132
	IPM ₁₆ (Ours)	10.679±4.351	22.448±1.307	29.633±1.739	11.982±4.683	11.989±5.584
	IPM ₃₂ (Ours)	2.236±0.249	7.685±2.917	19.310±4.806	2.003±0.472	1.856±0.370
	IPM-G ₁₆ (Ours)	10.715±5.344	12.170±5.604	14.648±8.498	10.692±5.573	9.694±6.355
	IPM-G ₃₂ (Ours)	1.661±0.199	4.961±1.219	3.462±0.692	1.648±0.238	1.350±0.243
	Feas. ₁₆ (Ours)	0.119±0.013	0.948±0.111	5.867±0.667	0.118±0.062	0.127±0.002
	Feas. ₃₂ (Ours)	0.049±0.015	0.615±0.064	4.839±0.602	0.045±0.011	0.046±0.007
	Feas.-G ₁₆ (Ours)	0.163±0.003	1.480±0.049	8.609±0.660	0.180±0.037	0.184±0.005
	Feas.-G ₃₂ (Ours)	0.070±0.004	0.991±0.031	7.607±0.607	0.077±0.010	0.071±0.005
	Naive 2024	0.012±0.004	0.053±0.002	0.099±0.002	0.014±0.002	0.014±0.002
	Naive-G 2024	0.018±0.001	0.050±0.004	0.095±0.006	0.017±0.001	0.017±0.001
	IPM 2024	0.013±0.001	0.048±0.002	0.092±0.003	0.012±0.001	0.011±0.001
	IPM-G 2024	0.016±0.0003	0.048±0.002	0.089±0.003	0.016±0.001	0.016±0.0003
	IPM ₁₆ (Ours)	0.028±0.008	0.040±0.006	0.064±0.006	0.028±0.008	0.027±0.008
	IPM ₃₂ (Ours)	0.031±0.008	0.050±0.006	0.078±0.007	0.030±0.009	0.030±0.008
IPM-G ₁₆ (Ours)	0.026±0.007	0.048±0.007	0.069±0.004	0.026±0.008	0.026±0.007	
IPM-G ₃₂ (Ours)	0.029±0.009	0.053±0.007	0.076±0.004	0.029±0.009	0.028±0.009	
Feas. ₁₆ (Ours)	9.786×10^{-8}	1.138×10^{-7}	1.279×10^{-7}	1.093×10^{-7}	1.178×10^{-7}	
Feas. ₃₂ (Ours)	1.215×10^{-7}	1.376×10^{-7}	1.516×10^{-7}	1.318×10^{-7}	1.396×10^{-7}	
Feas.-G ₁₆ (Ours)	9.080×10^{-8}	1.161×10^{-7}	1.546×10^{-7}	1.021×10^{-7}	1.148×10^{-7}	
Feas.-G ₃₂ (Ours)	1.142×10^{-7}	1.447×10^{-7}	1.769×10^{-7}	1.228×10^{-7}	1.346×10^{-7}	

A.7. Omitted proofs

Here, we outline the missing proofs from the main paper.

A.7.1. MPNNS CAN SIMULATE IPMS

Here we prove Theorem 1 from the main paper in detail.

Lemma 3. *There exists an MPNN $f_{MPNN,IPM}$ composed of $\mathcal{O}(1)$ layers and $\mathcal{O}(m+n)$ successive message-passing steps that reproduces each iteration of the IPM algorithm for LCQPs, in the sense that for any LCQP instance $I = (\mathbf{Q}, \mathbf{A}, \mathbf{b}, \mathbf{c})$ and any primal-dual point $(\mathbf{x}^{(t)}, \boldsymbol{\lambda}^{(t)}, \mathbf{s}^{(t)})$ with $t > 0$, $f_{MPNN,IPM}$ maps the graph $G(I)$ carrying $[\mathbf{x}^{(t-1)}, \mathbf{s}^{(t-1)}]$ on the variable nodes, $[\boldsymbol{\lambda}^{(t-1)}]$ on the constraint nodes, and $[\mu, \sigma]$ on the global node to the same graph $G(I)$ carrying the output $[\mathbf{x}^{(t)}, \mathbf{s}^{(t)}]$ and $[\boldsymbol{\lambda}^{(t)}]$ of Algorithm 7 on the variable and constraint nodes, respectively.*

Proof. For a QP instance I , we construct an undirected, heterogeneous graph $G(I)$ with three node types, variable nodes $V(I)$, constraint nodes $C(I)$, and a single global node $\{g(I)\}$, as already described in Section 2. The corresponding node embedding matrices are denoted as $\mathbf{V}, \mathbf{C}, \mathbf{G}$ respectively. Across different node types, we have four edge types. The intra-variable-nodes connections are given by the non-zero entries of the \mathbf{Q} matrix, and we use the values Q_{ij} as the edge attributes. For the edges connecting variable and constraint nodes, we use the non-zero entries of the \mathbf{A} matrix and also the values A_{ij} as the edge attributes. We design the global node to be connected to all variable and constraint nodes with uniform edge attributes. By default, we assume all the vectors to be *column* vectors, but we refer to a row i of a matrix \mathbf{M} in the form of M_i and assume it to be a *row* vector. Specifically, we construct the graph with node feature matrices initialized as follows,

$$\begin{aligned} \mathbf{V}^{(\text{init},0)} &:= [\mathbf{x} \quad \mathbf{s} \quad \mathbf{c}] \in \mathbb{R}^{n \times 3}, \\ \mathbf{C}^{(\text{init},0)} &:= [\boldsymbol{\lambda} \quad \mathbf{b}] \in \mathbb{R}^{m \times 2}, \\ \mathbf{G}^{(\text{init},0)} &:= [\sigma \mu] \in \mathbb{R}. \end{aligned}$$

Note that we use superscripts of the form (phase, i) where phase stands for the initialization or some iteration t in Algorithm 6,

Table 17. Computational efficiency on various problems trained with GCN architecture. The GCN was trained on datasets of smaller size and evaluated on larger sizes. The larger instances are generated by increasing the problem size and fixing the density parameters. We compare both our methods at 16 and 32 iterations against the naive MPNN approach Chen et al. (2024), the fix-step IPM-MPNN Qian et al. (2024) and three traditional QP solvers. The methods with postfix -G are with the global node. We report the neural networks based results with three models pretrained with various random seeds, with the mean and standard deviation reported.

Problem Size	Generic			SVM			Portfolio		
	400*	600	800	400*	600	800	800*	1000	1200
CVXOPT	0.764±0.198	2.181±0.168	5.177±0.757	0.495±0.050	1.205±0.331	2.503±0.606	0.178±0.063	0.214±0.077	0.411±0.085
OSQP	0.485±0.165	1.470±0.109	3.865±0.259	0.019±0.001	0.072±0.008	0.270±0.085	0.040±0.006	0.065±0.013	0.121±0.042
Gurobi	0.813±0.088	2.691±0.158	6.682±0.579	0.013±0.001	0.057±0.016	0.125±0.018	0.221±0.032	0.303±0.022	0.520±0.063
Naive 2024	0.010±0.002	0.026±0.008	0.018±0.005	0.015±0.003	0.017±0.003	0.010±0.004	0.008±0.002	0.009±0.003	0.010±0.005
Naive-G 2024	0.021±0.005	0.045±0.061	0.061±0.007	0.022±0.006	0.025±0.005	0.028±0.005	0.022±0.006	0.023±0.007	0.024±0.009
IPM 2024	0.014±0.002	0.031±0.002	0.048±0.001	0.010±0.001	0.010±0.001	0.013±0.002	0.012±0.003	0.018±0.002	0.017±0.001
IPM-G 2024	0.025±0.0004	0.036±0.002	0.057±0.003	0.022±0.004	0.025±0.003	0.026±0.002	0.022±0.002	0.022±0.002	0.019±0.002
IPM ₁₆ (Ours)	0.150±0.009	0.377±0.006	0.704±0.002	0.136±0.010	0.137±0.002	0.138±0.003	0.136±0.009	0.124±0.002	0.152±0.009
IPM ₃₂ (Ours)	0.298±0.010	0.751±0.003	1.410±0.005	0.256±0.014	0.247±0.011	0.238±0.007	0.261±0.017	0.254±0.009	0.289±0.007
IPM-G ₁₆ (Ours)	0.277±0.003	0.479±0.006	0.824±0.001	0.256±0.008	0.238±0.002	0.240±0.005	0.274±0.010	0.242±0.006	0.259±0.006
IPM-G ₃₂ (Ours)	0.533±0.006	0.980±0.004	1.612±0.001	0.497±0.008	0.459±0.009	0.488±0.007	0.500±0.008	0.494±0.005	0.522±0.006
Prep.	0.052±0.002	0.148±0.010	0.314±0.005	0.034±0.001	0.091±0.002	0.184±0.009	0.002±0.0004	0.004±0.001	0.005±0.001
Feas. ₁₆ (Ours)	0.177±0.003	0.382±0.001	0.704±0.001	0.161±0.001	0.166±0.002	0.140±0.001	0.177±0.005	0.171±0.002	0.170±0.004
Feas. ₃₂ (Ours)	0.294±0.001	0.756±0.004	1.414±0.002	0.295±0.005	0.283±0.006	0.264±0.002	0.305±0.020	0.299±0.011	0.310±0.010
Feas.-G ₁₆ (Ours)	0.324±0.006	0.482±0.001	0.821±0.001	0.297±0.001	0.255±0.001	0.254±0.001	0.262±0.009	0.276±0.008	0.270±0.002
Feas.-G ₃₂ (Ours)	0.602±0.025	0.955±0.003	1.652±0.014	0.482±0.002	0.508±0.005	0.481±0.013	0.470±0.015	0.517±0.018	0.543±0.015

and i is an index for intermediate operations that appears when necessary. We set edge features

$$\begin{aligned}
 e_{v \rightarrow u} &:= \mathbf{Q}_{vu}, \forall v, u \in V(I) \\
 e_{c \rightarrow v} &:= \mathbf{A}_{cv}, \forall c \in C(I), v \in V(I) \\
 e_{v \rightarrow g} &:= 1, \forall v \in V(I) \\
 e_{c \rightarrow g} &:= 1, \forall c \in C(I).
 \end{aligned}$$

From now on, we drop the notations of e and use \mathbf{Q} , \mathbf{A} for ease of notation.

In principle, we would like all the message-passing steps to fall in the framework of the following synchronous, heterogeneous message-passing functions,

$$\begin{aligned}
 \mathbf{V}_v^{(t)} &:= \text{UPD}_v^{(t)} \left[\mathbf{V}_v^{(t-1)}, \right. \\
 &\quad \text{AGG}_{c \rightarrow v}^{(t)} \left(\left\{ \left\{ \text{MSG}_{c \rightarrow v}^{(t)} \left(\mathbf{C}_c^{(t-1)}, \mathbf{A}_{cv} \right) \mid c \in N(v) \cap C(I) \right\} \right\} \right), \\
 &\quad \text{AGG}_{v \rightarrow v}^{(t)} \left(\left\{ \left\{ \text{MSG}_{v \rightarrow v}^{(t)} \left(\mathbf{V}_u^{(t-1)}, \mathbf{Q}_{vu} \right) \mid u \in N(v) \cap V(I) \right\} \right\} \right), \\
 &\quad \left. \text{MSG}_{g \rightarrow v}^{(t)} \left(\mathbf{G}^{(t-1)} \right) \right], \forall v \in V(I). \\
 \mathbf{C}_c^{(t)} &:= \text{UPD}_c^{(t)} \left[\mathbf{C}_c^{(t-1)}, \right. \\
 &\quad \text{AGG}_{v \rightarrow c}^{(t)} \left(\left\{ \left\{ \text{MSG}_{v \rightarrow c}^{(t)} \left(\mathbf{V}_v^{(t-1)}, \mathbf{A}_{cv} \right) \mid v \in N(c) \cap V(I) \right\} \right\} \right), \\
 &\quad \left. \text{MSG}_{g \rightarrow c}^{(t)} \left(\mathbf{G}^{(t-1)} \right) \right], \forall c \in C(I). \\
 \mathbf{G}^{(t)} &:= \text{UPD}_g^{(t)} \left[\mathbf{G}^{(t-1)}, \right. \\
 &\quad \text{AGG}_{v \rightarrow g}^{(t)} \left(\left\{ \left\{ \text{MSG}_{v \rightarrow g}^{(t)} \left(\mathbf{V}_v^{(t-1)} \right) \mid v \in V(I) \right\} \right\} \right), \\
 &\quad \left. \text{AGG}_{c \rightarrow g}^{(t)} \left(\left\{ \left\{ \text{MSG}_{c \rightarrow g}^{(t)} \left(\mathbf{C}_c^{(t-1)} \right) \mid c \in C(I) \right\} \right\} \right) \right],
 \end{aligned} \tag{21}$$

where $\text{UPD}_v^{(t)}$ is the update function shared by all the variable nodes $v \in V(I)$, similar with $\text{UPD}_c^{(t)}$ and $\text{UPD}_g^{(t)}$. Functions

Algorithm 5 Standard conjugate gradient algorithm for reference.

Require: An equation $\mathbf{A}\mathbf{x} = \mathbf{b}$, where $\mathbf{A} \in \mathbb{R}^{n \times n}$ is a real-valued, symmetric, positive-definite matrix.

```

1:  $\mathbf{r}^{(0)} \leftarrow \mathbf{b}$ 
2:  $\mathbf{x}^{(0)} \leftarrow \mathbf{0}$ 
3:  $\mathbf{p}^{(0)} \leftarrow \mathbf{r}^{(0)}$ 
4: for  $t \in [n]$  do
5:    $\alpha^{(t)} \leftarrow \frac{\mathbf{r}^{(t-1)\top} \mathbf{r}^{(t-1)}}{\mathbf{r}^{(t-1)\top} \mathbf{A} \mathbf{r}^{(t-1)}}$ 
6:    $\mathbf{x}^{(t)} \leftarrow \mathbf{x}^{(t-1)} + \alpha^{(t)} \mathbf{p}^{(t-1)}$ 
7:    $\mathbf{r}^{(t)} \leftarrow \mathbf{r}^{(t-1)} - \alpha^{(t)} \mathbf{A} \mathbf{p}^{(t-1)}$ 
8:    $\beta^{(t)} \leftarrow \frac{\mathbf{r}^{(t)\top} \mathbf{r}^{(t)}}{\mathbf{r}^{(t-1)\top} \mathbf{r}^{(t-1)}}$ 
9:    $\mathbf{p}^{(t)} \leftarrow \beta^{(t)} \mathbf{p}^{(t-1)} + \mathbf{r}^{(t)}$ 
10: end for
11: return Solution  $\mathbf{x}^{(n)}$ .
```

$\text{AGG}_{\circ \rightarrow \odot}^{(t)}$ and $\text{MSG}_{\circ \rightarrow \odot}^{(t)}$ represent the aggregation and message functions from a node type \circ to another \odot , also shared on the edges with the same edge type. We assume all the UPD, AGG, MSG are arbitrary continuous functions.

In the following, we show how a message-passing architecture can simulate the CG algorithm Algorithm 6.

Lines 4-6 Let us first take a look at the initialization

$$\mathbf{r}^{(0)} \leftarrow \begin{bmatrix} \mathbf{X}^{-1} \sigma \mu \mathbf{1} - \mathbf{Q} \mathbf{x} - \mathbf{c} + \mathbf{A}^\top \boldsymbol{\lambda} \\ \mathbf{A} \mathbf{x} - \mathbf{b} \end{bmatrix}.$$

That is, we need the vector $\mathbf{X}^{-1} \sigma \mu \mathbf{1} - \mathbf{Q} \mathbf{x} - \mathbf{c} + \mathbf{A}^\top \boldsymbol{\lambda}$ to be stored in the variable nodes, and $\mathbf{A} \mathbf{x} - \mathbf{b}$ in the constraint nodes. We notice that $\mathbf{Q} \mathbf{x}$ is a simple graph convolution on the intra-variable nodes, and $\mathbf{A}^\top \boldsymbol{\lambda}$ is convolution from constraint nodes to variable nodes. Therefore, we can compute $\mathbf{X}^{-1} \sigma \mu \mathbf{1} - \mathbf{Q} \mathbf{x} - \mathbf{c} + \mathbf{A}^\top \boldsymbol{\lambda}$ with one message-passing step by constructing the message functions for every variable node $v \in V(I)$,

$$\begin{aligned} \text{MSG}_{\mathbf{g} \rightarrow \mathbf{v}}^{(\text{init},1)}(\mathbf{G}^{(\text{init},0)}) &:= \mathbf{G}^{(\text{init},0)} = \sigma \mu, \\ \text{MSG}_{\mathbf{c} \rightarrow \mathbf{v}}^{(\text{init},1)}(\mathbf{C}_c^{(\text{init},0)}, \mathbf{A}_{cv}) &:= \mathbf{A}_{cv} \mathbf{C}_c^{(\text{init},0)} \begin{bmatrix} 1 \\ 0 \end{bmatrix} = \mathbf{A}_{cv} \boldsymbol{\lambda}_c, \forall c \in N(v) \cap C(I), \\ \text{MSG}_{\mathbf{v} \rightarrow \mathbf{v}}^{(\text{init},1)}(\mathbf{V}_u^{(\text{init},0)}, \mathbf{Q}_{vu}) &:= \mathbf{Q}_{vu} \mathbf{V}_u^{(\text{init},0)} \begin{bmatrix} 1 \\ 0 \\ 0 \end{bmatrix} = \mathbf{Q}_{vu} \mathbf{x}_u, \forall u \in N(v) \cap V(I), \end{aligned} \quad (22)$$

and the aggregation functions,

$$\begin{aligned} \text{AGG}_{\mathbf{c} \rightarrow \mathbf{v}}^{(\text{init},1)}(\{\{\mathbf{A}_{cv} \boldsymbol{\lambda}_c \mid c \in N(v) \cap C(I)\}\}) &:= \sum_{c \in N(v) \cap C(I)} \mathbf{A}_{cv} \boldsymbol{\lambda}_c = \mathbf{A}_v^\top \boldsymbol{\lambda}, \\ \text{AGG}_{\mathbf{v} \rightarrow \mathbf{v}}^{(\text{init},1)}(\{\{\mathbf{Q}_{vu} \mathbf{x}_u \mid u \in N(v) \cap V(I)\}\}) &:= \sum_{u \in N(v) \cap V(I)} \mathbf{Q}_{vu} \mathbf{x}_u = \mathbf{Q}_v \mathbf{x}, \end{aligned} \quad (23)$$

and finally, we design the update function,

$$\begin{aligned} \mathbf{V}_v^{(\text{init},1)} &:= \text{UPD}_v^{(\text{init},1)}[\mathbf{V}_v^{(\text{init},0)}, \mathbf{A}_v^\top \boldsymbol{\lambda}, \mathbf{Q}_v \mathbf{x}, \sigma \mu] \\ &= \frac{\sigma \mu}{\mathbf{V}_v^{(\text{init},0)} \begin{bmatrix} 1 \\ 0 \\ 0 \end{bmatrix}} - \mathbf{Q}_v \mathbf{x} + \mathbf{A}_v^\top \boldsymbol{\lambda} - \mathbf{V}_v^{(\text{init},0)} \begin{bmatrix} 0 \\ 0 \\ 1 \end{bmatrix} \\ &= \frac{\sigma \mu}{\mathbf{x}_v} - \mathbf{Q}_v \mathbf{x} + \mathbf{A}_v^\top \boldsymbol{\lambda} - \mathbf{c}_v. \end{aligned} \quad (24)$$

Algorithm 6 Conjugate gradient algorithm for the linear equations Equation (20).

Require: A QP instance (Q, A, b, c) , initial solution $x, s > 0, \lambda \in \mathbb{R}^m$, hyperparameter σ, μ .

- 1: $X \leftarrow \text{diag}(x)$
- 2: $S \leftarrow \text{diag}(s)$
- 3: $P \leftarrow \begin{bmatrix} Q + X^{-1}S & -A^\top \\ -A & 0 \end{bmatrix}$
- 4: $r^{(0)} \leftarrow \begin{bmatrix} X^{-1}\sigma\mu\mathbf{1} - Qx - c + A^\top\lambda \\ Ax - b \end{bmatrix}$
- 5: $w^{(0)} \leftarrow \mathbf{0}$
- 6: $p^{(0)} \leftarrow r^{(0)}$
- 7: **for** $t \in [n + m]$ **do**
- 8: $\alpha^{(t)} \leftarrow \frac{r^{(t-1)\top} r^{(t-1)}}{r^{(t-1)\top} P r^{(t-1)}}$
- 9: $w^{(t)} \leftarrow w^{(t-1)} + \alpha^{(t)} p^{(t-1)}$
- 10: $r^{(t)} \leftarrow r^{(t-1)} - \alpha^{(t)} P p^{(t-1)}$
- 11: $\beta^{(t)} \leftarrow \frac{r^{(t)\top} r^{(t)}}{r^{(t-1)\top} r^{(t-1)}}$
- 12: $p^{(t)} \leftarrow \beta^{(t)} p^{(t-1)} + r^{(t)}$
- 13: **end for**
- 14: $\Delta x \leftarrow w_{[1:n]}^{(n+m)}$
- 15: $\Delta \lambda \leftarrow w_{[n+1:n+m]}^{(n+m)}$
- 16: **return** Solution $\Delta x, \Delta \lambda$.

The above functions form the framework in Equation (21). When we stack all the values $V_v^{(\text{init},1)}$ into a vector, we end up with the needed vector $X^{-1}\sigma\mu\mathbf{1} - Qx - c + A^\top\lambda$. Note that $X^{-1}\mathbf{1} = \frac{1}{x}$ can be obtained by element-wise reciprocal operation as a non-linear activation function.

The functions Equations (22) to (24) give us a first impression of how our proof by construction works. For convenience, we store the previous vectors x, s in the node embedding matrices for the upcoming operations. Besides the initialization for $r^{(0)}$ above, we need to copy $r^{(0)}$ into $p^{(0)}$, and assign some trivial values to $w^{(0)}$. Hence, we need to modify the update functions,

$$\begin{aligned} V_v^{(\text{init},1)} &:= \text{UPD}_v^{(\text{init},1)} \left[V_v^{(\text{init},0)}, A_v^\top \lambda, Q_v x, \sigma\mu \right] \\ &= \left(\frac{\sigma\mu}{V_v^{(\text{init},0)} \begin{bmatrix} 1 \\ 0 \\ 0 \end{bmatrix}} - Q_v x + A_v^\top \lambda - V_v^{(\text{init},0)} \begin{bmatrix} 0 \\ 0 \\ 1 \end{bmatrix} \right) \begin{bmatrix} 1 & 1 & 0 & 0 & 0 \end{bmatrix} \\ &\quad + V_v^{(\text{init},0)} \begin{bmatrix} 0 & 0 & 0 & 1 & 0 \\ 0 & 0 & 0 & 0 & 1 \\ 0 & 0 & 0 & 0 & 0 \end{bmatrix} \\ &= \begin{bmatrix} \frac{\sigma\mu}{x_v} - Q_v x + A_v^\top \lambda - c_v & \frac{\sigma\mu}{x_v} - Q_v x + A_v^\top \lambda - c_v & 0 & x_v & s_v \end{bmatrix} \in \mathbb{R}^5, \end{aligned}$$

giving us a row vector for node v .

Similarly, we need the result $Ax - b$ for the initialization of the constraint nodes. Notice that Ax is a simple graph convolution from the variable to the constraint nodes. We construct the message functions for each constraint node $c \in C(I)$,

$$\text{MSG}_{v \rightarrow c}^{(\text{init},1)} \left(V_v^{(\text{init},0)}, A_{cv} \right) := A_{cv} V_v^{(\text{init},0)} \begin{bmatrix} 1 \\ 0 \\ 0 \end{bmatrix} = A_{cv} x_v, \forall v \in N(c) \cap V(I),$$

and the aggregation function,

$$\text{AGG}_{v \rightarrow c}^{(\text{init},1)}(\{\{\mathbf{A}_{cv}\mathbf{x}_v \mid v \in N(c) \cap V(I)\}\}) := \sum_{v \in N(c) \cap V(I)} \mathbf{A}_{cv}\mathbf{x}_v = \mathbf{A}_c\mathbf{x},$$

and the update function,

$$\begin{aligned} \mathbf{C}_c^{(\text{init},1)} &:= \text{UPD}_c^{(\text{init},1)}\left[\mathbf{C}_c^{(\text{init},0)}, \mathbf{A}_c\mathbf{x}\right] \\ &= \mathbf{A}_c\mathbf{x} - \mathbf{C}_c^{(\text{init},0)} \begin{bmatrix} 0 \\ 1 \end{bmatrix} \\ &= \mathbf{A}_c\mathbf{x} - \mathbf{b}_c. \end{aligned}$$

We get $\mathbf{A}\mathbf{x} - \mathbf{b}$ by stacking up all the nodes $c \in C(I)$. Still, we would like to store the vector $\boldsymbol{\lambda}$ in the updated node embeddings, and initialize $\mathbf{p}^{(0)}$ and $\mathbf{w}^{(0)}$. Hence, we modify the update function as

$$\begin{aligned} \mathbf{C}_c^{(\text{init},1)} &:= \text{UPD}_c^{(\text{init},1)}\left[\mathbf{C}_c^{(\text{init},0)}, \mathbf{A}_c\mathbf{x}\right] \\ &= \left(\mathbf{A}_c\mathbf{x} - \mathbf{C}_c^{(\text{init},0)} \begin{bmatrix} 0 \\ 1 \end{bmatrix}\right) \begin{bmatrix} 1 & 1 & 0 & 0 \end{bmatrix} \\ &\quad + \mathbf{C}_c^{(\text{init},0)} \begin{bmatrix} 0 & 0 & 0 & 1 \\ 0 & 0 & 0 & 0 \end{bmatrix} \\ &= \begin{bmatrix} \mathbf{A}_c\mathbf{x} - \mathbf{b}_c & \mathbf{A}_c\mathbf{x} - \mathbf{b}_c & 0 & \boldsymbol{\lambda}_c \end{bmatrix} \in \mathbb{R}^4. \end{aligned}$$

Thus, we accomplish the the initialization of $\mathbf{r}^{(0)}$, $\mathbf{p}^{(0)}$, $\mathbf{w}^{(0)}$ with one message-passing step. We notice that we can always split a joint vector, e.g., $\mathbf{r} \in \mathbb{R}^{n+m}$ (superscript omitted), into $\mathbf{r} = \begin{bmatrix} \mathbf{r}_1 \in \mathbb{R}^n \\ \mathbf{r}_2 \in \mathbb{R}^m \end{bmatrix}$ with \mathbf{r}_1 and \mathbf{r}_2 stored in variable and constraint nodes. Therefore, we will always refer to their two distributed parts as $\mathbf{r}_1, \mathbf{r}_2$ from now on, same with the vectors \mathbf{p}, \mathbf{w} .

After the lines 4-6 in Algorithm 6, we now have the node embedding matrices

$$\begin{aligned} \mathbf{V}^{(\text{init},1)} &:= \begin{bmatrix} \mathbf{r}_1^{(0)} & \mathbf{p}_1^{(0)} & \mathbf{w}_1^{(0)} & \mathbf{x} & \mathbf{s} \end{bmatrix} \in \mathbb{R}^{n \times 5} \\ \mathbf{C}^{(\text{init},1)} &:= \begin{bmatrix} \mathbf{r}_2^{(0)} & \mathbf{p}_2^{(0)} & \mathbf{w}_2^{(0)} & \boldsymbol{\lambda} \end{bmatrix} \in \mathbb{R}^{m \times 4}, \end{aligned}$$

which we now redefine as $\mathbf{V}^{(0)}$ and $\mathbf{C}^{(0)}$, and we do not care about $\mathbf{G}^{(0)}$ at the moment. Now, we are ready for the iterations in Algorithm 6.

Line 8 Let us look at each iteration t in Algorithm 6. With the information of $\mathbf{r}_1^{(t-1)}, \mathbf{r}_2^{(t-1)}$ already in the nodes, the numerator of $\alpha^{(t)}$, $\mathbf{r}^{(t-1)\top} \mathbf{r}^{(t-1)} = \mathbf{r}_1^{(t-1)\top} \mathbf{r}_1^{(t-1)} + \mathbf{r}_2^{(t-1)\top} \mathbf{r}_2^{(t-1)}$ can be computed with one convolution from variable and constraint nodes to the global node. The right part of the denominator, $\mathbf{P}\mathbf{r}^{(t-1)} = \begin{bmatrix} \mathbf{Q} + \mathbf{X}^{-1}\mathbf{S} & -\mathbf{A}^\top \\ -\mathbf{A} & \mathbf{0} \end{bmatrix} \begin{bmatrix} \mathbf{r}_1^{(t-1)} \\ \mathbf{r}_2^{(t-1)} \end{bmatrix} = \begin{bmatrix} \mathbf{Q}\mathbf{r}_1^{(t-1)} + \frac{\mathbf{s}\mathbf{r}_1^{(t-1)}}{\mathbf{x}} - \mathbf{A}^\top \mathbf{r}_2^{(t-1)} \\ -\mathbf{A}\mathbf{r}_1^{(t-1)} \end{bmatrix}$, can be done with one step of message passing between variable and constraint nodes.

Following Equation (21), we can construct message functions from constraint nodes to variable nodes

$$\text{MSG}_{v \rightarrow c}^{(t,1)}\left(\mathbf{V}_v^{(t-1)}, \mathbf{A}_{cv}\right) := \mathbf{A}_{cv} \mathbf{V}_v^{(t-1)} \begin{bmatrix} 1 \\ 0 \\ 0 \\ 0 \\ 0 \end{bmatrix} = \mathbf{A}_{cv} \left(\mathbf{r}_1^{(t-1)}\right)_v, f v \in N(c) \cap V(I),$$

and aggregation function

$$\text{AGG}_{v \rightarrow c}^{(t,1)} \left(\left\{ \mathbf{A}_{cv} \left(\mathbf{r}_1^{(t-1)} \right)_v \mid v \in N(c) \cap V(I) \right\} \right) := \sum_{v \in N(c) \cap V(I)} \mathbf{A}_{cv} \left(\mathbf{r}_1^{(t-1)} \right)_v = \mathbf{A}_c \mathbf{r}_1^{(t-1)},$$

and the update function

$$\begin{aligned} \mathbf{C}_c^{(t,1)} &:= \text{UPD}_c^{(t,1)} \left[\mathbf{C}_c^{(t-1)}, \mathbf{A}_c \mathbf{r}_1^{(t-1)} \right] \\ &= \mathbf{A}_c \mathbf{r}_1^{(t-1)} \begin{bmatrix} -1 \\ 0 \\ 0 \\ 0 \\ 0 \end{bmatrix} + \mathbf{C}_c^{(t-1)} \begin{bmatrix} 0 & 1 & 0 & 0 & 0 \\ 0 & 0 & 1 & 0 & 0 \\ 0 & 0 & 0 & 1 & 0 \\ 0 & 0 & 0 & 0 & 1 \end{bmatrix} \\ &= \left[-\mathbf{A}_c \mathbf{r}_1^{(t-1)} \quad \left(\mathbf{r}_2^{(t-1)} \right)_c \quad \left(\mathbf{p}_2^{(t-1)} \right)_c \quad \left(\mathbf{w}_2^{(t-1)} \right)_c \quad \lambda_c \right]. \end{aligned} \quad (25)$$

For the other direction, i.e., from constraint nodes to variable nodes, we have message functions,

$$\begin{aligned} \text{MSG}_{c \rightarrow v}^{(t,1)} \left(\mathbf{C}_c^{(t-1)}, \mathbf{A}_{cv} \right) &:= \mathbf{A}_{cv} \mathbf{C}_c^{(t-1)} \begin{bmatrix} 1 \\ 0 \\ 0 \\ 0 \end{bmatrix} = \mathbf{A}_{cv} \left(\mathbf{r}_2^{(t-1)} \right)_c, \forall c \in N(v) \cap C(I) \\ \text{MSG}_{v \rightarrow v}^{(t,1)} \left(\mathbf{V}_v^{(t-1)}, \mathbf{Q}_{vu} \right) &:= \mathbf{Q}_{vu} \mathbf{V}_v^{(t-1)} \begin{bmatrix} 1 \\ 0 \\ 0 \\ 0 \\ 0 \end{bmatrix} = \mathbf{Q}_{vu} \left(\mathbf{r}_1^{(t-1)} \right)_u, \forall u \in N(v) \cap V(I), \end{aligned}$$

and aggregation function,

$$\begin{aligned} \text{AGG}_{c \rightarrow v}^{(t,1)} \left(\left\{ \mathbf{A}_{cv} \left(\mathbf{r}_2^{(t-1)} \right)_c \mid c \in N(v) \cap C(I) \right\} \right) &:= \sum_{c \in N(v) \cap C(I)} \mathbf{A}_{cv} \left(\mathbf{r}_2^{(t-1)} \right)_c = \mathbf{A}_v^\top \mathbf{r}_2^{(t-1)} \\ \text{AGG}_{v \rightarrow v}^{(t,1)} \left(\left\{ \mathbf{Q}_{vu} \left(\mathbf{r}_1^{(t-1)} \right)_u \mid u \in N(v) \cap V(I) \right\} \right) &:= \sum_{u \in N(v) \cap V(I)} \mathbf{Q}_{vu} \left(\mathbf{r}_1^{(t-1)} \right)_u = \mathbf{Q}_v \mathbf{r}_1^{(t-1)}, \end{aligned}$$

and the update function,

$$\begin{aligned} \mathbf{V}_v^{(t,1)} &:= \text{UPD}_v^{(t,1)} \left[\mathbf{V}_v^{(t-1)}, \mathbf{A}_v^\top \mathbf{r}_2^{(t-1)}, \mathbf{Q}_v \mathbf{r}_1^{(t-1)} \right] \\ &= \mathbf{V}_v^{(t-1)} \begin{bmatrix} 0 & 1 & 0 & 0 & 0 & 0 \\ 0 & 0 & 1 & 0 & 0 & 0 \\ 0 & 0 & 0 & 1 & 0 & 0 \\ 0 & 0 & 0 & 0 & 1 & 0 \\ 0 & 0 & 0 & 0 & 0 & 1 \end{bmatrix} \\ &\quad + \left(\begin{array}{c} \mathbf{V}_v^{(t-1)} \begin{bmatrix} 0 & 0 & 0 & 0 & 0 \\ 0 & 0 & 0 & 0 & 0 \\ 0 & 0 & 0 & 0 & 0 \\ 0 & 0 & 0 & 0 & 0 \\ 1 & 0 & 0 & 0 & 0 \end{bmatrix} \left(\mathbf{V}_v^{(t-1)} \right)^\top \\ \mathbf{Q}_v \mathbf{r}_1^{(t-1)} - \mathbf{A}_v^\top \mathbf{r}_2^{(t-1)} + \frac{\begin{bmatrix} 0 \\ 0 \\ 0 \\ 0 \\ 1 \\ 0 \end{bmatrix}}{\mathbf{V}_v^{(t-1)} \begin{bmatrix} 0 \\ 0 \\ 0 \\ 0 \\ 1 \\ 0 \end{bmatrix}} \end{array} \right) \begin{bmatrix} 1 & 0 & 0 & 0 & 0 & 0 \end{bmatrix} \\ &= \left[\mathbf{Q}_v \mathbf{r}_1^{(t-1)} - \mathbf{A}_v^\top \mathbf{r}_2^{(t-1)} + \frac{\mathbf{s}_v \left(\mathbf{r}_1^{(t-1)} \right)_v}{\mathbf{x}_v} \quad \left(\mathbf{r}_1^{(t-1)} \right)_v \quad \left(\mathbf{p}_1^{(t-1)} \right)_v \quad \left(\mathbf{w}_1^{(t-1)} \right)_v \quad \mathbf{x}_v \quad \mathbf{s}_v \right]. \end{aligned} \quad (26)$$

If we stack up the per-node embeddings in Equation (25) and Equation (26), we will have the matrix representation,

$$\begin{aligned}
 \mathbf{V}^{(t,1)} &:= \begin{bmatrix} \mathbf{Q}\mathbf{r}_1^{(t-1)} - \mathbf{A}^\top\mathbf{r}_2^{(t-1)} + \frac{\mathbf{s}\mathbf{r}_1^{(t-1)}}{\mathbf{x}} & \mathbf{r}_1^{(t-1)} & \mathbf{p}_1^{(t-1)} & \mathbf{w}_1^{(t-1)} & \mathbf{x} & \mathbf{s} \end{bmatrix} \\
 &= \begin{bmatrix} (\mathbf{P}\mathbf{r}^{(t-1)})_1 & \mathbf{r}_1^{(t-1)} & \mathbf{p}_1^{(t-1)} & \mathbf{w}_1^{(t-1)} & \mathbf{x} & \mathbf{s} \end{bmatrix} \\
 \mathbf{C}^{(t,1)} &:= \begin{bmatrix} -\mathbf{A}\mathbf{r}_1^{(t-1)} & \mathbf{r}_2^{(t-1)} & \mathbf{p}_2^{(t-1)} & \mathbf{w}_2^{(t-1)} & \boldsymbol{\lambda} \end{bmatrix} \\
 &= \begin{bmatrix} (\mathbf{P}\mathbf{r}^{(t-1)})_2 & \mathbf{r}_2^{(t-1)} & \mathbf{p}_2^{(t-1)} & \mathbf{w}_2^{(t-1)} & \boldsymbol{\lambda} \end{bmatrix}.
 \end{aligned}$$

Further, $\mathbf{r}^{(t-1)\top}\mathbf{P}\mathbf{r}^{(t-1)} = \begin{bmatrix} \mathbf{r}_1^{(t-1)} & \mathbf{r}_2^{(t-1)} \end{bmatrix} \begin{bmatrix} (\mathbf{P}\mathbf{r}^{(t-1)})_1 \\ (\mathbf{P}\mathbf{r}^{(t-1)})_2 \end{bmatrix}$ can be computed with one additional message passing from variable and constraint nodes to the global node. Together with the numerator $\mathbf{r}^{(t-1)\top}\mathbf{r}^{(t-1)}$, we can now construct the functions for the global node. Hence, the message function are set to,

$$\begin{aligned}
 \text{MSG}_{\mathbf{c} \rightarrow \mathbf{g}}^{(t,2)}(\mathbf{C}_c^{(t,1)}) &:= \mathbf{C}_c^{(t,1)} \begin{bmatrix} 0 & 1 & 0 & 0 & 0 \\ 0 & 0 & 0 & 0 & 0 \\ 0 & 0 & 0 & 0 & 0 \\ 0 & 0 & 0 & 0 & 0 \\ 0 & 0 & 0 & 0 & 0 \end{bmatrix} (\mathbf{C}_c^{(t,1)})^\top \begin{bmatrix} 1 & 0 \end{bmatrix} \\
 &+ \mathbf{C}_c^{(t,1)} \begin{bmatrix} 0 & 0 & 0 & 0 & 0 \\ 0 & 1 & 0 & 0 & 0 \\ 0 & 0 & 0 & 0 & 0 \\ 0 & 0 & 0 & 0 & 0 \\ 0 & 0 & 0 & 0 & 0 \end{bmatrix} (\mathbf{C}_c^{(t,1)})^\top \begin{bmatrix} 0 & 1 \end{bmatrix} \\
 &= \left[((\mathbf{P}\mathbf{r}^{(t-1)})_2)_c (\mathbf{r}_2^{(t-1)})_c \quad (\mathbf{r}_2^{(t-1)})_c^2 \right], \forall c \in C(I), \\
 \text{MSG}_{\mathbf{v} \rightarrow \mathbf{g}}^{(t,2)}(\mathbf{V}_v^{(t,1)}) &:= \mathbf{V}_v^{(t,1)} \begin{bmatrix} 0 & 1 & 0 & 0 & 0 & 0 \\ 0 & 0 & 0 & 0 & 0 & 0 \\ 0 & 0 & 0 & 0 & 0 & 0 \\ 0 & 0 & 0 & 0 & 0 & 0 \\ 0 & 0 & 0 & 0 & 0 & 0 \\ 0 & 0 & 0 & 0 & 0 & 0 \end{bmatrix} (\mathbf{V}_v^{(t,1)})^\top \begin{bmatrix} 1 & 0 \end{bmatrix} \\
 &+ \mathbf{V}_v^{(t,1)} \begin{bmatrix} 0 & 0 & 0 & 0 & 0 & 0 \\ 0 & 1 & 0 & 0 & 0 & 0 \\ 0 & 0 & 0 & 0 & 0 & 0 \\ 0 & 0 & 0 & 0 & 0 & 0 \\ 0 & 0 & 0 & 0 & 0 & 0 \\ 0 & 0 & 0 & 0 & 0 & 0 \end{bmatrix} (\mathbf{V}_v^{(t,1)})^\top \begin{bmatrix} 0 & 1 \end{bmatrix} \\
 &= \left[((\mathbf{P}\mathbf{r}^{(t-1)})_1)_v (\mathbf{r}_1^{(t-1)})_v \quad (\mathbf{r}_1^{(t-1)})_v^2 \right], \forall v \in V(I),
 \end{aligned}$$

and the aggregation function for the global node is,

$$\begin{aligned}
 \text{AGG}_{\mathcal{V} \rightarrow \mathcal{g}}^{(t,2)} & \left(\left\{ \left[\left((\mathbf{P}\mathbf{r}^{(t-1)})_1 \right)_v \left(\mathbf{r}_1^{(t-1)} \right)_v \left(\mathbf{r}_1^{(t-1)} \right)_v^2 \mid v \in V(I) \right\} \right) \\
 & := \sum_{v \in V(I)} \left[\left((\mathbf{P}\mathbf{r}^{(t-1)})_1 \right)_v \left(\mathbf{r}_1^{(t-1)} \right)_v \left(\mathbf{r}_1^{(t-1)} \right)_v^2 \right] \\
 & = \left[\left(\mathbf{r}_1^{(t-1)} \right)^\top (\mathbf{P}\mathbf{r}^{(t-1)})_1 \left(\mathbf{r}_1^{(t-1)} \right)^\top \mathbf{r}_1^{(t-1)} \right], \\
 \text{AGG}_{\mathcal{C} \rightarrow \mathcal{g}}^{(t,2)} & \left(\left\{ \left[\left((\mathbf{P}\mathbf{r}^{(t-1)})_2 \right)_c \left(\mathbf{r}_2^{(t-1)} \right)_c \left(\mathbf{r}_2^{(t-1)} \right)_c^2 \mid c \in C(I) \right\} \right) \\
 & := \sum_{c \in C(I)} \left[\left((\mathbf{P}\mathbf{r}^{(t-1)})_2 \right)_c \left(\mathbf{r}_2^{(t-1)} \right)_c \left(\mathbf{r}_2^{(t-1)} \right)_c^2 \right] \\
 & = \left[\left(\mathbf{r}_2^{(t-1)} \right)^\top (\mathbf{P}\mathbf{r}^{(t-1)})_2 \left(\mathbf{r}_2^{(t-1)} \right)^\top \mathbf{r}_2^{(t-1)} \right].
 \end{aligned}$$

The update function for the global node, without using the previous state of $\mathbf{G}^{(t-1)}$,

$$\begin{aligned}
 \mathbf{G}^{(t,2)} & := \text{UPD}_{\mathcal{g}}^{(t,2)} \left[\left[\left(\mathbf{r}_1^{(t-1)} \right)^\top (\mathbf{P}\mathbf{r}^{(t-1)})_1 \left(\mathbf{r}_1^{(t-1)} \right)^\top \mathbf{r}_1^{(t-1)} \right], \right. \\
 & \left. \left[\left(\mathbf{r}_2^{(t-1)} \right)^\top (\mathbf{P}\mathbf{r}^{(t-1)})_2 \left(\mathbf{r}_2^{(t-1)} \right)^\top \mathbf{r}_2^{(t-1)} \right] \right] \\
 & = \frac{\left(\left[\left(\mathbf{r}_1^{(t-1)} \right)^\top (\mathbf{P}\mathbf{r}^{(t-1)})_1 \left(\mathbf{r}_1^{(t-1)} \right)^\top \mathbf{r}_1^{(t-1)} \right] + \left[\left(\mathbf{r}_2^{(t-1)} \right)^\top (\mathbf{P}\mathbf{r}^{(t-1)})_2 \left(\mathbf{r}_2^{(t-1)} \right)^\top \mathbf{r}_2^{(t-1)} \right] \right) \begin{bmatrix} 0 \\ 1 \end{bmatrix}}{\left(\left[\left(\mathbf{r}_1^{(t-1)} \right)^\top (\mathbf{P}\mathbf{r}^{(t-1)})_1 \left(\mathbf{r}_1^{(t-1)} \right)^\top \mathbf{r}_1^{(t-1)} \right] + \left[\left(\mathbf{r}_2^{(t-1)} \right)^\top (\mathbf{P}\mathbf{r}^{(t-1)})_2 \left(\mathbf{r}_2^{(t-1)} \right)^\top \mathbf{r}_2^{(t-1)} \right] \right) \begin{bmatrix} 1 \\ 0 \end{bmatrix}} \\
 & = \frac{\left(\mathbf{r}_1^{(t-1)} \right)^\top \mathbf{r}_1^{(t-1)} + \left(\mathbf{r}_2^{(t-1)} \right)^\top \mathbf{r}_2^{(t-1)}}{\left(\mathbf{r}_1^{(t-1)} \right)^\top (\mathbf{P}\mathbf{r}^{(t-1)})_1 + \left(\mathbf{r}_2^{(t-1)} \right)^\top (\mathbf{P}\mathbf{r}^{(t-1)})_2} = \frac{\left(\mathbf{r}^{(t-1)} \right)^\top \mathbf{r}^{(t-1)}}{\left(\mathbf{r}^{(t-1)} \right)^\top \mathbf{P}\mathbf{r}^{(t-1)}} = \alpha^{(t)}.
 \end{aligned}$$

Thus, the calculation of $\alpha^{(t)}$ in line 8 in Algorithm 6 consists of two steps of message passing, with the result stored in the global node as $\mathbf{G}^{(t,2)}$ after the second message passing step. As for $\mathbf{V}^{(t,2)}$ and $\mathbf{C}^{(t,2)}$, we can discard the intermediate matrix-vector product $\mathbf{P}\mathbf{r}^{(t-1)}$ by designing a simple update function,

$$\begin{aligned}
 \mathbf{V}_v^{(t,2)} & := \text{UPD}_{\mathcal{V}}^{(t,2)} \left[\mathbf{V}_v^{(t,1)} \right] \\
 & = \mathbf{V}_v^{(t,1)} \begin{bmatrix} 0 & 0 & 0 & 0 & 0 \\ 1 & 0 & 0 & 0 & 0 \\ 0 & 1 & 0 & 0 & 0 \\ 0 & 0 & 1 & 0 & 0 \\ 0 & 0 & 0 & 1 & 0 \\ 0 & 0 & 0 & 0 & 1 \end{bmatrix} \\
 & = \left[\left(\mathbf{r}_1^{(t-1)} \right)_v \left(\mathbf{p}_1^{(t-1)} \right)_v \left(\mathbf{w}_1^{(t-1)} \right)_v \quad \mathbf{x}_v \quad \mathbf{s}_v \right], \\
 \mathbf{C}_c^{(t,2)} & := \text{UPD}_{\mathcal{C}}^{(t,2)} \left[\mathbf{C}_c^{(t,1)} \right] \\
 & = \mathbf{C}_c^{(t,1)} \begin{bmatrix} 0 & 0 & 0 & 0 \\ 1 & 0 & 0 & 0 \\ 0 & 1 & 0 & 0 \\ 0 & 0 & 1 & 0 \\ 0 & 0 & 0 & 1 \end{bmatrix} \\
 & = \left[\left(\mathbf{r}_2^{(t-1)} \right)_c \left(\mathbf{p}_2^{(t-1)} \right)_c \left(\mathbf{w}_2^{(t-1)} \right)_c \quad \boldsymbol{\lambda}_c \right].
 \end{aligned}$$

To quickly recap, after line 8, we have

$$\begin{aligned}\mathbf{V}^{(t,2)} &:= \begin{bmatrix} \mathbf{r}_1^{(t-1)} & \mathbf{p}_1^{(t-1)} & \mathbf{w}_1^{(t-1)} & \mathbf{x} & \mathbf{s} \end{bmatrix} \\ \mathbf{C}^{(t,2)} &:= \begin{bmatrix} \mathbf{r}_2^{(t-1)} & \mathbf{p}_2^{(t-1)} & \mathbf{w}_2^{(t-1)} & \boldsymbol{\lambda} \end{bmatrix} \\ \mathbf{G}^{(t,2)} &:= \alpha^{(t)}.\end{aligned}$$

Line 9 The update of $\mathbf{w}^{(t-1)}$ in line 9 is quite simple by updating the variable and constraint node embeddings with the scalar $\alpha^{(t)}$ in the global node, so one single step of message passing. We can define the message from the global node as,

$$\begin{aligned}\text{MSG}_{\mathbf{g} \rightarrow \mathbf{v}}^{(t,3)}(\mathbf{G}^{(t,2)}) &:= \mathbf{G}^{(t,2)} = \alpha^{(t)} \\ \text{MSG}_{\mathbf{g} \rightarrow \mathbf{c}}^{(t,3)}(\mathbf{G}^{(t,2)}) &:= \mathbf{G}^{(t,2)} = \alpha^{(t)}.\end{aligned}$$

Then, the variable and constraint nodes update their embeddings locally,

$$\begin{aligned}\mathbf{V}_v^{(t,3)} &:= \text{UPD}_v^{(t,3)}[\mathbf{V}_v^{(t,2)}, \alpha^{(t)}] \\ &= \mathbf{V}_v^{(t,2)} + \alpha^{(t)} \mathbf{V}_v^{(t,2)} \begin{bmatrix} 0 & 0 & 0 & 0 & 0 \\ 0 & 0 & 1 & 0 & 0 \\ 0 & 0 & 0 & 0 & 0 \\ 0 & 0 & 0 & 0 & 0 \\ 0 & 0 & 0 & 0 & 0 \end{bmatrix} \\ &= \begin{bmatrix} \left(\mathbf{r}_1^{(t-1)}\right)_v & \left(\mathbf{p}_1^{(t-1)}\right)_v & \left(\mathbf{w}_1^{(t-1)}\right)_v & \mathbf{x}_v & \mathbf{s}_v \end{bmatrix} \\ &\quad + \alpha^{(t)} \begin{bmatrix} 0 & 0 & \left(\mathbf{p}_1^{(t-1)}\right)_v & 0 & 0 \end{bmatrix} \\ &= \begin{bmatrix} \left(\mathbf{r}_1^{(t-1)}\right)_v & \left(\mathbf{p}_1^{(t-1)}\right)_v & \left(\mathbf{w}_1^{(t)}\right)_v & \mathbf{x}_v & \mathbf{s}_v \end{bmatrix}. \\ \mathbf{C}_c^{(t,3)} &:= \text{UPD}_c^{(t,3)}[\mathbf{C}_c^{(t,2)}, \alpha^{(t)}] \\ &= \mathbf{C}_c^{(t,2)} + \alpha^{(t)} \mathbf{C}_c^{(t,2)} \begin{bmatrix} 0 & 0 & 0 & 0 \\ 0 & 0 & 1 & 0 \\ 0 & 0 & 0 & 0 \\ 0 & 0 & 0 & 0 \end{bmatrix} \\ &= \begin{bmatrix} \left(\mathbf{r}_2^{(t-1)}\right)_c & \left(\mathbf{p}_2^{(t-1)}\right)_c & \left(\mathbf{w}_2^{(t-1)}\right)_c & \boldsymbol{\lambda}_c \end{bmatrix} + \alpha^{(t)} \begin{bmatrix} 0 & 0 & \left(\mathbf{p}_2^{(t-1)}\right)_c & 0 \end{bmatrix} \\ &= \begin{bmatrix} \left(\mathbf{r}_2^{(t-1)}\right)_c & \left(\mathbf{p}_2^{(t-1)}\right)_c & \left(\mathbf{w}_2^{(t)}\right)_c & \boldsymbol{\lambda}_c \end{bmatrix}.\end{aligned}$$

Thereafter, we have the updated node embeddings,

$$\begin{aligned}\mathbf{V}^{(t,3)} &:= \begin{bmatrix} \mathbf{r}_1^{(t-1)} & \mathbf{p}_1^{(t-1)} & \mathbf{w}_1^{(t)} & \mathbf{x} & \mathbf{s} \end{bmatrix} \\ \mathbf{C}^{(t,3)} &:= \begin{bmatrix} \mathbf{r}_2^{(t-1)} & \mathbf{p}_2^{(t-1)} & \mathbf{w}_2^{(t)} & \boldsymbol{\lambda} \end{bmatrix}.\end{aligned}$$

Line 10 In line 10, the matrix-vector product $\mathbf{P}\mathbf{p}^{(t-1)} = \begin{bmatrix} \mathbf{Q} + \mathbf{X}^{-1}\mathbf{S} & -\mathbf{A}^\top \\ -\mathbf{A} & \mathbf{0} \end{bmatrix} \begin{bmatrix} \mathbf{p}_1^{(t-1)} \\ \mathbf{p}_2^{(t-1)} \end{bmatrix} = \begin{bmatrix} \mathbf{Q}\mathbf{p}_1^{(t-1)} + \frac{\mathbf{s}\mathbf{p}_1^{(t-1)}}{\mathbf{x}} - \mathbf{A}^\top\mathbf{p}_2^{(t-1)} \\ -\mathbf{A}\mathbf{p}_1^{(t-1)} \end{bmatrix} = \begin{bmatrix} (\mathbf{P}\mathbf{p}^{(t-1)})_1 \\ (\mathbf{P}\mathbf{p}^{(t-1)})_2 \end{bmatrix}$ can be done with one step of message passing, similar to the discussion of $\mathbf{P}\mathbf{r}^{(t-1)}$ above.

Explicitly, the message functions from constraint nodes to variable nodes,

$$\text{MSG}_{v \rightarrow c}^{(t,4)}\left(\mathbf{V}_v^{(t,3)}, \mathbf{A}_{cv}\right) := \mathbf{A}_{cv} \mathbf{V}_v^{(t,3)} \begin{bmatrix} 0 \\ 1 \\ 0 \\ 0 \\ 0 \end{bmatrix} = \mathbf{A}_{cv} \left(\mathbf{p}_1^{(t-1)}\right)_v, v \in N(c) \cap V(I),$$

and the aggregation function

$$\text{AGG}_{v \rightarrow c}^{(t,4)}\left(\left\{\mathbf{A}_{cv} \left(\mathbf{p}_1^{(t-1)}\right)_v \mid v \in N(c) \cap V(I)\right\}\right) := \sum_{v \in N(c) \cap V(I)} \mathbf{A}_{cv} \left(\mathbf{p}_1^{(t-1)}\right)_v = \mathbf{A}_c \mathbf{p}_1^{(t-1)},$$

and the update function,

$$\begin{aligned} \mathbf{C}_c^{(t,4)} &:= \text{UPD}_c^{(t,4)}\left[\mathbf{C}_c^{(t,3)}, \mathbf{A}_c \mathbf{p}_1^{(t-1)}\right] \\ &= \mathbf{A}_c \mathbf{p}_1^{(t-1)} \begin{bmatrix} -1 \\ 0 \\ 0 \\ 0 \\ 0 \end{bmatrix} + \mathbf{C}_c^{(t,3)} \begin{bmatrix} 0 & 1 & 0 & 0 & 0 \\ 0 & 0 & 1 & 0 & 0 \\ 0 & 0 & 0 & 1 & 0 \\ 0 & 0 & 0 & 0 & 1 \end{bmatrix} \\ &= \left[-\mathbf{A}_c \mathbf{p}_1^{(t-1)} \quad \left(\mathbf{r}_2^{(t-1)}\right)_c \quad \left(\mathbf{p}_2^{(t-1)}\right)_c \quad \left(\mathbf{w}_2^{(t)}\right)_c \quad \lambda_c \right] \\ &= \left[\left(\left(\mathbf{P}\mathbf{r}^{(t-1)}\right)_2\right)_c \quad \left(\mathbf{r}_2^{(t-1)}\right)_c \quad \left(\mathbf{p}_2^{(t-1)}\right)_c \quad \left(\mathbf{w}_2^{(t)}\right)_c \quad \lambda_c \right]. \end{aligned}$$

From constraint nodes to variable nodes, we have the message functions,

$$\begin{aligned} \text{MSG}_{c \rightarrow v}^{(t,4)}\left(\mathbf{C}_c^{(t,3)}, \mathbf{A}_{cv}\right) &:= \mathbf{A}_{cv} \mathbf{C}_c^{(t,3)} \begin{bmatrix} 0 \\ 1 \\ 0 \\ 0 \end{bmatrix} = \mathbf{A}_{cv} \left(\mathbf{p}_2^{(t-1)}\right)_c, c \in N(v) \cap C(I), \\ \text{MSG}_{v \rightarrow v}^{(t,4)}\left(\mathbf{V}_u^{(t,3)}, \mathbf{Q}_{vu}\right) &:= \mathbf{Q}_{vu} \mathbf{V}_u^{(t,3)} \begin{bmatrix} 0 \\ 1 \\ 0 \\ 0 \\ 0 \end{bmatrix} = \mathbf{Q}_{vu} \left(\mathbf{p}_1^{(t-1)}\right)_u, u \in N(v) \cap V(I), \end{aligned}$$

and the aggregation function,

$$\begin{aligned} \text{AGG}_{c \rightarrow v}^{(t,4)}\left(\left\{\mathbf{A}_{cv} \left(\mathbf{p}_2^{(t-1)}\right)_c \mid c \in N(v) \cap C(I)\right\}\right) &:= \sum_{c \in N(v) \cap C(I)} \mathbf{A}_{cv} \left(\mathbf{p}_2^{(t-1)}\right)_c = \mathbf{A}_v^T \mathbf{p}_2^{(t-1)}, \\ \text{AGG}_{v \rightarrow v}^{(t,4)}\left(\left\{\mathbf{Q}_{vu} \left(\mathbf{p}_1^{(t-1)}\right)_u \mid u \in N(v) \cap V(I)\right\}\right) &:= \sum_{u \in N(v) \cap V(I)} \mathbf{Q}_{vu} \left(\mathbf{p}_1^{(t-1)}\right)_u = \mathbf{Q}_v \mathbf{p}_1^{(t-1)}, \end{aligned}$$

and the update function,

$$\begin{aligned}
 \mathbf{V}_v^{(t,4)} &:= \text{UPD}_v^{(t,4)} \left[\mathbf{V}_v^{(t,3)}, \mathbf{A}_v^\top \mathbf{p}_2^{(t-1)}, \mathbf{Q}_v \mathbf{p}_1^{(t-1)} \right] \\
 &= \mathbf{V}_v^{(t,3)} \begin{bmatrix} 0 & 1 & 0 & 0 & 0 & 0 \\ 0 & 0 & 1 & 0 & 0 & 0 \\ 0 & 0 & 0 & 1 & 0 & 0 \\ 0 & 0 & 0 & 0 & 1 & 0 \\ 0 & 0 & 0 & 0 & 0 & 1 \end{bmatrix} \\
 &\quad + \left(\begin{array}{c} \mathbf{Q}_v \mathbf{p}_1^{(t-1)} - \mathbf{A}_v^\top \mathbf{p}_2^{(t-1)} + \frac{\mathbf{V}_v^{(t,3)} \begin{bmatrix} 0 & 0 & 0 & 0 & 0 \\ 0 & 0 & 0 & 0 & 1 \\ 0 & 0 & 0 & 0 & 0 \\ 0 & 0 & 0 & 0 & 0 \\ 0 & 0 & 0 & 0 & 0 \end{bmatrix} (\mathbf{V}_v^{(t,3)})^\top}{\mathbf{V}_v^{(t,3)} \begin{bmatrix} 0 \\ 0 \\ 0 \\ 1 \\ 0 \end{bmatrix}} \begin{bmatrix} 0 \\ 0 \\ 0 \\ 0 \\ 0 \end{bmatrix} \\ \hline \end{array} \right) [1 \ 0 \ 0 \ 0 \ 0 \ 0] \\
 &= \begin{bmatrix} \mathbf{Q}_v \mathbf{p}_1^{(t-1)} - \mathbf{A}_v^\top \mathbf{p}_2^{(t-1)} + \frac{\mathbf{s}_v (\mathbf{p}_1^{(t-1)})_v}{\mathbf{x}_v} & (\mathbf{r}_1^{(t-1)})_v & (\mathbf{p}_1^{(t-1)})_v & (\mathbf{w}_1^{(t)})_v & \mathbf{x}_v & \mathbf{s}_v \end{bmatrix} \\
 &= \left[((\mathbf{P}\mathbf{p}^{(t-1)})_1)_v \quad (\mathbf{r}_1^{(t-1)})_v \quad (\mathbf{p}_1^{(t-1)})_v \quad (\mathbf{w}_1^{(t)})_v \quad \mathbf{x}_v \quad \mathbf{s}_v \right].
 \end{aligned}$$

Now, we have updated node embeddings,

$$\begin{aligned}
 \mathbf{V}^{(t,4)} &:= \left[(\mathbf{P}\mathbf{p}^{(t-1)})_1 \quad \mathbf{r}_1^{(t-1)} \quad \mathbf{p}_1^{(t-1)} \quad \mathbf{w}_1^{(t)} \quad \mathbf{x} \quad \mathbf{s} \right], \\
 \mathbf{C}^{(t,4)} &:= \left[(\mathbf{P}\mathbf{p}^{(t-1)})_1 \quad \mathbf{r}_2^{(t-1)} \quad \mathbf{p}_2^{(t-1)} \quad \mathbf{w}_2^{(t)} \quad \boldsymbol{\lambda} \right], \\
 \mathbf{G}^{(t,4)} &:= \alpha^{(t)}.
 \end{aligned}$$

We notice that $\mathbf{G}^{(t,4)}$ is inherited from $\mathbf{G}^{(t,2)}$ as we have never updated it. We convey the message from $\mathbf{G}^{(t,4)}$ with an identity mapping,

$$\begin{aligned}
 \text{MSG}_{\mathbf{g} \rightarrow \mathbf{v}}^{(t,5)} \left(\mathbf{G}^{(t,4)} \right) &:= \mathbf{G}^{(t,4)} = \alpha^{(t)}, \\
 \text{MSG}_{\mathbf{g} \rightarrow \mathbf{c}}^{(t,5)} \left(\mathbf{G}^{(t,4)} \right) &:= \mathbf{G}^{(t,4)} = \alpha^{(t)}.
 \end{aligned}$$

Now, we can update the vector \mathbf{r} with a simple update function,

$$\begin{aligned}
 \mathbf{V}_v^{(t,5)} &:= \text{UPD}_v^{(t,5)} \left[\mathbf{V}_v^{(t,4)}, \alpha^{(t)} \right] \\
 &= \mathbf{V}_v^{(t,4)} \begin{bmatrix} 0 & 0 & 0 & 0 & 0 & 0 \\ 1 & 1 & 0 & 0 & 0 & 0 \\ 0 & 0 & 1 & 0 & 0 & 0 \\ 0 & 0 & 0 & 1 & 0 & 0 \\ 0 & 0 & 0 & 0 & 1 & 0 \\ 0 & 0 & 0 & 0 & 0 & 1 \end{bmatrix} - \alpha^{(t)} \mathbf{V}_v^{(t,4)} \begin{bmatrix} 1 & 0 & 0 & 0 & 0 & 0 \\ 0 & 0 & 0 & 0 & 0 & 0 \\ 0 & 0 & 0 & 0 & 0 & 0 \\ 0 & 0 & 0 & 0 & 0 & 0 \\ 0 & 0 & 0 & 0 & 0 & 0 \\ 0 & 0 & 0 & 0 & 0 & 0 \end{bmatrix} \\
 &= \left[(\mathbf{r}_1^{(t)})_v \quad (\mathbf{r}_1^{(t-1)})_v \quad (\mathbf{p}_1^{(t-1)})_v \quad (\mathbf{w}_1^{(t)})_v \quad \mathbf{x}_v \quad \mathbf{s}_v \right],
 \end{aligned}$$

and

$$\begin{aligned}
 \mathbf{C}_c^{(t,5)} &:= \text{UPD}_c^{(t,5)} \left[\mathbf{C}_c^{(t,4)}, \alpha^{(t)} \right] \\
 &= \mathbf{C}_c^{(t,4)} \begin{bmatrix} 0 & 0 & 0 & 0 & 0 \\ 1 & 1 & 0 & 0 & 0 \\ 0 & 0 & 1 & 0 & 0 \\ 0 & 0 & 0 & 1 & 0 \\ 0 & 0 & 0 & 0 & 1 \end{bmatrix} - \alpha^{(t)} \mathbf{C}_c^{(t,4)} \begin{bmatrix} 1 & 0 & 0 & 0 & 0 \\ 0 & 0 & 0 & 0 & 0 \\ 0 & 0 & 0 & 0 & 0 \\ 0 & 0 & 0 & 0 & 0 \\ 0 & 0 & 0 & 0 & 0 \end{bmatrix} \\
 &= \left[\left(\mathbf{r}_2^{(t)} \right)_c \quad \left(\mathbf{r}_2^{(t-1)} \right)_c \quad \left(\mathbf{p}_2^{(t-1)} \right)_c \quad \left(\mathbf{w}_2^{(t)} \right)_c \quad \lambda_c \right].
 \end{aligned}$$

We now obtain the node embeddings

$$\begin{aligned}
 \mathbf{V}^{(t,5)} &:= \begin{bmatrix} \mathbf{r}_1^{(t)} & \mathbf{r}_1^{(t-1)} & \mathbf{p}_1^{(t-1)} & \mathbf{w}_1^{(t)} & \mathbf{x} & \mathbf{s} \end{bmatrix} \\
 \mathbf{C}^{(t,5)} &:= \begin{bmatrix} \mathbf{r}_2^{(t)} & \mathbf{r}_2^{(t-1)} & \mathbf{p}_2^{(t-1)} & \mathbf{w}_2^{(t)} & \lambda \end{bmatrix}.
 \end{aligned}$$

Line 11 Line 11 can also be done with one step from variable and constraint nodes to the global node. The message functions are,

$$\begin{aligned}
 \text{MSG}_{v \rightarrow g}^{(t,6)} \left(\mathbf{V}_v^{(t,5)} \right) &:= \mathbf{V}_v^{(t,5)} \begin{bmatrix} 1 & 0 & 0 & 0 & 0 & 0 \\ 0 & 0 & 0 & 0 & 0 & 0 \\ 0 & 0 & 0 & 0 & 0 & 0 \\ 0 & 0 & 0 & 0 & 0 & 0 \\ 0 & 0 & 0 & 0 & 0 & 0 \\ 0 & 0 & 0 & 0 & 0 & 0 \end{bmatrix} \left(\mathbf{V}_v^{(t,5)} \right)^\top \begin{bmatrix} 1 & 0 \end{bmatrix} \\
 &+ \mathbf{V}_v^{(t,5)} \begin{bmatrix} 0 & 0 & 0 & 0 & 0 & 0 \\ 0 & 1 & 0 & 0 & 0 & 0 \\ 0 & 0 & 0 & 0 & 0 & 0 \\ 0 & 0 & 0 & 0 & 0 & 0 \\ 0 & 0 & 0 & 0 & 0 & 0 \\ 0 & 0 & 0 & 0 & 0 & 0 \end{bmatrix} \left(\mathbf{V}_v^{(t,5)} \right)^\top \begin{bmatrix} 0 & 1 \end{bmatrix} \\
 &= \left[\left(\mathbf{r}_1^{(t)} \right)_v^2 \quad \left(\mathbf{r}_1^{(t-1)} \right)_v^2 \right], v \in V(I), \\
 \text{MSG}_{c \rightarrow g}^{(t,6)} \left(\mathbf{C}_c^{(t,5)} \right) &:= \mathbf{C}_c^{(t,5)} \begin{bmatrix} 1 & 0 & 0 & 0 & 0 \\ 0 & 0 & 0 & 0 & 0 \\ 0 & 0 & 0 & 0 & 0 \\ 0 & 0 & 0 & 0 & 0 \\ 0 & 0 & 0 & 0 & 0 \end{bmatrix} \left(\mathbf{C}_c^{(t,5)} \right)^\top \begin{bmatrix} 1 & 0 \end{bmatrix} \\
 &+ \mathbf{C}_c^{(t,5)} \begin{bmatrix} 0 & 0 & 0 & 0 & 0 \\ 0 & 1 & 0 & 0 & 0 \\ 0 & 0 & 0 & 0 & 0 \\ 0 & 0 & 0 & 0 & 0 \\ 0 & 0 & 0 & 0 & 0 \end{bmatrix} \left(\mathbf{C}_c^{(t,5)} \right)^\top \begin{bmatrix} 0 & 1 \end{bmatrix} \\
 &= \left[\left(\mathbf{r}_2^{(t)} \right)_c^2 \quad \left(\mathbf{r}_2^{(t-1)} \right)_c^2 \right], c \in C(I),
 \end{aligned}$$

and the aggregation function for the global node is,

$$\begin{aligned}
 \text{AGG}_{v \rightarrow g}^{(t,6)} & \left(\left\{ \left[\left(\mathbf{r}_1^{(t)} \right)_v^2 \quad \left(\mathbf{r}_1^{(t-1)} \right)_v^2 \right] \mid v \in V(I) \right\} \right) \\
 & := \sum_{v \in V(I)} \left[\left(\mathbf{r}_1^{(t)} \right)_v^2 \quad \left(\mathbf{r}_1^{(t-1)} \right)_v^2 \right] \\
 & = \left[\left(\mathbf{r}_1^{(t)} \right)^\top \mathbf{r}_1^{(t)} \quad \left(\mathbf{r}_1^{(t-1)} \right)^\top \mathbf{r}_1^{(t-1)} \right], \\
 \text{AGG}_{c \rightarrow g}^{(t,6)} & \left(\left\{ \left[\left(\mathbf{r}_2^{(t)} \right)_c^2 \quad \left(\mathbf{r}_2^{(t-1)} \right)_c^2 \right] \mid c \in C(I) \right\} \right) \\
 & := \sum_{c \in C(I)} \left[\left(\mathbf{r}_2^{(t)} \right)_c^2 \quad \left(\mathbf{r}_2^{(t-1)} \right)_c^2 \right] \\
 & = \left[\left(\mathbf{r}_2^{(t)} \right)^\top \mathbf{r}_2^{(t)} \quad \left(\mathbf{r}_2^{(t-1)} \right)^\top \mathbf{r}_2^{(t-1)} \right],
 \end{aligned}$$

and the update function for the global node,

$$\begin{aligned}
 \mathbf{G}^{(t,6)} & := \text{UPD}_g^{(t,6)} \left[\left[\left(\mathbf{r}_1^{(t)} \right)^\top \mathbf{r}_1^{(t)} \quad \left(\mathbf{r}_1^{(t-1)} \right)^\top \mathbf{r}_1^{(t-1)} \right], \left[\left(\mathbf{r}_2^{(t)} \right)^\top \mathbf{r}_2^{(t)} \quad \left(\mathbf{r}_2^{(t-1)} \right)^\top \mathbf{r}_2^{(t-1)} \right] \right] \\
 & = \frac{\left(\left[\left(\mathbf{r}_1^{(t)} \right)^\top \mathbf{r}_1^{(t)} \quad \left(\mathbf{r}_1^{(t-1)} \right)^\top \mathbf{r}_1^{(t-1)} \right] + \left[\left(\mathbf{r}_2^{(t)} \right)^\top \mathbf{r}_2^{(t)} \quad \left(\mathbf{r}_2^{(t-1)} \right)^\top \mathbf{r}_2^{(t-1)} \right] \right) \begin{bmatrix} 1 \\ 0 \end{bmatrix}}{\left(\left[\left(\mathbf{r}_1^{(t)} \right)^\top \mathbf{r}_1^{(t)} \quad \left(\mathbf{r}_1^{(t-1)} \right)^\top \mathbf{r}_1^{(t-1)} \right] + \left[\left(\mathbf{r}_2^{(t)} \right)^\top \mathbf{r}_2^{(t)} \quad \left(\mathbf{r}_2^{(t-1)} \right)^\top \mathbf{r}_2^{(t-1)} \right] \right) \begin{bmatrix} 0 \\ 1 \end{bmatrix}} \\
 & = \frac{\left(\mathbf{r}_1^{(t)} \right)^\top \mathbf{r}_1^{(t)} + \left(\mathbf{r}_2^{(t)} \right)^\top \mathbf{r}_2^{(t)}}{\left(\mathbf{r}_1^{(t-1)} \right)^\top \mathbf{r}_1^{(t-1)} + \left(\mathbf{r}_2^{(t-1)} \right)^\top \mathbf{r}_2^{(t-1)}} = \frac{\left(\mathbf{r}^{(t)} \right)^\top \mathbf{r}^{(t)}}{\left(\mathbf{r}^{(t-1)} \right)^\top \mathbf{r}^{(t-1)}} = \beta^{(t)}.
 \end{aligned}$$

Hence, $\beta^{(t)}$ is stored in the global node. Meanwhile we can discard the unnecessary $\mathbf{r}^{(t-1)}$ with simple update function,

$$\begin{aligned}
 \mathbf{C}_c^{(t,6)} & := \text{UPD}_c^{(t,6)} \left[\mathbf{C}_c^{(t,5)} \right] \\
 & = \mathbf{C}_c^{(t,5)} \begin{bmatrix} 1 & 0 & 0 & 0 \\ 0 & 0 & 0 & 0 \\ 0 & 1 & 0 & 0 \\ 0 & 0 & 1 & 0 \\ 0 & 0 & 0 & 1 \end{bmatrix} \\
 & = \left[\left(\mathbf{r}_2^{(t)} \right)_c \quad \left(\mathbf{p}_2^{(t-1)} \right)_c \quad \left(\mathbf{w}_2^{(t)} \right)_c \quad \lambda_c \right],
 \end{aligned}$$

and,

$$\begin{aligned}
 \mathbf{V}_v^{(t,6)} & := \text{UPD}_v^{(t,6)} \left[\mathbf{V}_v^{(t,5)} \right] \\
 & = \mathbf{V}_v^{(t,5)} \begin{bmatrix} 1 & 0 & 0 & 0 & 0 \\ 0 & 0 & 0 & 0 & 0 \\ 0 & 1 & 0 & 0 & 0 \\ 0 & 0 & 1 & 0 & 0 \\ 0 & 0 & 0 & 1 & 0 \\ 0 & 0 & 0 & 0 & 1 \end{bmatrix} \\
 & = \left[\left(\mathbf{r}_1^{(t)} \right)_v \quad \left(\mathbf{p}_1^{(t-1)} \right)_v \quad \left(\mathbf{w}_1^{(t)} \right)_v \quad \mathbf{x}_v \quad \mathbf{s}_v \right],
 \end{aligned}$$

which leads us to,

$$\begin{aligned}
 \mathbf{V}^{(t,6)} & := \begin{bmatrix} \mathbf{r}_1^{(t)} & \mathbf{p}_1^{(t-1)} & \mathbf{w}_1^{(t)} & \mathbf{x} & \mathbf{s} \end{bmatrix} \\
 \mathbf{C}^{(t,6)} & := \begin{bmatrix} \mathbf{r}_2^{(t)} & \mathbf{p}_2^{(t-1)} & \mathbf{w}_2^{(t)} & \lambda \end{bmatrix},
 \end{aligned}$$

after stacking up the nodes.

Line 12 What is left now is updating $\mathbf{p}^{(t-1)}$ in line 12 with one message passing step. Again, we need to retrieve the information from the global node for all the nodes,

$$\begin{aligned}\text{MSG}_{\mathbf{g} \rightarrow \mathbf{v}}^{(t,7)}(\mathbf{G}^{(t,6)}) &:= \mathbf{G}^{(t,6)} = \beta^{(t)}, \\ \text{MSG}_{\mathbf{g} \rightarrow \mathbf{c}}^{(t,7)}(\mathbf{G}^{(t,6)}) &:= \mathbf{G}^{(t,6)} = \beta^{(t)}.\end{aligned}$$

Now, we update for the $\mathbf{p}^{(t-1)}$,

$$\begin{aligned}\mathbf{C}_c^{(t,7)} &:= \text{UPD}_c^{(t,7)}[\mathbf{C}_c^{(t,6)}, \beta^{(t)}] \\ &= \beta^{(t)} \mathbf{C}_c^{(t,6)} \begin{bmatrix} 0 & 0 & 0 & 0 \\ 0 & 1 & 0 & 0 \\ 0 & 0 & 0 & 0 \\ 0 & 0 & 0 & 0 \end{bmatrix} + \mathbf{C}_c^{(t,6)} \begin{bmatrix} 1 & 1 & 0 & 0 \\ 0 & 0 & 0 & 0 \\ 0 & 0 & 1 & 0 \\ 0 & 0 & 0 & 1 \end{bmatrix} \\ &= \begin{bmatrix} (\mathbf{r}_2^{(t)})_c & (\mathbf{p}_2^{(t)})_c & (\mathbf{w}_2^{(t)})_c & \lambda_c \end{bmatrix},\end{aligned}$$

and

$$\begin{aligned}\mathbf{V}_v^{(t,7)} &:= \text{UPD}_v^{(t,7)}[\mathbf{V}_v^{(t,6)}, \beta^{(t)}] \\ &= \beta^{(t)} \mathbf{V}_v^{(t,6)} \begin{bmatrix} 0 & 0 & 0 & 0 & 0 \\ 0 & 1 & 0 & 0 & 0 \\ 0 & 0 & 0 & 0 & 0 \\ 0 & 0 & 0 & 0 & 0 \\ 0 & 0 & 0 & 0 & 0 \end{bmatrix} + \mathbf{V}_v^{(t,6)} \begin{bmatrix} 1 & 1 & 0 & 0 & 0 \\ 0 & 0 & 0 & 0 & 0 \\ 0 & 0 & 1 & 0 & 0 \\ 0 & 0 & 0 & 1 & 0 \\ 0 & 0 & 0 & 0 & 1 \end{bmatrix} \\ &= \begin{bmatrix} (\mathbf{r}_1^{(t)})_v & (\mathbf{p}_1^{(t)})_v & (\mathbf{w}_1^{(t)})_v & \mathbf{x}_v & \mathbf{s}_v \end{bmatrix}.\end{aligned}$$

Finally, we have

$$\begin{aligned}\mathbf{V}^{(t)} &:= \mathbf{V}^{(t,7)} = \begin{bmatrix} \mathbf{r}_1^{(t)} & \mathbf{p}_1^{(t)} & \mathbf{w}_1^{(t)} & \mathbf{x} & \mathbf{s} \end{bmatrix} \\ \mathbf{C}^{(t)} &:= \mathbf{C}^{(t,7)} = \begin{bmatrix} \mathbf{r}_2^{(t)} & \mathbf{p}_2^{(t)} & \mathbf{w}_2^{(t)} & \lambda \end{bmatrix},\end{aligned}$$

and we can proceed with the next iteration.

In summary, the initialization of Algorithm 6 takes one step of message passing, while each iteration takes seven. Hence, the runtime complexity is $\mathcal{O}(m + n)$, i.e., linear time in the problem size. However, if we take a closer look at the UPD, MSG, AGG functions, we will notice they are specifically parametrized and shared across different t . Therefore, we need only 1 + 7, a constant number of message-passing layers, with the first executed once and the rest executed in a loop repeatedly.

At the end of the algorithm, we take the third column of the node embeddings $\mathbf{V}^{(n+m)}$ and $\mathbf{C}^{(n+m)}$ as the solution for $\Delta \mathbf{x}$ and $\Delta \lambda$.

□

Given the CG algorithm that can solve for $\Delta \mathbf{x}, \Delta \lambda$, we can construct the algorithm for solving the QP problem in Algorithm 7.

Theorem 4. *There exists an MPNN $f_{\text{MPNN,IPM}}$ composed of $\mathcal{O}(1)$ layers and $\mathcal{O}(m + n)$ successive message-passing steps that reproduces each iteration of Algorithm 7, in the sense that for any QP instance $I = (\mathbf{Q}, \mathbf{A}, \mathbf{b}, \mathbf{c})$ and any primal-dual point $(\mathbf{x}^{(t)}, \lambda^{(t)}, \mathbf{s}^{(t)})$ with $t > 0$, $f_{\text{MPNN,IPM}}$ maps the graph $G(I)$ carrying $[\mathbf{x}^{(t-1)}, \mathbf{s}^{(t-1)}]$ on the variable nodes, $[\lambda^{(t-1)}]$ on the constraint nodes. and $[\mu, \sigma]$ on the global node to the same graph $G(I)$ carrying the output $[\mathbf{x}^{(t)}, \mathbf{s}^{(t)}]$ and $[\lambda^{(t)}]$ of Algorithm 7 on the variable nodes and constraint nodes, respectively.*

Algorithm 7 Practical IPM for QPs

Require: An instance $(\mathbf{Q}, \mathbf{A}, \mathbf{b}, \mathbf{c})$, a barrier reduction hyperparameter $\sigma \in (0,1)$, initial solution $(\mathbf{x}^{(0)}, \boldsymbol{\lambda}^{(0)}, \mathbf{s}^{(0)})$ with $\mathbf{x}^{(0)}, \mathbf{s}^{(0)} > \mathbf{0}$ and $\boldsymbol{\mu}^{(0)} = \mathbf{x}^{(0)\top} \mathbf{s}^{(0)} / n$.

- 1: $t \leftarrow 1$
- 2: **repeat**
- 3: Compute $\Delta \mathbf{x}^{(t)}, \Delta \boldsymbol{\lambda}^{(t)}$ by solving Equation (20) using Algorithm 6
- 4: Compute $\Delta \mathbf{s}^{(t)}$ with Appendix A.6
- 5: $\alpha^{(t)} \leftarrow \min\{1, \sup\{\alpha \mid \mathbf{x}^{(t)} + \alpha \Delta \mathbf{x}^{(t)} \geq \mathbf{0}\}, \sup\{\alpha \mid \mathbf{s}^{(t)} + \alpha \Delta \mathbf{s}^{(t)} \geq \mathbf{0}\}\}$
- 6: $\mathbf{x}^{(t)} \leftarrow \mathbf{x}^{(t-1)} + 0.99\alpha^{(t)} \Delta \mathbf{x}^{(t)}$
- 7: $\mathbf{s}^{(t)} \leftarrow \mathbf{s}^{(t-1)} + 0.99\alpha^{(t)} \Delta \mathbf{s}^{(t)}$
- 8: $\boldsymbol{\lambda}^{(t)} \leftarrow \boldsymbol{\lambda}^{(t-1)} + 0.99\alpha^{(t)} \Delta \boldsymbol{\lambda}^{(t)}$
- 9: $\boldsymbol{\mu}^{(t)} \leftarrow \sigma \boldsymbol{\mu}^{(t-1)}$
- 10: $t \leftarrow t + 1$
- 11: **until** convergence of $(\mathbf{x}, \boldsymbol{\lambda}, \mathbf{s})$
- 12: **return** the point \mathbf{x}

Proof. For the details of the construction $G(I)$, we follow Lemma 3. At the beginning of the algorithm, we construct the graph with node feature matrices initialized as following,

$$\begin{aligned} \mathbf{V}^{(0)} &:= [\mathbf{x}^{(0)} \quad \mathbf{s}^{(0)} \quad \mathbf{c}] \in \mathbb{R}^{n \times 3}, \\ \mathbf{C}^{(0)} &:= [\boldsymbol{\lambda}^{(0)} \quad \mathbf{b}] \in \mathbb{R}^{m \times 2}, \\ \mathbf{G}^{(0)} &:= [\sigma \quad \boldsymbol{\mu}] \in \mathbb{R}^2. \end{aligned}$$

Line 3 For $t > 0$, we have the vectors $\Delta \mathbf{x}^{(t)}, \Delta \boldsymbol{\lambda}^{(t)}$ given by Algorithm 6. Following the MPNN framework Equation (21), we compute the update functions for variable nodes,

$$\begin{aligned} \mathbf{V}_v^{(t,1)} &:= \text{UPD}_v^{(t,1)} \left[\mathbf{V}_v^{(t-1)}, \Delta \mathbf{x}_v^{(t)} \right] \\ &= \Delta \mathbf{x}_v^{(t)} [1 \quad 0 \quad 0 \quad 0] + \mathbf{V}_v^{(t-1)} \begin{bmatrix} 0 & 0 & 0 & 0 \\ 0 & 1 & 0 & 0 \\ 0 & 0 & 1 & 0 \\ 0 & 0 & 0 & 1 \end{bmatrix} \\ &= \begin{bmatrix} \Delta \mathbf{x}_v^{(t)} & \mathbf{x}_v^{(t-1)} & \mathbf{s}_v^{(t-1)} & \mathbf{c}_v \end{bmatrix}, \end{aligned}$$

and constraint nodes,

$$\begin{aligned} \mathbf{C}_c^{(t,1)} &:= \text{UPD}_c^{(t,1)} \left[\mathbf{C}_c^{(t-1)}, \Delta \boldsymbol{\lambda}_c^{(t)} \right] \\ &= \Delta \boldsymbol{\lambda}_c^{(t)} [1 \quad 0 \quad 0] + \mathbf{C}_c^{(t-1)} \begin{bmatrix} 0 & 0 & 0 \\ 0 & 1 & 0 \\ 0 & 0 & 1 \end{bmatrix} \\ &= \begin{bmatrix} \Delta \boldsymbol{\lambda}_c^{(t)} & \boldsymbol{\lambda}_c^{(t-1)} & \mathbf{b}_c \end{bmatrix}. \end{aligned}$$

Line 4 During the derivation of IPM, we eliminated $\Delta \mathbf{s}$, now we can recover it as $\Delta \mathbf{s}^{(t)} := -\frac{\mathbf{s}^{(t-1)} \Delta \mathbf{x}^{(t)}}{\mathbf{x}^{(t-1)}} - \mathbf{s}^{(t-1)} + \frac{\sigma \boldsymbol{\mu}}{\mathbf{x}^{(t-1)}}$. To do that, we need a message function from the global to the variable nodes,

$$\text{MSG}_{\mathbf{g} \rightarrow \mathbf{v}}^{(t,2)} \left(\mathbf{G}^{(t-1)} \right) := \mathbf{G}^{(t-1)} \begin{bmatrix} 0 & 0 \\ 1 & 0 \end{bmatrix} \left(\mathbf{G}^{(t-1)} \right)^\top = \boldsymbol{\mu} \sigma,$$

and the update function,

$$\begin{aligned}
 \mathbf{V}_v^{(t,2)} &:= \text{UPD}_v^{(t,2)} \left[\mathbf{V}_v^{(t,1)}, \mu\sigma \right] \\
 &= \mathbf{V}_v^{(t,1)} \begin{bmatrix} 1 & 0 & 0 & 0 & 0 \\ 0 & 0 & 1 & 0 & 0 \\ 0 & 0 & 0 & 1 & 0 \\ 0 & 0 & 0 & 0 & 1 \end{bmatrix} \\
 &= \left(\frac{\mu\sigma + \mathbf{V}_v^{(t,1)} \begin{bmatrix} 0 & 0 & 1 & 0 \\ 0 & 0 & 0 & 0 \\ 0 & 0 & 0 & 0 \\ 0 & 0 & 0 & 0 \end{bmatrix} (\mathbf{V}_v^{(t,1)})^\top}{\mathbf{V}_v^{(t,1)} \begin{bmatrix} 0 \\ 1 \\ 0 \\ 0 \end{bmatrix}} - \mathbf{V}_v^{(t,1)} \begin{bmatrix} 0 \\ 0 \\ 1 \\ 0 \end{bmatrix} \right) [0 \ 1 \ 0 \ 0 \ 0] \\
 &= [\Delta \mathbf{x}_v^{(t)} \quad \Delta \mathbf{s}_v^{(t)} \quad \mathbf{x}_v^{(t-1)} \quad \mathbf{s}_v^{(t-1)} \quad \mathbf{c}_v].
 \end{aligned}$$

Line 5 Simulating the line search for the step size $\alpha^{(t)}$ is cumbersome. We need to calculate a vector $\alpha_x^{(t)}$ w.r.t. $\mathbf{x}^{(t-1)}$ and $\Delta \mathbf{x}^{(t)}$. Each element in the vector is defined as

$$\left(\alpha_x^{(t)} \right)_v := \begin{cases} -\frac{\mathbf{x}_v^{(t-1)}}{\Delta \mathbf{x}_v^{(t)}} & \text{if } \Delta \mathbf{x}_v^{(t)} < 0 \\ +\infty & \text{else.} \end{cases} \quad (27)$$

Then we take $\alpha_x^{(t)} := \inf \left\{ \left(\alpha_x^{(t)} \right)_v \mid v \in V(I) \right\} \in \mathbb{R}_{>0} \cup \{+\infty\}$. We repeat the same process for slack variables \mathbf{s} . We then calculate $\alpha^{(t)} := \min \left\{ 1, \alpha_x^{(t)}, \alpha_s^{(t)} \right\}$, where 1 is a constant coefficient that can be replaced by any positive number to avoid the step size being unlimited.

However, the definition in Equation (27) is not continuous as it contains $+\infty$ term. We introduce a small number $\epsilon > 0$ and modify it to be

$$\left(\alpha_x^{(t)} \right)_v := \begin{cases} -\frac{\mathbf{x}_v^{(t-1)}}{\Delta \mathbf{x}_v^{(t)}} & \text{if } \Delta \mathbf{x}_v^{(t)} \leq -\epsilon \\ \frac{\mathbf{x}_v^{(t-1)}}{\epsilon} & \text{else,} \end{cases}$$

so that $\left(\alpha_x^{(t)} \right)_v$ is continuous w.r.t. $\mathbf{x}^{(t-1)}$ and $\Delta \mathbf{x}^{(t)}$, thus compatible with neural networks.

Now, we can design functions for the message passing. We construct the message function from variable nodes to the global

node as,

$$\begin{aligned}
 \text{MSG}_{v \rightarrow g}^{(t,3)}(\mathbf{V}_v^{(t,2)}) &:= \frac{\mathbf{V}_v^{(t,2)} \begin{bmatrix} 0 \\ 0 \\ 1 \\ 0 \\ 0 \end{bmatrix}}{-\min \left\{ -\epsilon, \mathbf{V}_v^{(t,2)} \begin{bmatrix} 1 \\ 0 \\ 0 \\ 0 \\ 0 \end{bmatrix} \right\}} [1 \ 0] + \frac{\mathbf{V}_v^{(t,2)} \begin{bmatrix} 0 \\ 0 \\ 0 \\ 1 \\ 0 \end{bmatrix}}{-\min \left\{ -\epsilon, \mathbf{V}_v^{(t,2)} \begin{bmatrix} 0 \\ 1 \\ 0 \\ 0 \\ 0 \end{bmatrix} \right\}} [0 \ 1] \\
 &= \begin{bmatrix} \mathbf{x}_v^{(t-1)} & \mathbf{s}_v^{(t-1)} \\ -\min \left\{ -\epsilon, \Delta \mathbf{x}_v^{(t)} \right\} & -\min \left\{ -\epsilon, \Delta \mathbf{s}_v^{(t)} \right\} \end{bmatrix} \\
 &= \begin{bmatrix} (\boldsymbol{\alpha}_x^{(t)})_v & (\boldsymbol{\alpha}_s^{(t)})_v \end{bmatrix}.
 \end{aligned}$$

Unlike other sum aggregation functions that we have used so far, here we need a min aggregation function,

$$\begin{aligned}
 \text{AGG}_{v \rightarrow g}^{(t,3)}(\{ \begin{bmatrix} (\boldsymbol{\alpha}_x^{(t)})_v & (\boldsymbol{\alpha}_s^{(t)})_v \end{bmatrix} \mid v \in V(I) \}) \\
 &:= \min_{v \in V(I)} \begin{bmatrix} (\boldsymbol{\alpha}_x^{(t)})_v & (\boldsymbol{\alpha}_s^{(t)})_v \end{bmatrix} \\
 &= \begin{bmatrix} \alpha_x^{(t)} & \alpha_s^{(t)} \end{bmatrix},
 \end{aligned}$$

and the update function of the global node,

$$\begin{aligned}
 \mathbf{G}^{(t,3)} &:= \text{UPD}_g^{(t,3)} \left[\mathbf{G}^{(t,2)}, \begin{bmatrix} \alpha_x^{(t)} & \alpha_s^{(t)} \end{bmatrix} \right] \\
 &= \mathbf{G}^{(t,2)} [1 \ 0 \ 0] + \left(\min \left\{ 1, \begin{bmatrix} \alpha_x^{(t)} & \alpha_s^{(t)} \end{bmatrix} \begin{bmatrix} 1 \\ 0 \end{bmatrix}, \begin{bmatrix} \alpha_x^{(t)} & \alpha_s^{(t)} \end{bmatrix} \begin{bmatrix} 0 \\ 1 \end{bmatrix} \right\} \right) [0 \ 0 \ 1] \\
 &= [\sigma \ \mu \ \alpha^{(t)}].
 \end{aligned}$$

Line 6-8 The update of the variables is straightforward. We notice that $\mathbf{V}_v^{(t,3)}$ is inherited from $\mathbf{V}_v^{(t,2)}$ and $\mathbf{C}_c^{(t,3)}$ from $\mathbf{C}_c^{(t,1)}$ as we have never updated them. We need the step size information from the global node,

$$\begin{aligned}
 \text{MSG}_{g \rightarrow v}^{(t,4)}(\mathbf{G}^{(t,3)}) &:= \mathbf{G}^{(t,3)} [0 \ 0 \ 1] = \alpha^{(t)} \\
 \text{MSG}_{g \rightarrow c}^{(t,4)}(\mathbf{G}^{(t,3)}) &:= \mathbf{G}^{(t,3)} [0 \ 0 \ 1] = \alpha^{(t)},
 \end{aligned}$$

and the update function,

$$\begin{aligned}
 \mathbf{V}_v^{(t,4)} &:= \text{UPD}_v^{(t,4)} \left[\mathbf{V}_v^{(t,3)}, \alpha^{(t)} \right] \\
 &= \mathbf{V}_v^{(t,3)} \begin{bmatrix} 0 & 0 & 0 \\ 0 & 0 & 0 \\ 1 & 0 & 0 \\ 0 & 1 & 0 \\ 0 & 0 & 1 \end{bmatrix} + 0.99\alpha^{(t)} \mathbf{V}_v^{(t,3)} \begin{bmatrix} 1 & 0 & 0 \\ 0 & 1 & 0 \\ 0 & 0 & 0 \\ 0 & 0 & 0 \\ 0 & 0 & 0 \end{bmatrix} \\
 &= \begin{bmatrix} \mathbf{x}_v^{(t-1)} & \mathbf{s}_v^{(t-1)} & \mathbf{c}_v \end{bmatrix} + 0.99\alpha^{(t)} \begin{bmatrix} \Delta \mathbf{x}_v^{(t)} & \Delta \mathbf{s}_v^{(t)} & 0 \end{bmatrix} \\
 &= \begin{bmatrix} \mathbf{x}_v^{(t)} & \mathbf{s}_v^{(t)} & \mathbf{c}_v \end{bmatrix}, \\
 \mathbf{C}_c^{(t,4)} &:= \text{UPD}_c^{(t,4)} \left[\mathbf{C}_c^{(t,3)}, \alpha^{(t)} \right] \\
 &= \mathbf{C}_c^{(t,3)} \begin{bmatrix} 0 & 0 \\ 1 & 0 \\ 0 & 1 \end{bmatrix} + 0.99\alpha^{(t)} \mathbf{C}_c^{(t,3)} \begin{bmatrix} 1 & 0 \\ 0 & 0 \\ 0 & 0 \end{bmatrix} \\
 &= \begin{bmatrix} \boldsymbol{\lambda}_c^{(t-1)} & \mathbf{b}_c \end{bmatrix} + 0.99\alpha^{(t)} \begin{bmatrix} \Delta \boldsymbol{\lambda}_c^{(t)} & 0 \end{bmatrix} \\
 &= \begin{bmatrix} \boldsymbol{\lambda}_c^{(t)} & \mathbf{b}_c \end{bmatrix}.
 \end{aligned}$$

We can update the global node by dropping the used $\alpha^{(t)}$ and scale it,

$$\begin{aligned}
 \mathbf{G}^{(t,4)} &:= \text{UPD}_g^{(t,4)} \left[\mathbf{G}^{(t,3)} \right] \\
 &= \mathbf{G}^{(t,3)} \begin{bmatrix} 1 & 0 \\ 0 & 0 \\ 0 & 0 \end{bmatrix} + \mathbf{G}^{(t,3)} \begin{bmatrix} 0 & 1 & 0 \\ 0 & 0 & 0 \\ 0 & 0 & 0 \end{bmatrix} \left(\mathbf{G}^{(t,3)} \right)^\top \begin{bmatrix} 0 & 1 \end{bmatrix} = \begin{bmatrix} \sigma & \sigma\mu \end{bmatrix},
 \end{aligned}$$

where we overwrite $\mu := \sigma\mu$.

To wrap up, at the end of each iteration, we now have,

$$\begin{aligned}
 \mathbf{G}^{(t)} &= \mathbf{G}^{(t,4)} = \begin{bmatrix} \sigma & \mu \end{bmatrix}, \\
 \mathbf{C}^{(t)} &= \mathbf{C}^{(t,4)} = \begin{bmatrix} \boldsymbol{\lambda}^{(t)} & \mathbf{b} \end{bmatrix}, \\
 \mathbf{V}^{(t)} &= \mathbf{V}^{(t,4)} = \begin{bmatrix} \mathbf{x}^{(t)} & \mathbf{s}^{(t)} & \mathbf{c} \end{bmatrix},
 \end{aligned}$$

and we are ready for the next iteration.

Observing the functions we have defined, we see that they are shared across different iterations t . Combining the results from Lemma 3, we have an MPNN with $\mathcal{O}(1)$ layers and $\mathcal{O}(m+n)$ message passing steps that can reproduce an iteration in Theorem 4. \square

A.7.2. MPNNs CAN PREDICT DISPLACEMENT

Let us quickly recap the QP graph representation from Chen et al. (2024) with our notations. They consider LCQPs of the form

$$\begin{aligned}
 \min_{\mathbf{x}} \quad & \frac{1}{2} \mathbf{x}^\top \mathbf{Q} \mathbf{x} + \mathbf{c}^\top \mathbf{x} \\
 \text{s.t.} \quad & \mathbf{A} \mathbf{x} \circ \mathbf{b} \\
 & \mathbf{x} \in \mathbb{Q}^n, \mathbf{l} \leq \mathbf{x} \leq \mathbf{u},
 \end{aligned} \tag{28}$$

where $\circ \in \{\leq, =, \geq\}^m$, $\mathbf{l} \in (\mathbb{Q} \cup -\infty)^n$, and $\mathbf{u} \in (\mathbb{Q} \cup \infty)^n$. They encode an LCQP into a graph with variable and constraint node types, where \mathbf{Q} and \mathbf{A} are represented within the intra- and inter-node edges, respectively. Particularly, the

node embeddings are initialized as

$$\begin{aligned} \mathbf{h}_c^{(0)} &:= \text{INIT}_c(\mathbf{b}_c, \circ_c), \forall c \in C(I), \\ \mathbf{h}_v^{(0)} &:= \text{INIT}_v(\mathbf{c}_v, \mathbf{l}_v, \mathbf{u}_v), \forall v \in V(I). \end{aligned} \quad (29)$$

The message-passing steps in their work would be,

$$\begin{aligned} \mathbf{h}_c^{(l)} &:= \text{UPD}_c^{(l)} \left[\mathbf{h}_c^{(l-1)}, \sum_{v \in N(c) \cap V(I)} \mathbf{A}_{cv} \mathbf{h}_v^{(l-1)} \right] \in \mathbb{Q}^d, \\ \mathbf{h}_v^{(l)} &:= \text{UPD}_v^{(l)} \left[\mathbf{h}_v^{(l-1)}, \sum_{u \in N(v) \cap V(I)} \mathbf{Q}_{vu} \mathbf{h}_u^{(l-1)}, \right. \\ &\quad \left. \sum_{c \in N(v) \cap C(I)} \mathbf{A}_{cv} \mathbf{h}_c^{(l-1)} \right] \in \mathbb{Q}^d. \end{aligned} \quad (30)$$

Finally, the prediction head

$$\mathbf{x}_v := \text{READOUT} \left(\sum_{v \in V(I)} \mathbf{h}_v^{(L)}, \sum_{c \in C(I)} \mathbf{h}_c^{(L)}, \mathbf{h}_v^{(L)} \right) \in \mathbb{Q}. \quad (31)$$

They assume all the functions INIT, UPD, READOUT are parametrized by MLPs with ReLU activation functions.

Lemma 5. (Reformulation of Theorem 3.4 in Chen et al. (2024)) Given a LCQP instance I , assume I is feasible with solution \mathbf{x}^* , for any $\epsilon, \delta > 0$, there exists an MPNN $f_{\text{MPNN},1}$ of the form Equations (29) to (31), such that

$$P[\|f_{\text{MPNN},1}(I) - \mathbf{x}^*\|_2 > \delta] < \epsilon \quad (32)$$

Proof. See Chen et al. (2024) for a proof. □

We now make some slight modifications to Equation (29). We remove $\circ_c, c \in C(I)$, and $\mathbf{l}_v, \mathbf{u}_v, v \in V(I)$ from the initializations. Instead, we add an initial solution $\mathbf{x}^{(0)}$ as an extra input for INIT_v . Specifically, now we have the initialization,

$$\begin{aligned} \mathbf{h}_c^{(0)} &:= \text{INIT}_c(\mathbf{b}_c), \forall c \in C(I), \\ \mathbf{h}_v^{(0)} &:= \text{INIT}_v(\mathbf{c}_v, \mathbf{x}_v^{(0)}), v \in V(I), \end{aligned}$$

and we get the following result.

Theorem 6. Given an LCQP instance I , assume I is feasible with solution \mathbf{x}^* , $\mathbf{x}^{(0)} \geq \mathbf{0}$ is an initial point, for any $\epsilon, \delta > 0$, there exists an MPNN $f_{\text{MPNN},2}$ of the form Appendix A.7.2 and Equations (30) and (31), such that

$$P\left[\|f_{\text{MPNN},2}(I, \mathbf{x}^{(0)}) - (\mathbf{x}^* - \mathbf{x}^{(0)})\|_2 > \delta\right] < \epsilon.$$

Proof. For now, we assume the MLPs in $f_{\text{MPNN},1}$ all have the form

$$\text{MLP}(\mathbf{x}) := \mathbf{W}^{(L)} \sigma \left(\dots \sigma \left(\mathbf{W}^{(1)} \mathbf{x} + \mathbf{w}^{(1)} \right) \right) + \mathbf{w}^{(L)},$$

where σ is a ReLU activation function not applied to the last layer.

Let us remove the dependency on $\circ, \mathbf{l}, \mathbf{u}$. In our case, we restrict the problem instances to have equality constraints, and the bound of variables is always $[0, +\infty)$. Therefore, the $\circ_c, c \in C(I)$ and $\mathbf{l}_v, \mathbf{u}_v, v \in V(I)$ are constant for all the variables and constraints, for all the instances, not contributing to the distinguish of variables or QP instances. We can formulate the initialization in Equation (29) as

$$\mathbf{h}_c^{(0)} := \text{INIT}_{c,1}(\mathbf{b}_c, \circ_c) = \mathbf{W}_{(1)}^{(L)} \sigma \left(\dots \sigma \left(\mathbf{W}_{(1)}^{(1)} \mathbf{b}_c + \text{const} + \mathbf{w}_{(1)}^{(1)} \right) \right) + \mathbf{w}_{(1)}^{(L)}.$$

Therefore, it is clear that we can find an initialization $\text{INIT}_{c,1'}$ that has a bias $\mathbf{w}_{(1')}^{(1)} := \mathbf{w}_{(1)}^{(1)} + \text{const}$, while other parameters remaining the same, that can recover $\text{INIT}_{c,1}$ without the input \circ_c . Similarly, we can construct $\text{INIT}_{v,1'}$ that takes \mathbf{c}_v only as the input.

Now, we would like to have further $\mathbf{x}^{(0)}$ as the input and add it to the output of $f_{\text{MPNN},1}$. We concatenate $\mathbf{x}_c^{(0)}$ to \mathbf{c}_v , and we construct the initialization as following,

$$\begin{aligned} & \text{INIT}_{v,2}(\mathbf{c}_v, \mathbf{x}_c^{(0)}) \\ &= \begin{bmatrix} \mathbf{W}_{(L)}^{(1)} & 0 \\ 0 & 1 \end{bmatrix} \sigma \left(\dots \sigma \left(\begin{bmatrix} \mathbf{W}_{(1)}^{(1)} & 0 \\ 0 & 1 \end{bmatrix} \begin{bmatrix} \mathbf{c}_v \\ \mathbf{x}_c^{(0)} \end{bmatrix} + \begin{bmatrix} \mathbf{w}_{(1')}^{(1)} \\ 0 \end{bmatrix} \right) \right) + \begin{bmatrix} \mathbf{w}_{(1)}^{(L)} \\ 0 \end{bmatrix} \\ &= \begin{bmatrix} \mathbf{h}_v^{(0)} \\ \mathbf{x}_c^{(0)} \end{bmatrix}. \end{aligned}$$

The final equation holds, for $\mathbf{x}^{(0)}$ is assumed to be non-negative $\mathbf{x}^{(0)} \geq \mathbf{0}$, therefore the ReLU activation function does not have any effect. For the initialization of $\mathbf{h}_c^{(0)}$, we can concatenate a zero vector to the input \mathbf{b}_c and modify the weight matrices and biases in the same way and obtain $\begin{bmatrix} \mathbf{h}_c^{(0)} \\ 0 \end{bmatrix}$. For the following message passing steps, we also pad the weight

matrices \mathbf{W} and biases \mathbf{w} so that the information $\mathbf{x}^{(0)}$ is carried to the end of embedding $\begin{bmatrix} \mathbf{h}_v^{(L)} \\ \mathbf{x}_c^{(0)} \end{bmatrix}$. Finally, we need to modify the last layer of the READOUT function by modifying the weights and biases the same way and padding a ones vector column at the last weight matrix $\begin{bmatrix} \mathbf{W}^{(L)} & \mathbf{1} \end{bmatrix}$. Therefore, the input $\mathbf{x}^{(0)}$ will be finally added to the output, i.e.,

$$f_{\text{MPNN},2}(I, \mathbf{x}^{(0)}) = f_{\text{MPNN},1}(I) + \mathbf{x}^{(0)}.$$

Hence, we immediately have the conclusion that $f_{\text{MPNN},2}$ can approximate $\mathbf{x}^* - \mathbf{x}^{(0)}$ arbitrarily well. □